2006

Shear-Wave Velocities and Derivative Mapping For the Upper Mississippi Embayment

David M. Vance
University of Kentucky, davey1977@yahoo.com

Abstract

Shear-Wave Velocities and Derivative Mapping
For the Upper Mississippi Embayment

During the past two decades, University of Kentucky researchers have been acquiring seismic refraction/reflection data, as well as seismic downhole data, for characterizing the seismic velocity models of the soil/sediment overburden in the central United States. The dataset includes densely spaced measurements for urban microzonation studies and coarsely spaced measurements for regional assessments. The 519 measurements and their derivative products often were not in an organized electronic form, however, limiting their accessibility for use by other researchers. In order to make these data more accessible, this project constructed a database using the ArcGIS 9.1 software. The data have been formatted and integrated into a system serving a wider array of users. The seismic shear-wave velocity models collected at various locations are archived with corresponding x-, y-, and z-coordinate information. Flexibility has been included to allow input of additional data in the future (e.g., seismograms, strong ground-motion parameters and time histories, weak-motion waveform data, etc.). Using the completed database, maps of the region showing derivative dynamic site period (DSP) and weighted shear-wave velocity of the upper 30 m of soil (V_{30}) were created using the ArcGIS 9.1 Geostatistical Analyst extension for examination of the distribution of pertinent dynamic properties for seismic hazard assessments. Both geostatistical and deterministic techniques were employed. Interpolation of V_{30} data yielded inaccurate predictions because of the high lateral variation in soil layer lithology in the Jackson Purchase Region. As a result of the relatively uniform distribution of depths to bedrock, the predictions of DSP values suggested a high degree of accuracy.

Keywords: GIS, geodatabase, kriging, shear-wave velocity, dynamic site period

Shear-Wave Velocity Database and Derivative Mapping For the Upper Mississippi Embayment

By

David M. Vance

Dr. Edward W. Woolery
Director of Thesis

Dr. Sue Rimmer
Director of Graduate Studies

Rules for the Use of Thesis

Unpublished theses submitted for the Master's degree and deposited in the University of Kentucky Library are as a rule open for inspection, but are to be used only with due regard to the rights of the authors. Bibliographical references may be noted, but quotations or summaries of parts may be published only with the permission of the author, and with the usual scholarly acknowledgements.

Extensive copying or publication of the thesis in whole or in part also requires the consent of the Dean of the Graduate School of the University of Kentucky.

A library that borrows this thesis for use by its patrons is expected to secure the signature of each user.

THESIS

David M. Vance

The Graduate School

University of Kentucky

2006

SHEAR-WAVE VELOCITY DATABASE AND DERIVATIVE MAPPING FOR THE UPPER MISSISSIPPI EMBAYMENT

THESIS

A thesis submitted in partial fulfillment of the
requirements of the degree of Master of Science in the
College of Arts and Sciences
at the University of Kentucky

By

David M. Vance

Director: Dr. Edward W. Woolery, University of Kentucky
Department of Earth and Environmental Sciences

Lexington, Kentucky

2006

For Laura Leigh Vance

Acknowledgments

The completion of this project would not have been possible without the support of many friends and colleagues. First, I'd like to thank the Kentucky Geological Survey for providing both financial and technical support. In particular, Jackie Silvers and Mandy Long were dependable sources of help throughout the process. Mark C. Thompson was invaluable in keeping the computer network and software available and running. I'd also like to thank Dr. Zhenming Wang and Dr. John Kiefer for excellent advice and suggestions concerning the development of this project. I appreciate the comments, insights, and suggestions of Josh Sexton, James Ward, James Whitt, and Ken Macpherson, as well.

Dr. Ed Woolery, in addition to being my supervisor, has been an outstanding mentor. I greatly appreciate his advice, support, and knowledge. I'm grateful for the learning opportunities he afforded me, both as an undergraduate and at the graduate level.

Finally, I'd like to thank my family for their encouragement and especially my wife, Laura, for her incredible love and support throughout this process. Without her inspiration and encouragement this project would not have been possible.

Table of Contents

List of Tables

List of Figures

List of Files

VanceThesis06.pdf

1.0 Introduction

1.1 The Dataset

During the last two decades, researchers at the University of Kentucky have collected numerous seismic velocity data, especially in the vicinity of the New Madrid Seismic Zone, including western Kentucky, southeastern Missouri, northeastern Arkansas, northwestern Tennessee; and the Wabash Valley Seismic Zone, located in southern Indiana and Illinois. Additional microzonation data have been collected in the Kentucky cities of Paducah, Henderson, Louisville, and Maysville (Figure 1).

In addition to seismic velocity, the data provided the depth to bedrock at each site, thicknesses of overlying soil layers, and location coordinates. The weighted average shear-wave velocity of the upper 30 meters (V_{30}) of soil/bedrock, calculated according to the 1997 National Earthquake Hazard Reduction Program (NEHRP) provisions (BSSC, 1997), were included in some of the studies from which the data were taken. The V_{30} values were manually calculated and added to the dataset in which they were not originally included. Dynamic site periods (DSP) were also included in some of the original studies and calculated for studies in which they were not originally included. Other associated data from the original sources, such as the site name, site classification, average sediment and bedrock velocities, elevation, soil type, collection date, and topographic map name were also included.

The purpose of these data is to characterize and model the soil/sediment overburden in the central United States in order to determine the ground-motion site effects during an earthquake. Flexibility in the database is built in for future additions of new data and data types. For this project, the Jackson Purchase Region of western Kentucky (Figure 2), because of its increasing development, particularly in the vicinity of Paducah, and because of its proximity to major geologic structures and seismically active zones, was selected for derivative mapping.

The seismic risk to engineered structures in the central United States necessitates the research to characterize earthquake site effects in the region. Several seismic zones are present in the central United States, including the Eastern Tennessee Seismic Zone, the South Carolina Seismic Zone, the Giles County Seismic Zone (in Virginia), the Anna, Ohio, Seismic Zone, the Northeastern Kentucky Seismic Zone, and the New Madrid Seismic Zone, which dominates the overall seismic hazard. The influence of local geologic/soil conditions on the amplitude, frequency content, and duration of any size earthquake ground motion is referred to as “site

effects." Site effects may have a more profound influence on ground motions than the magnitude in areas with a thick sediment overburden (Street et al., 1997). Ground-motion parameters can be either amplified or attenuated by the dynamic soil properties (e.g., sediment velocity, natural period), the subsurface geometry at both one-dimensional local and two- and three-dimensional basin scales, and surface topography. Only one-dimensional local site effects were considered in this project. Neglecting material damping and scattering effects, for example, as a seismic wave passes into a region of low impedance from a region of high impedance, the resistance to motion decreases and the wave amplitude must increase to maintain energy conservation.

The effect of near-surface geometry is evident in the case of a site with dynamic soil properties remaining the same, changing only the thickness (H) of the sediments above bedrock. According to the equation for the frequency of the soil, $f_s = \beta/4H$, where β = shear-wave velocity, an increase in thickness of the sediments results in a decrease in frequency. The dynamic site period (DSP), the period at which the fundamental mode of resonance occurs, is the inverse of the frequency and is used to design structures with fundamental periods that differ from the DSP, avoiding in-phase resonance between the structure and soil column and therefore minimizing damage during an earthquake (Street et al., 1997).

The weighted shear-wave velocity of the upper 30 m of soil/bedrock (V_{30}), as calculated in accordance with the 1997 NEHRP Recommended Provisions for Seismic Regulations for New Buildings (BSSC, 1997), is used for site classification of the more poorly consolidated sediments of the near-surface soils. These site classifications can then be used to calculate site-dependent seismic coefficients, which are used to produce soil amplification maps (Street et al., 2001).

Derivative maps generated using the Geostatistical Analyst extension of ArcGIS 9.1 are useful for providing DSP estimates across the study area. Researchers can use the maps for examination of the distribution of the values, which would otherwise be impossible without sample locations at every point.

To support ongoing earthquake site-effects research, the objectives of this project were to 1) retrieve seismic velocity data collected by University of Kentucky researchers from various media (e.g., journals, theses, dissertations, reports), 2) digitize the data and organize by project, 3) use methods to interpolate pertinent dynamic properties for seismic hazard assessments (i.e., V_{30} and DSP values), and 4) interpret the resultant derivative maps.

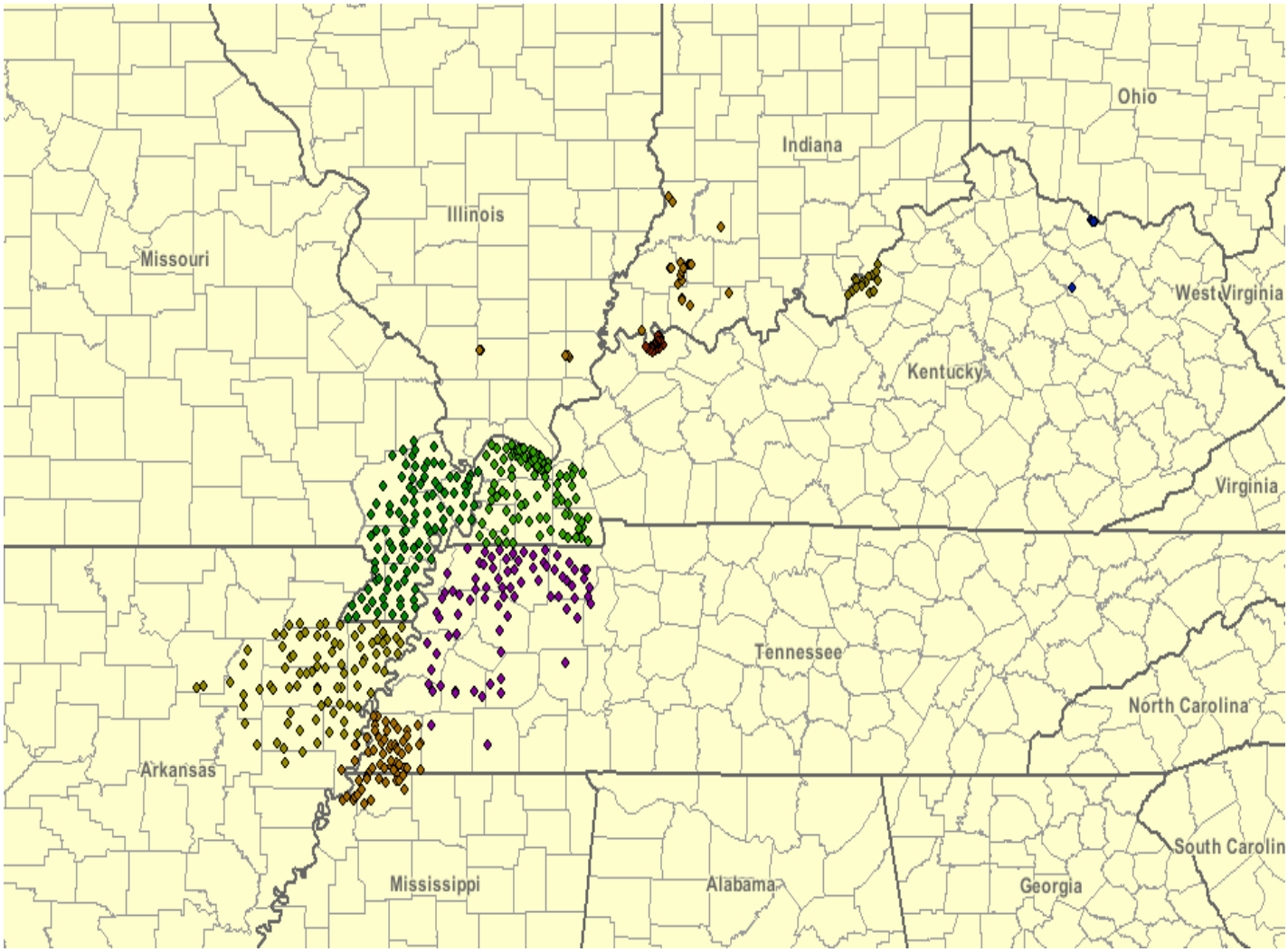

Figure 1. Geographic distribution of the 519 sample locations contained in the database.

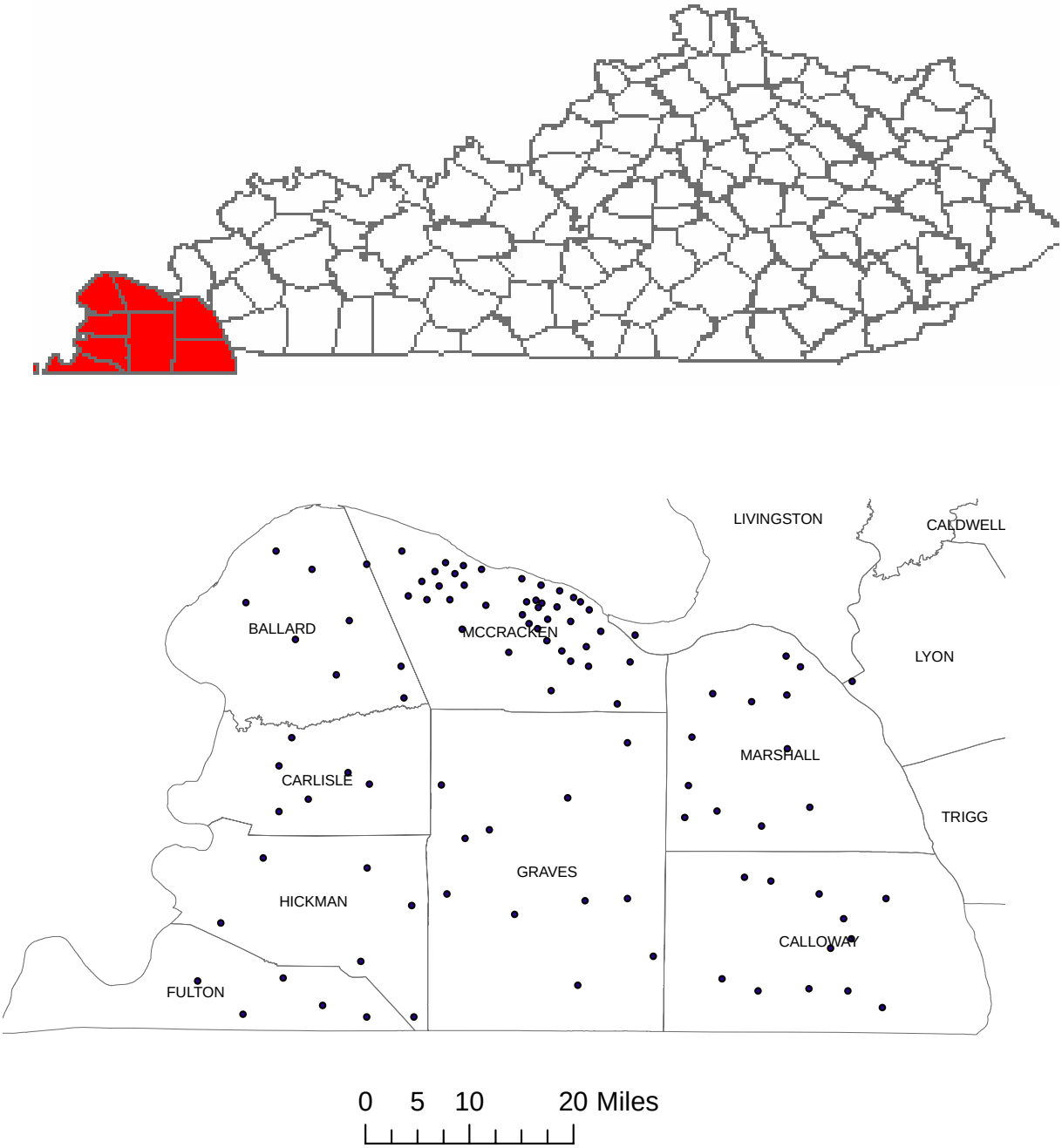

Figure 2. The Jackson Purchase Region of western Kentucky (highlighted in red). The lower figure shows the distribution of sample locations in the study area. The concentration of sample sites in McCracken County centers around the Paducah urban area and the samples were collected by Harris (1992). The remaining samples were collected by Street et al. (1997).

1.2 Data Accessibility

The usefulness of 519 seismic velocity soundings has been limited because of the inaccessibility of the data. Often, the data did not exist in electronic form, requiring researchers to spend time and energy locating the data in published reports, theses, and journal articles. The existence of data was sometimes unknown. In addition, examination of the data to identify trends and to derive useful information was often difficult because there was no easy way to plot the data for spatial representation and perform rapid manipulation of the dataset. Therefore, another goal of this project was to digitize the database in a manner that would allow queries and spatial representation in map form. Specifically, this digitization provides a view of the sample site distribution and allows statistical analyses that would be overly cumbersome to perform by hand.

1.3 The GIS Database

For this project, the ArcGIS version 9.1 suite of applications, including ArcCatalog, ArcMap, and ArcToolbox, developed by the Environmental Systems Research Institute (ESRI), was selected because of its comprehensive database management tools, geostatistical analysis capabilities, and wide acceptance in the scientific community. Dowdy (1998) compared ArcGIS to various other GIS software packages, such as Rockworks, TerraSoft, and MapInfo.

The data in this study were organized in the geographic database, or *geodatabase*, by name of researcher and study area location. This design allows a user to examine data and perform operations on data from specific areas, since future studies will likely focus on a particular area rather than an entire region. The data may easily be reconfigured to allow operations on the full dataset, however. The *personal geodatabase, feature dataset,* and *feature classes* were created directly in ArcCatalog with no data initially contained within. Data were entered into the geodatabase manually by transfer from other digital sources or directly from printed sources. Each dataset from a single source forms a *point feature class* and all feature classes are included in a single-feature dataset to enforce a common spatial reference. This ensures that all data points will be projected at the appropriate locations on the map. The feature dataset and all included data are stored in a personal geodatabase (Figure 3). *Metadata* were created to document the source, quality, and other information related to the data using the template available in ArcCatalog.

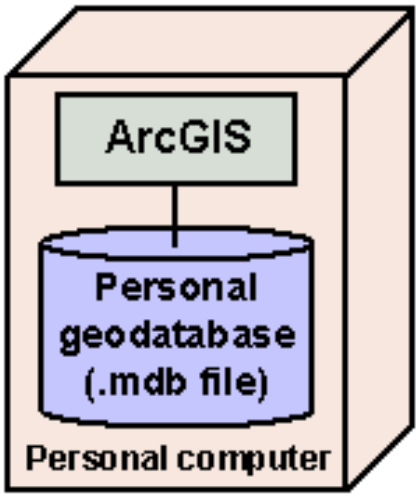

Figure 3. A personal geodatabase handles small to moderately sized (~2 GB) datasets (from ESRI, 2004).

1.3.1 Application 1: ArcGIS Functionality

ArcGIS 9.1 includes the Geostatistical Analyst extension, which was used to demonstrate two applications of ArcGIS functionality: specifically, derivative maps of the mean dynamic site period (DSP) and weighted shear-wave velocity of the upper 30 meters of soil (V_{30}) distributions. Geostatistical Analyst provides tools such as histograms, Voronoi maps, Quantile-Quantile (QQ) plots, trend analysis, and semivariogram/covariance clouds for exploratory spatial data analysis (ESDA), which is used to examine the data for trends and to identify data outliers. Application of these tools assists the parameter selection process, resulting in more accurate prediction maps. An explanation of the available tools for ESDA was included in this text, and comparisons between interpolation methods were made using the root-mean-square (RMS) and other prediction error measurements, also provided in Geostatistical Analyst, to identify the most accurate method.

1.3.2 Application 2: Interpolated Maps

Although geophysical knowledge of an entire area such as the Jackson Purchase is desirable, the collection of such an enormous amount of data is both logistically and fiscally unrealistic. For this reason, interpolation of the data between data points over the study area, using deterministic and stochastic methods based on the limited samples already collected,

allows prediction of values of a particular geophysical property at any given location with a finite amount of accuracy. Deterministic methods, such as splines, apply mathematical functions to the dataset for the interpolation process. Stochastic methods, such as kriging, also use mathematical functions but include geostatistical methods as well to account for the randomness inherent in geologic and data collection processes. Therefore, stochastic methods provide measures of accuracy and a level of confidence in the predictions. The methodology for producing such interpolated maps is documented and then demonstrated using the real dataset from the Jackson Purchase area.

2.0 Geographic Information System (GIS)

In addition to having human and organizational components, a geographic Information system (GIS) is defined as:

> *An integrated collection of computer software and data used to view and manage information about geographic places, analyze spatial relationships, and model spatial processes. A GIS provides a framework for gathering and organizing spatial data and related information so that it can be displayed and analyzed* (ESRI GIS Dictionary).

The utility of GIS spans multiple industries, and GIS has been used to integrate the operations of organizations in more powerful ways than in the past. Specifically, in the past organizations relied on hard copies of information and data in the form of compact disks and paper files, often resulting in duplication of work. The use of shared geodatabases has reduced operation time and costs and prevented the duplication of work already accomplished.

2.1 Development of Geographic Information Systems

The historical development of GIS is based in a variety of disciplines and is well documented (Foresman, 1998). Developments in the separate fields of geographic information systems and spatial data analysis and their convergence can be traced beginning in the 1950s and 1960s. One expression of this convergence is found in the ArcGIS Geostatistical Analyst extension of ArcGIS 9.1. The Geostatistical Analyst extension is used for application of statistical methods to datasets and production of derivative maps.

The ArcGIS software package was developed by the Environmental Systems Research Institute (ESRI) with capabilities for handling geoprocessing, database management, and digital

cartographic projects. The release of ArcGIS 8 in 1999 introduced ArcCatalog, ArcMap, ArcToolbox, and several extensions for data viewing and manipulation (ArcCatalog), projection and analysis (ArcMap), conversion and processing (ArcToolbox), and utilization for various specific applications (extensions such as Geostatistical Analyst, Spatial Analyst, and 3D Analyst). Subsequent versions such as 8.1, 8.3, 9.0, and 9.1 build upon previous versions to enhance functionality, usability, and performance.

2.2 Applicability

Data collected by researchers at the University of Kentucky existed primarily in paper form (e.g., journals, theses, dissertations, reports), making the data difficult to access and manipulate. Often, the existence of previously collected data was overlooked. ArcGIS provides an efficient platform for the storage and display of data and offers the Geostatistical Analyst extension and accompanying Exploratory Spatial Data Analysis (ESDA) environment for data analysis. The GIS technology was used to enhance seismic research efforts by organizing data in digital form and creating derivative maps of dynamic soil properties for regional assessment of seismic hazard.

2.2.1 ArcGIS (ArcCatalog, ArcMap, ArcToolbox, and Extensions)

In this project, the ESRI ArcGIS 9.1 software package was used, and the Geostatistical Analyst extension of version 9.1 was of particular interest for its ability to apply statistical methods to spatial datasets and to determine trends, identify outliers, and produce derivative maps of a given attribute. The various interpolation methods also yield measures of uncertainty.

2.2.2 Geostatistical Analyst

Exploratory Spatial Data Analysis (ESDA)

ESDA is a component of Geostatistical Analyst that is used to apply statistical methods to the dataset. The available tools include histograms, Voronoi maps, normal and general QQ plots, trend analysis, semivariogram/covariance clouds, and crosscovariance clouds. Each method assists in identification of data outliers, trends in the data, spatial autocorrelation, and data distribution.

Histograms

Histograms show the frequency distribution of the data in one variable and calculate summary statistics such as the count, minimum and maximum values, mean, median, standard deviation, skewness, kurtosis, and first and third quartiles. Carr (1995) defined these terms that describe histogram characteristics.

Voronoi Maps

Voronoi maps are composed of polygons, each of which contains a sample point, and are constructed so that any given point within the polygon is closer to the sample point in that polygon than any other sample point on the map. Statistics calculated within Voronoi maps allow the identification of local smoothing, local variation, local outliers, and local influence. There are eight types of maps that can be produced with this tool, including simple, mean, mode, cluster, entropy, median, and standard deviation. Four of the eight types of Voronoi maps were used in this project and are described below. Table 1 shows the functional purpose of each type of Voronoi map.

- **Simple**: The value assigned to a cell is the value recorded at the sample point within that cell.
- **Mean**: The value assigned to a cell is the mean value that is calculated from the cell and its neighbors.
- **Cluster**: All cells are placed into five class intervals. If the class interval of a cell is different from each of its neighbors, the cell is colored gray to distinguish it from its neighbors.
- **Standard Deviation**: The value assigned to a cell is the standard deviation that is calculated from the cell and its neighbors.

Functional category	Voronoi statistics
Local Smoothing	Mean Mode Median
Local Variation	Standard deviation Interquartile range Entropy
Local Outliers	Cluster
Local Influence	Simple

Table 1. Various aspects of a dataset examined using Voronoi maps (ESRI, 2006).

Quantile-Quantile (QQ) Plots

A cumulative distribution for a dataset is produced by ordering the data and producing a graph of the ordered values versus cumulative distribution values calculated as $(i – 0.5)/n$ for the ith ordered value out of n total values (the percent of the data below a value) (ESRI, 2006). Normal QQ plots, used to determine if the data are normally distributed, are constructed by plotting data values with standard normal values that have equal cumulative distributions, as shown in Figure 4 (ESRI, 2006). General QQ plots, used to examine the similarity of distributions between two datasets, are constructed by plotting values from one dataset with values from a second dataset that have equal cumulative distributions (Figure 5).

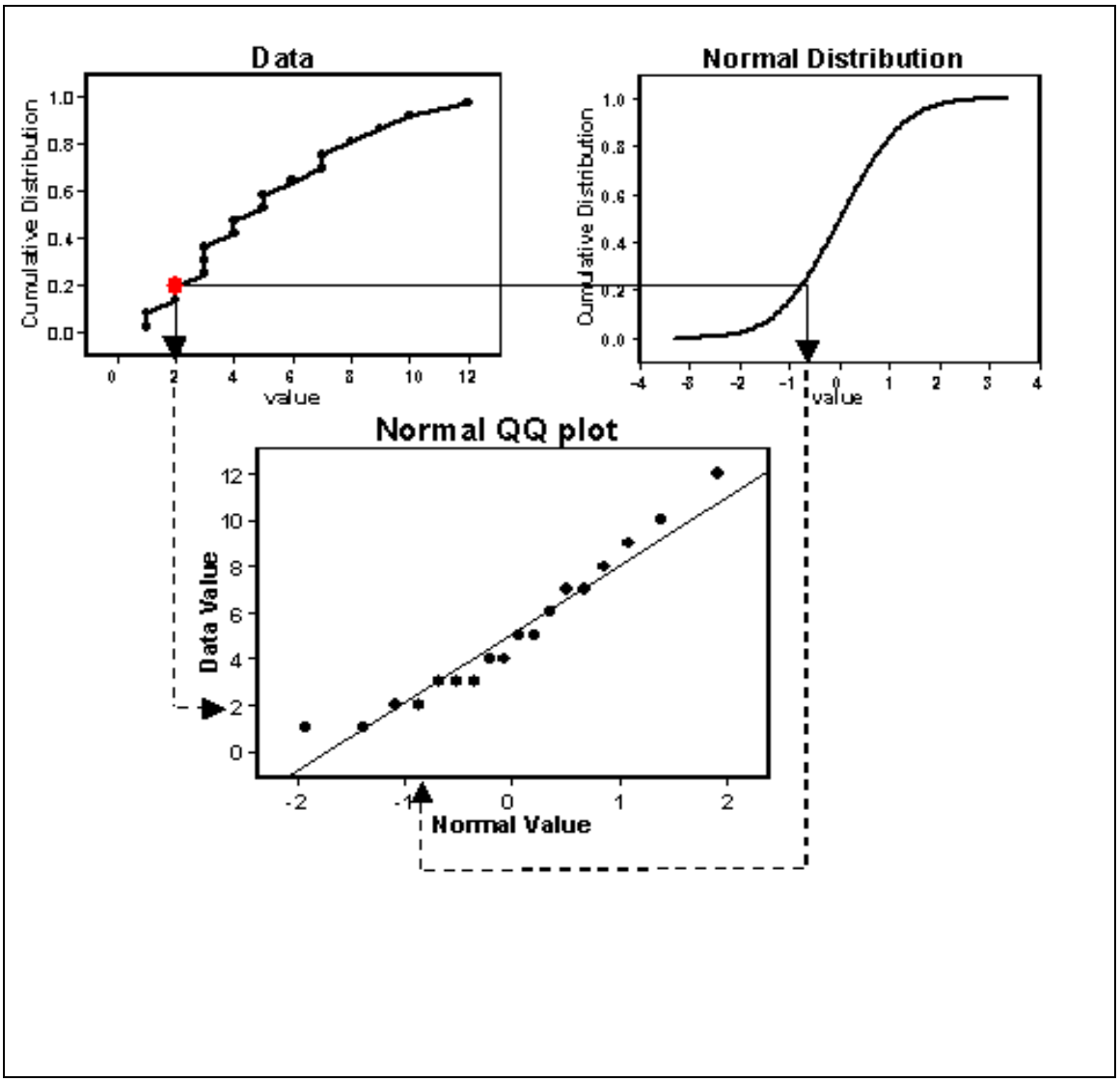

Figure 4. Construction of a normal QQ plot, which is used to examine the distribution of a dataset (ESRI, 2006).

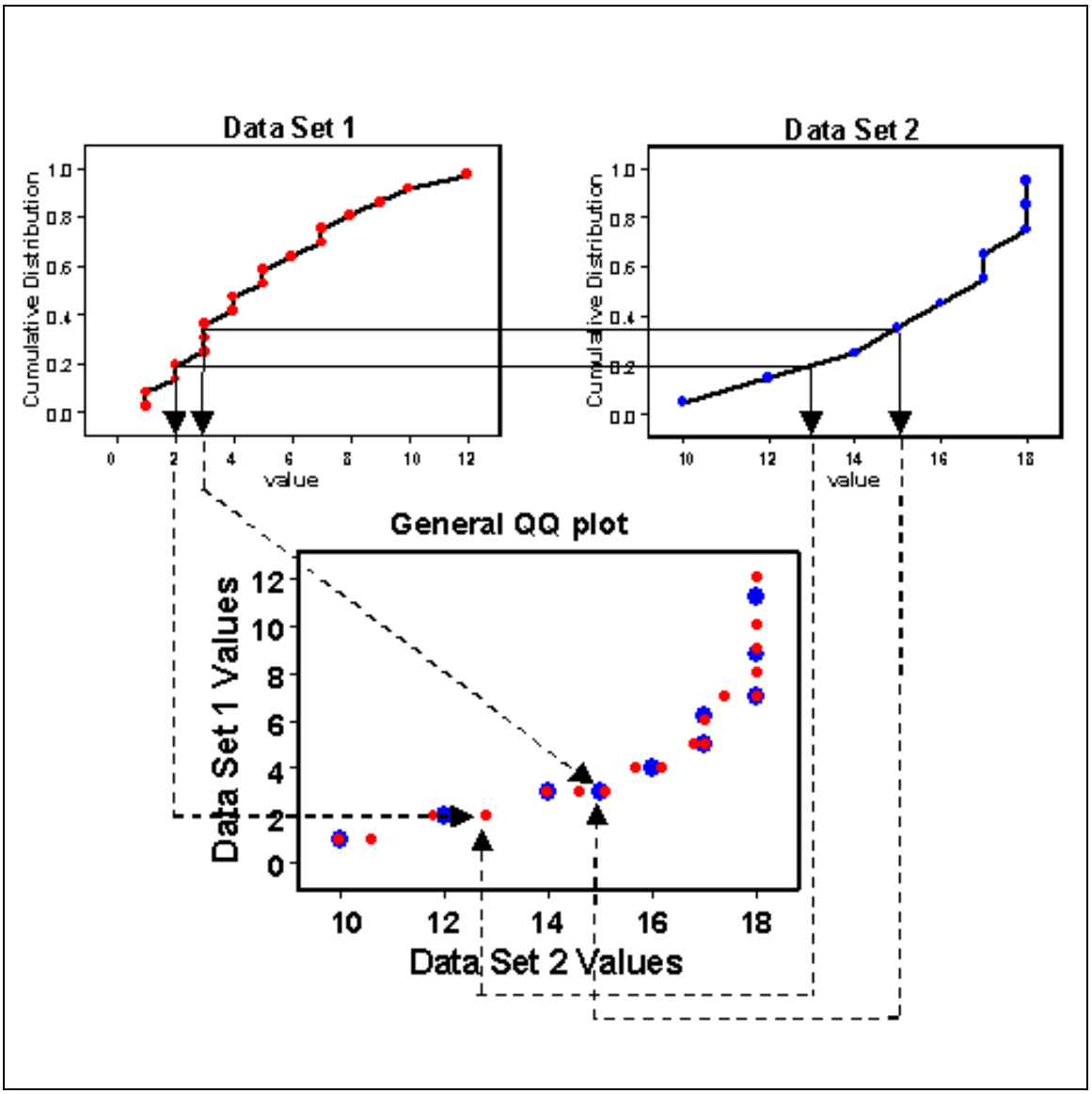

Figure 5. Construction of a general QQ plot, which is used to compare distributions of two datasets (ESRI, 2006).

Trend Analysis

To identify trends for mapping or removal, the trend analysis tool is used to view the data in a three-dimensional graph. The samples are plotted by location on the x, y plane. The z plane shows the values of the measured attribute of interest. The values are then projected on both the x, z plane and the y, z plane as scatter plots. Polynomial curves are fitted through the scatter plots to show trends. Additional features allow rotation of the graph and sample points to isolate directional trends, change of perspective, change of size and color of points and lines, removal of planes and points, and selection of the order of polynomial used to fit the scatter plots (Figure 6).

Semivariogram/Covariance Clouds

The semivariogram/covariance cloud, defined by Schabenberger and Gotway (2005), is used to examine spatial autocorrelation and identify data outliers and is constructed by plotting the difference squared between the values of two points for a designated attribute as a function of the distance between the pair of points. Thus, one dot on the cloud represents a pair of sample points.

Crosscovariance Clouds

Used to examine spatial autocorrelation between two datasets and to identify spatial shifts in correlation between the two datasets, the crosscovariance cloud is constructed by plotting the empirical crosscovariance for pairs of locations between two datasets as a function of the distance between them.

2.3 Surface Creation Using Interpolation Techniques

Geostatistical Analyst uses a finite set of sample points at known locations to calculate (predict) unknown values at unsampled locations and produce a map showing the distribution of values over an area. A fundamental geographic principle states that samples close together are more alike than samples farther apart. Based on this assumption, Geostatistical Analyst uses two types of interpolation techniques to derive surfaces based on limited datasets: *deterministic methods* and *geostatistical methods*. This assumption is often not applicable geologically. Specifically, the Jackson Purchase Region exhibits strong lateral variation in lithology over short distances, which resulted in higher prediction errors associated with the V_{30} derivative maps. This is attributed to the fact that V_{30} is calculated based on the thickness of individual soil layers, which vary appreciably over short distances. The DSP values, which are dependent on the total thickness of sediments above bedrock, demonstrated a more uniform distribution, resulting in low prediction errors.

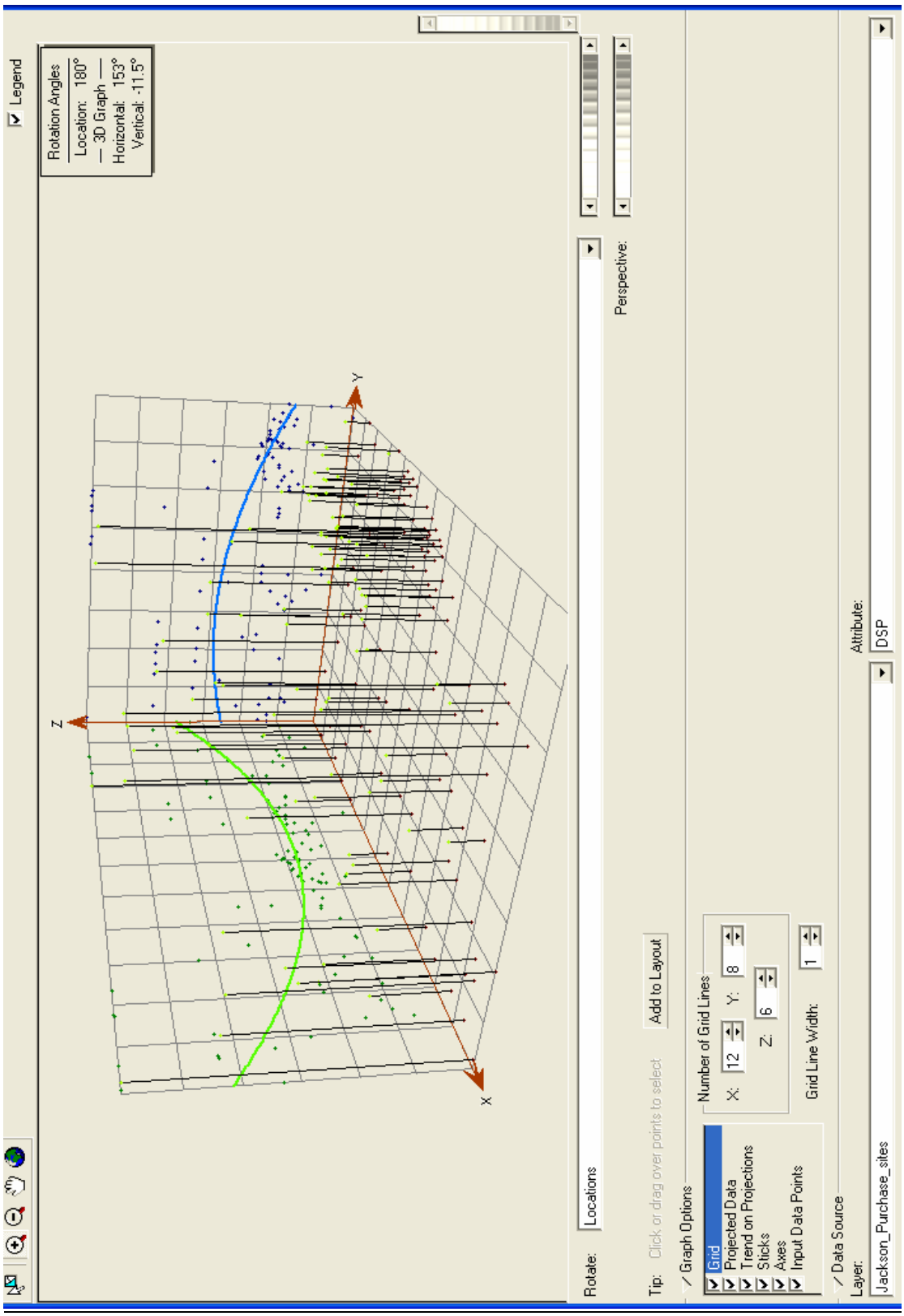

Figure 6. The trend analysis tool, showing distribution, trends, and magnitude of the DSP dataset**.**

2.3.1 Deterministic Methods

The deterministic interpolation methods can be characterized as global or local, exact or inexact, and are based on either extent of similarity between data points or degree of smoothing. Each method may be considered as a combination of one or more of these characterizations.

Global and Local Interpolators

Global interpolators (global polynomial) utilize the entire dataset when calculating the output surface, whereas local interpolators (inverse distance weighted, local polynomial, and radial basis functions) use search neighborhoods, which are smaller areas within the extent of the entire study area.

Exact and Inexact Interpolators

Exact interpolators (inverse distance weighted and radial basis functions) force the output surface to pass through the sample points, meaning the value of the derived surface is exactly equal to the measured value of the original dataset. Inexact interpolators (global polynomial and local polynomial) calculate values that vary slightly from the measured values, reducing sharp peaks that may occur in the output surface as a result of forcing the surface to pass through the measured sample points.

Extent of Similarity vs. Degree of Smoothing

Interpolators such as inverse distance weighted (IDW) perform interpolations based on the extent of similarity between data points. IDW gives more weight to points closer to the location at which a value is being calculated and gives progressively diminishing weight to points that are farther apart. Radial basis functions (RBF), such as splines, fit a surface through all data points while reducing the amount of curvature of the derived surface between points.

2.3.2 Geostatistical Methods

Geostatistical interpolation techniques involve both mathematical and statistical models. For this reason, these methods can be used to create maps showing the standard error and uncertainty in the prediction surfaces. The ability to produce error and uncertainty surfaces allows the user to attain a level of confidence in the accuracy of the derivative maps and is a distinguishing feature between the geostatistical and deterministic interpolators. Geostatistics is

dependent on the assumption that data are autocorrelated, meaning they are the result of random processes with dependence. The dependence rules are determined during the ESDA process (ESRI, 2006).

The group of interpolation techniques based on mathematical and statistical models is known collectively as *kriging*. Several varieties of kriging are available in Geostatistical Analyst including ordinary, simple, universal, indicator, probability, disjunctive, and cokriging. Advantages of using the geostatistical techniques include the ability to use semivariogram/covariance clouds, perform transformations, remove trends, and account for measurement error.

Ordinary Kriging

Ordinary kriging is modeled by the function

$$Z(\mathbf{s}) = \mu + \varepsilon(\mathbf{s})$$

where μ is an unknown constant mean and ε is autocorrelated error at location (s) (Figure 7). A constant mean across a large study area is probably unrealistic in most cases, but may be sufficiently flexible to achieve the desired result. Acceptable results are relative and depend greatly on the goals of the researcher.

Simple Kriging

The model used in ordinary kriging is also used in simple kriging, but here the mean, μ, is assumed to be known. Previously, when using ordinary kriging μ was unknown and estimated. Therefore, ε was also estimated. When ε is known, it is possible to make better estimations of autocorrelation and to produce more accurate derivative maps.

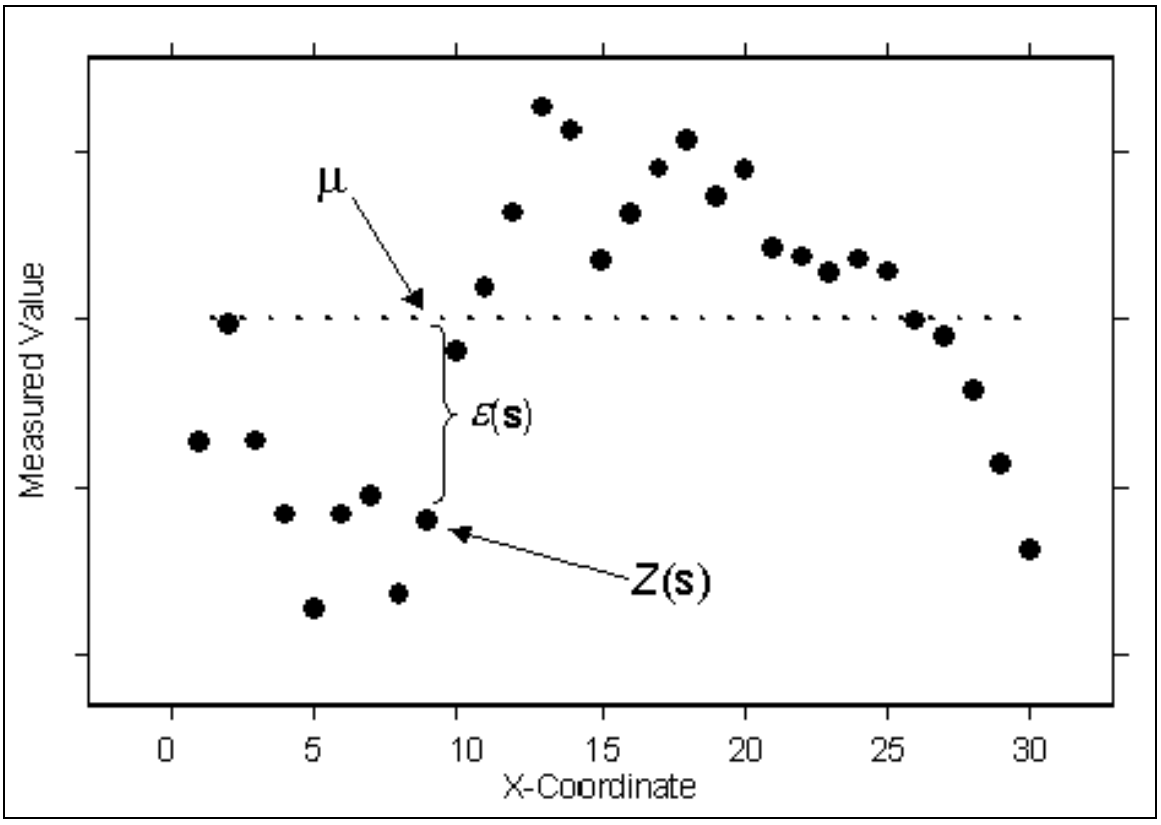

Figure 7. Ordinary kriging fits an unknown constant mean, μ, to the dataset with autocorrelated random errors, ε(s). Z(s) is a measured value, Z, at location (s) (ESRI, 2006).

Universal Kriging

Universal kriging uses a mathematical model similar to the previous two methods. The model used is

$$Z(\mathbf{s}) = \mu(s) + \varepsilon(\mathbf{s})$$

where μ(s) represents a deterministic function, rather than a known or unknown constant mean (Figure 8). The deterministic function is fitted to the data in Figure 8 as a second-order polynomial. Subtraction of the polynomial from the data results in a plot of autocorrelated errors. Universal kriging can be thought of as regression performed on spatial coordinate variables (ESRI, 2006).

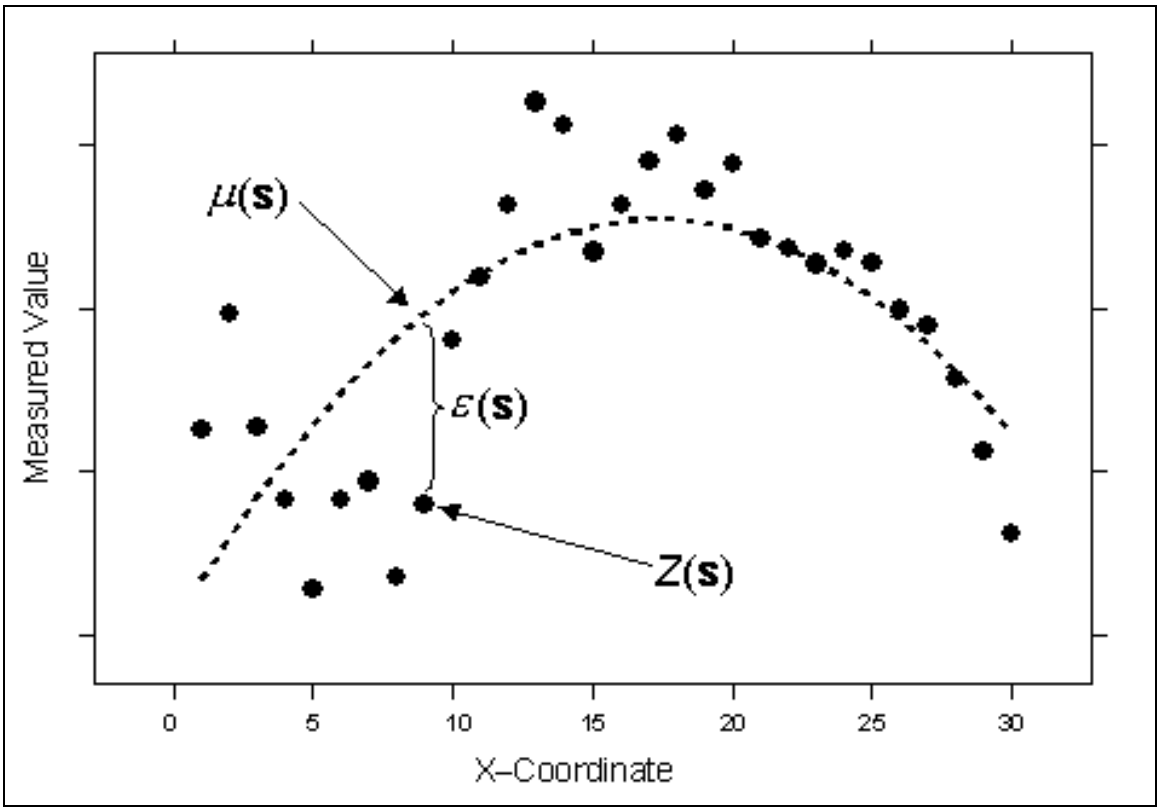

Figure 8. In universal kriging, the data are fitted with a deterministic function, μ(s). Errors, ε(s), are assumed to be autocorrelated (ESRI, 2006).

Indicator Kriging

Indicator kriging is defined by the equation

$$I(\mathbf{s}) = \mu + \varepsilon(\mathbf{s}),$$

where μ is an unknown constant and I(s) is a binary variable (ESRI, 2006). This method may be used on binary data or on binary data created by establishing a threshold on a continuous dataset. Otherwise, the procedure is the same as that for ordinary kriging (Figure 9).

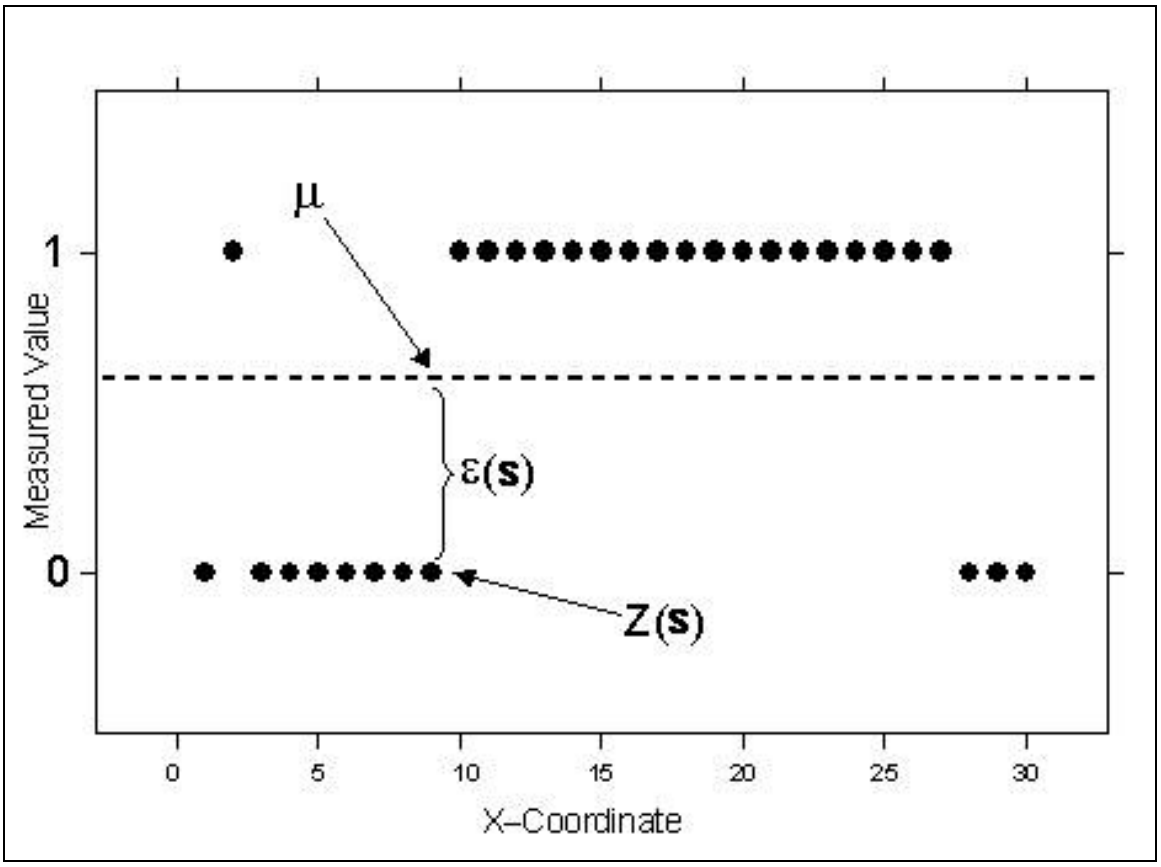

Figure 9. Indicator kriging interpolations indicate the probability of a given location having a value of 1, or in the case of a threshold applied to a dataset, the probability of the value at a point exceeding or not exceeding the threshold. Here, the dashed line indicates an unknown mean, μ. The measurement error, ε(s), is assumed to be autocorrelated. Multiple thresholds can be used to establish primary and secondary indicator variables, and interpolations can then be performed using the cokriging technique (ESRI, 2006).

Probability Kriging

The probability kriging method is defined by the equations

$$I(\mathbf{s}) = I(Z(\mathbf{s}) > c_t) = \mu_1 + \varepsilon_1(\mathbf{s})$$

$$Z(\mathbf{s}) = \mu_2 + \varepsilon_2(\mathbf{s}),$$

where μ_1 and μ_2 are unknown constants, and I(**s**) is a binary variable indicating exceedance or nonexceedance of a set threshold. This method is similar to indicator kriging, but uses cokriging rather than regular kriging, with the intent of producing more accurate results. The drawback is the extra estimation needed for autocorrelation of each variable and cross-correlation between datasets, potentially introducing more uncertainty.

Disjunctive Kriging

Disjunctive kriging is defined by the function

$$f(Z(s)) = \mu_1 + \varepsilon(s),$$

where μ_1 is an unknown constant and f(Z(s)) is an arbitrary function of Z(s) (ESRI, 2006). This model can also be written as $f(Z(s)) = I(Z(s) > c_t)$. The functions available are $Z(s_0)$ and $I(Z(s_0) > c_t)$. According to ESRI (2006), disjunctive kriging "requires the bivariate normality assumption and approximations to the functions $f_i(Z(s_i))$; the assumptions are difficult to verify, and the solutions are mathematically and computationally complicated."

Cokriging

Cokriging is potentially more powerful than kriging. In addition to the autocorrelation present in the main dataset of interest, information from another dataset is cross-correlated with the variable from the main dataset to achieve greater accuracy. If correlation does, in fact, exist between the two datasets, the resulting output surface should model reality more accurately. If there is no cross-correlation between datasets, the predictions are still made from the autocorrelation present in the original dataset. The risk involved comes from the added parameter estimations, which may introduce more variability, effectively negating any gains made from using the second dataset, possibly wasting the extra effort required to interpolate with more than one dataset.

Ordinary cokriging is defined by the mathematical models

$$Z_1(\mathbf{s}) = \mu_1 + \varepsilon_1(\mathbf{s})$$

$$Z_2(\mathbf{s}) = \mu_2 + \varepsilon_2(\mathbf{s}),$$

where μ_1 and μ_2 are unknown constants (Figure 10). Each of the kriging methods is also available as a cokriging method; in each case a second dataset is used to achieve greater accuracy.

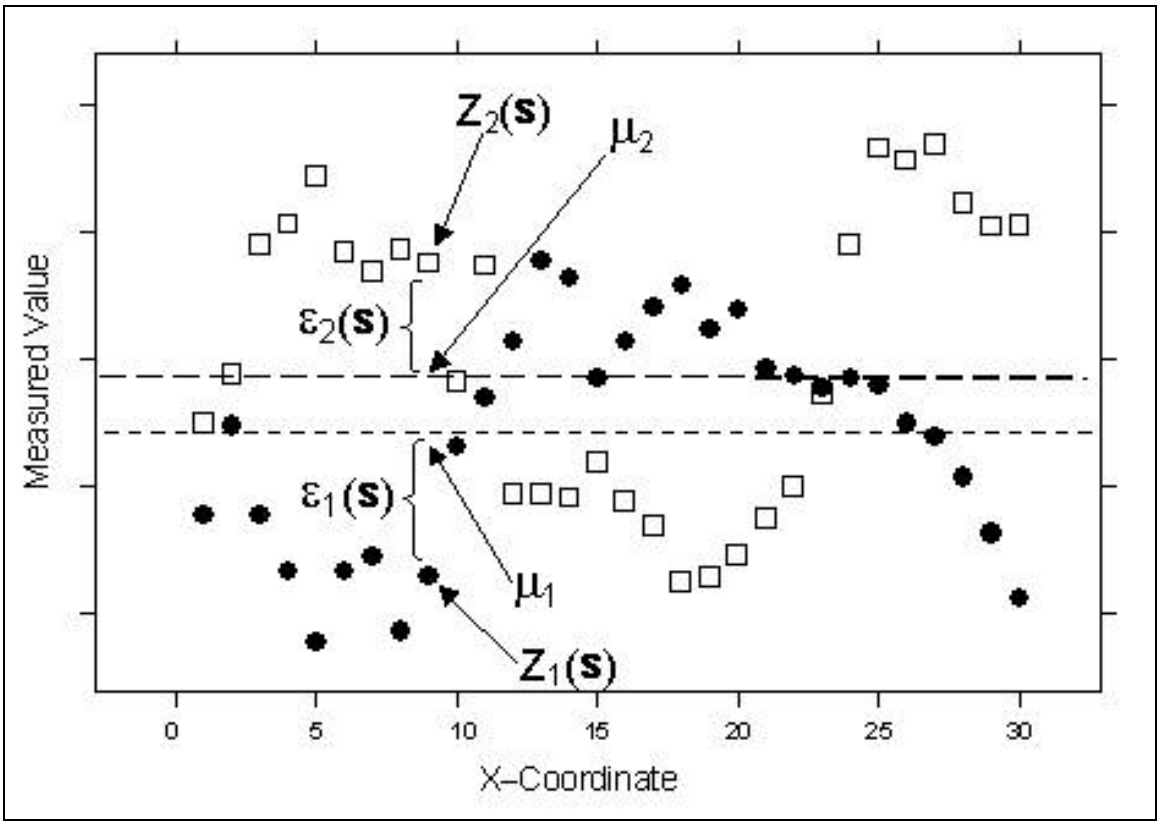

Figure 10. Similar to ordinary kriging, ordinary cokriging uses a second dataset with positive correlation to the original dataset to achieve greater accuracy (ESRI, 2006).

3.0 Application 1: Shear-Wave Velocity Database

Geophysical data were collected at 519 sites by researchers at the University of Kentucky, including Harris (1992), Al-Yazdi (1994), Higgins (1997), Street (1997), Street et al. (1997), Wood (2000), Lin (2003), Wang et al. (2004), and Street et al. (2005). Seismic-refraction surveys were conducted for the collection of SH-wave velocity data for all studies from which data were included in this database. This was typically accomplished using a seismograph with internal hard drive for signal data storage, connected to two inline spreads of horizontally polarized 4.5- or 30-Hz geophones. Spacing of geophones typically ranged from 2 to 10 m. The geophones detected seismic shear waves generated by an energy source, such as a section (approximately 12 kg) of steel H-pile beam struck horizontally by an approximately 4.5-kg sledgehammer. For maximum energy transmission, the H-pile beam was oriented perpendicular to the spread of geophones and was coupled with the ground surface by placing the edge against an asphalt surface or a prepared slit in the soil. SH-waves were used because the velocities at which they travel are characteristic of the soil medium, whereas P-waves travel

at velocities characteristic of water when generated in water-saturated sediments (Higgins, 1997).

To achieve the best possible signal-to-noise ratio, several strikes by the energy source at one location were stacked upon each other. This method allowed random noise generated by successive hammer blows to be cancelled out by destructive interference while coherent noise was constructively interfered to produce a more robust signal (Rutledge, 2004). In some instances, the hammer impacts were recorded for each side of the energy source and added together to enhance coherent SH-wave signals and to decimate other phases and random noise (Street et al., 1997).

The walkaway method was used, in which a 12- or 48-geophone spread remains fixed while the energy source is systematically struck and moved along a set of predetermined offsets dependent on geologic site conditions. Information gained from this method included velocities and intercepts of head-waves, identification of reflection events and interval velocities, and calculation of thicknesses of soil horizons and depths to bedrock (Street et al., 1997).

3.1 The Dataset and Database Development

The dataset includes seismic velocities, latitude/longitude coordinates, the depth to bedrock at each site, thicknesses of overlying soil layers, weighted-average shear-wave velocity of the upper 30 meters (V_{30}) of soil/bedrock, calculated according to the 1997 NEHRP provisions (BSSC, 1997), site name, site classification, average sediment and bedrock velocities, elevation, soil type, collection date, and topographic map name (Figure 11). The V_{30} values were manually calculated and added to the dataset in which they were not originally included. Dynamic site periods (DSP) were also included in some of the original studies and calculated for studies in which they were not originally included. Appendix A contains complete tables of all data currently stored in the database.

The current form of the database represents a template in which additional data can be included. New fields can be created and filled, and appropriate relationships established between data fields. The geodatabase (GDB) was created in ArcCatalog from Microsoft Excel files that were imported into the GDB using ArcCatalog's tools. Each table derived from the Excel files was converted to a feature class and stored in a feature dataset to ensure a common spatial reference. The feature classes were organized according to the researcher and geographic

location of the sites from which the data were collected. Figure 12 shows the process by which a geodatabase is created in ArcCatalog.

Different types of databases can be created in ArcGIS including *enterprise* (or *multiuser*) *geodatabases* and *personal geodatabases*. Enterprise geodatabases are typically used for handling large amounts of data (databases over 2 GB) in projects requiring multiple users for editing. ArcSDE is required for managing the database, and multiple storage models can be used, including IBM DB2, IBM Informix, Microsoft SQL Server, Oracle, and Oracle with Spatial or Locator. Versioning is supported in the enterprise geodatabase environment, allowing multiple users to edit the database simultaneously. Conflict resolution rules prevent separate users from editing the same feature at the same time in a contradictory manner. The personal geodatabase model is used for handling databases 2 GB or smaller, and is edited by a single user. The Microsoft Jet Engine (Access) is used for database management, and versioning is not supported. The smaller size of the dataset and the intended uses of the database make the personal geodatabase model ideally suited for this project. As the size of the database increases and new types of data are added, such as image files, conversion to the enterprise model may be necessary.

The data that were originally located in various journals, theses, and other hard-copy publications were initially digitized as Excel files and later imported into the GDB. ArcInfo is based on Microsoft Access, however, which can be used to create tables and databases directly. Empty feature classes and feature datasets can be created and placed in a geodatabase using ArcCatalog, and data can be subsequently entered. The choice of method for database creation is subjective, and the most efficient method depends highly on the pre-existing format of the data.

Metadata is defined as "data about data," and is used to describe the data being stored in the GDB. The purpose of metadata is to provide an efficient way for users to locate desired data and determine the source, usefulness, and quality of the data. Descriptions of data provenance, quality, and purpose were included in the GDB, and standard formats available from ESRI, found in ArcCatalog, provided the template.

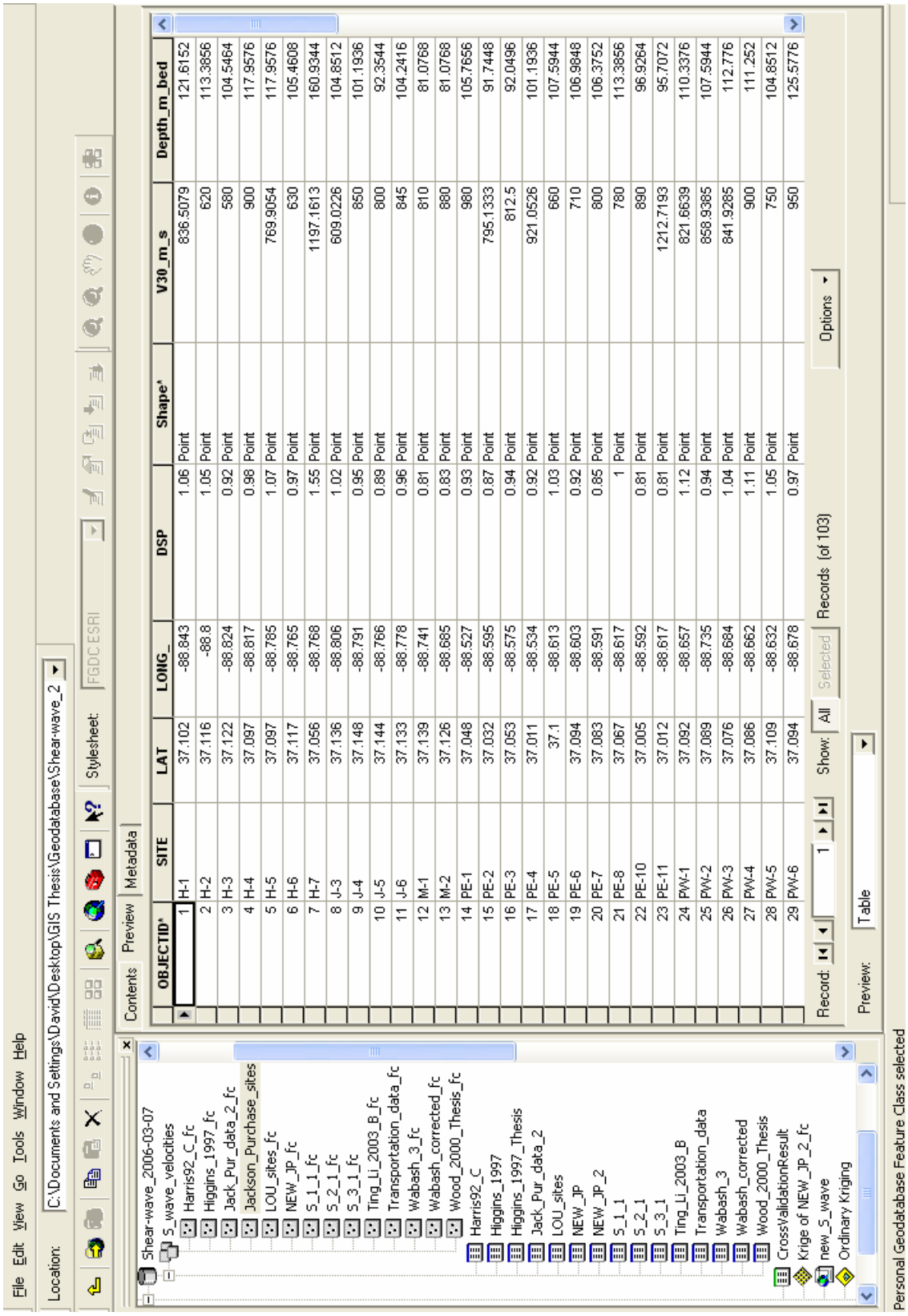

Figure 11. The Jackson Purchase sites feature class table in ArcCatalog. See Appendix A for data tables for all sources included in the database.

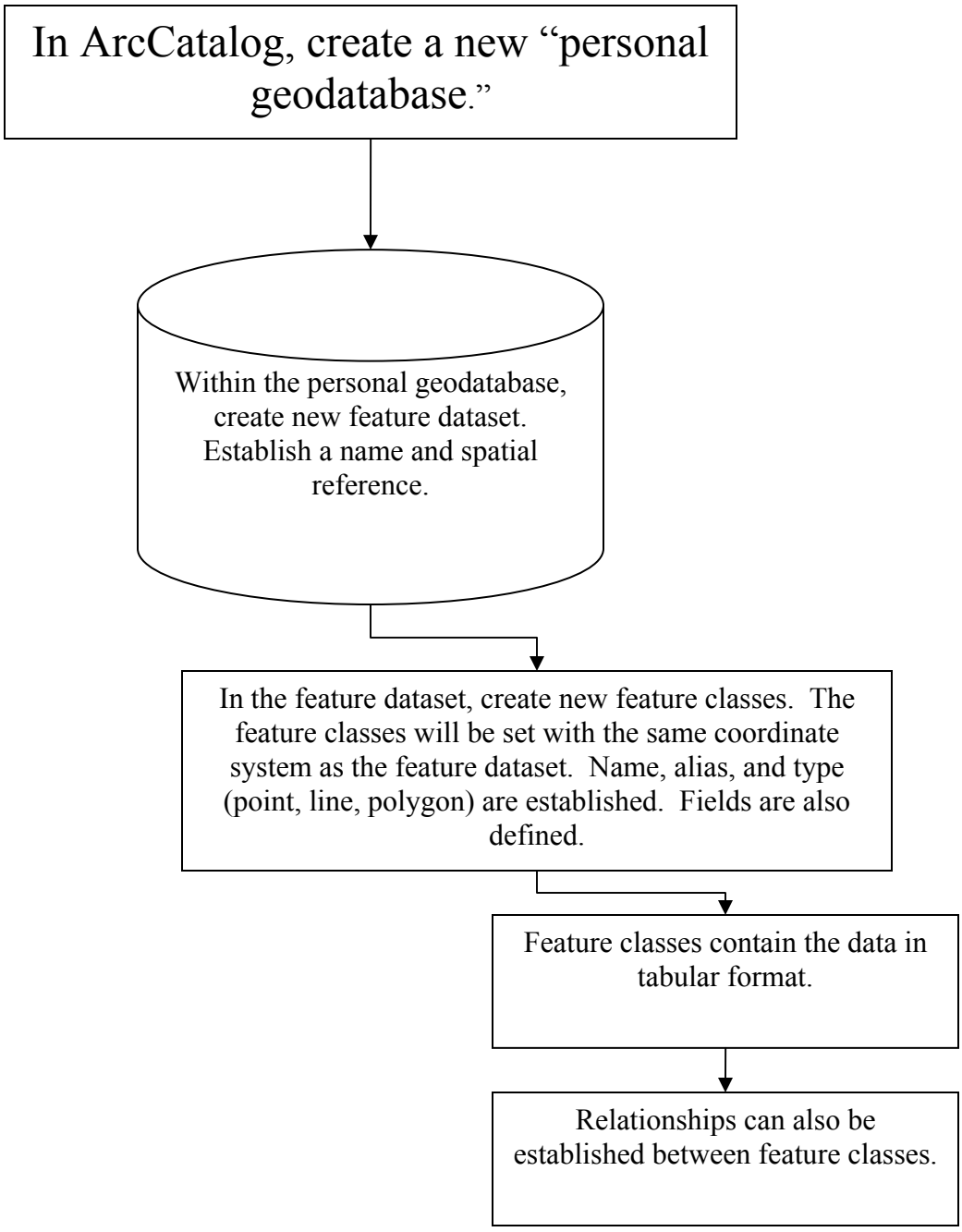

Figure 12. A personal geodatabase is created in ArcCatalog by using menu options. Feature datasets, feature classes, tables, and relationship classes can all be established within the geodatabase.

4.0 Application 2: Derivative Maps of the Jackson Purchase Region

4.0.1 Study Area: Geologic Setting of the Jackson Purchase

Seismic velocity models have been collected at sites throughout the central United States. Using some of the ArcGIS tools available for analyzing data stored in the geodatabase, the Jackson Purchase area of western Kentucky was selected to provide a regional overview of seismic hazard characteristics. The methods used are applicable to other areas in which similar data have been collected. The Jackson Purchase extends east–west from Kentucky Lake to the Ohio River, and north–south from the Ohio River to the Tennessee border. The city of Paducah is the most populous city in the area (population approximately 30,000) and is located adjacent to the Ohio River along the northern boundary of the Jackson Purchase.

Notably, the Jackson Purchase Region represents the northeasternmost part of the Mississippi Embayment. The Mississippi Embayment is a south-plunging syncline whose axis is roughly parallel to the course of the Mississippi River, filled with sediments ranging in age from Jurassic to Quaternary. These sediments overlie Ordovician and Mississippian bedrock (Davis, 1987). In the Jackson Purchase, Cretaceous to Quaternary sediments overlie the Paleozoic bedrock. The generalized stratigraphy of the Jackson Purchase area is shown in Table 2, and the post-Paleozoic sediment formations are described, from oldest to youngest, in Olive (1972):

Tuscaloosa Formation: The Tuscaloosa Formation rests unconformably on the Paleozoic bedrock surface and consists of chert gravel sediments and interspersed lenses of chert and silt. This formation was largely derived from rocks of Devonian and Mississippian age.

McNairy and Clayton Formations: Rest unconformably on the Tuscaloosa Formation and the Paleozoic bedrock. They are composed primarily of sand and sandy clay. Coal beds are present in some areas near the top of the formation.

Porters Creek Clay: Rests conformably on the McNairy and Clayton Formations in most places. The Porters Creek Clay is derived largely from weathered volcanic rocks deposited in nearshore or deltaic environments.

Wilcox Formation: Rests unconformably on the Porters Creek Clay and is composed predominantly of interbedded and interlensing sand, clay, and silt.

Claiborne Formation: Rests unconformably on the Wilcox Formation and Porters Creek Clay and is composed of quartz sand with lenses of silt and clay deposits.

Jackson Formation: Lies unconformably on the Claiborne Formation and is composed of silt and clay with quartz sand lenses.

Continental Deposits: Predominantly composed of chert and quartz gravel.

Loess: Consists of silt mixed with minor amounts of fine sand.

Alluvium and lacustrine deposits: Consist of silt, sand, and gravel and are rarely calcareous.

Other structures located in proximity to the study area include the Reelfoot Rift, a seismically active structure that extends from southwest to northeast and into the Jackson Purchase, and the Rough Creek Graben, a seismically inactive structure that extends east–west through most of western Kentucky. The structural and seismological relationship between the Reelfoot Rift and Rough Creek Graben is not well defined (Wheeler, 1997).

The New Madrid Seismic Zone, which extends from northeastern Arkansas into southeastern Missouri and the Jackson Purchase Region of western Kentucky, is situated within the boundaries of the Reelfoot Rift. Reactivation of the zones of weakness in the vicinity of the rift complex as a result of the regional stress field is thought to be the cause of seismicity in the area (Harris, 1992). Several large earthquakes ranging in magnitude from $m_{b,Lg}$ 7.0 to $m_{b,Lg}$ 7.3 occurred between December 1811 and February 1812 (Nuttli, 1973; Street, 1982). The New Madrid Seismic Zone is the most seismically active intracontinental area in the United States and represents the greatest earthquake threat east of the Rocky Mountains (Nuttli, 1973; Street, 1982; Johnston and Nava, 1985).

Research efforts in the Jackson Purchase Region and surrounding areas have attempted to delineate fault structures to establish controls on the timing of deformation and therefore to better determine locations and rates of seismicity, and to define the geophysical characteristics of the soil/sediment overburden for determining regional seismic hazards. The proximity to New Madrid seismicity, the presence of thick sediment deposits, and the location within the boundaries of the Mississippi Embayment (basin effects) make the Jackson Purchase ideal for emphasizing the objectives of this project.

Several maps were created using the shear-wave velocity database and the Geostatistical Analyst extension in ArcMap. Geostatistical methods were used to examine the data for trends and outliers with histograms, trend analysis diagrams, Voronoi maps, QQ plots, and semivariogram/covariance and crosscovariance clouds. The distribution of data values was examined and maps were generated for the purpose of interpolating characteristics between sites of physical measurements. Diagnostics were performed to determine the accuracy of each method. A summary of each method follows.

The techniques used for identifying trends and data outliers, and for producing derivative maps, depend on the assumption of stationarity in the data. In other words, the samples were collected from a spatially fixed and continuous field and are an incomplete representation of the entire surface. The purpose of this study is to predict with accuracy the magnitude of a particular attribute at all points within the study area.

System	Series	Group and Formation	Thickness
Quaternary	Holocene and Pleistocene	Alluvium and lacustrine deposits	0 – 56 m
	Pleistocene	Loess	0 – 24 m
Tertiary and Quaternary	Pliocene and Pleistocene	Continental deposits	0 – 30 m
Tertiary	Eocene	Jackson Fm.	~122 m
		Claiborne Fm.	~152 m
		Wilcox Fm.	0 – 107 m
	Paleocene	Porters Creek Clay	20 – 70 m
Cretaceous and Tertiary	Upper Cretaceous and Paleocene	McNairy and Clayton Fms.	38 – 83 m
Cretaceous	Upper Cretaceous	Tuscaloosa Fm.	0 – 50 m
Paleozoic Bedrock			

Table 2. Generalized stratigraphy in the Jackson Purchase Region (modified from Olive, 1972).

4.1 Exploratory Spatial Data Analysis (ESDA)

Prior to the application of spatial interpolation methods, exploratory spatial data analysis (ESDA) techniques were applied to better understand the distribution of values contained in the dataset. The tools used for ESDA included viewing histograms, Voronoi maps, normal and general QQ plots, trend analysis, semivariogram/covariance clouds, and crosscovariance clouds. Sample interpolations were performed on the V_{30} and DSP attributes using both stochastic and deterministic methods. Using the ESDA tools, outliers were identified, trends in the data were determined, and the distribution of the data was examined. Knowledge gained from the suite of ESDA tools was used to select interpolation parameters more accurately and consequently produce more accurate prediction and standard error maps. Figure 13 shows the distribution of sample sites across the study area.

4.1.1 ESDA Applied to the Mean Dynamic Site Period (DSP) Attribute

Histogram

To show the frequency distribution of the mean dynamic site period, the histogram tool was used (Figure 14). In this case the "Jackson Purchase sites" layer was chosen and the attribute to be studied was the mean dynamic site period (DSP). The attribute of interest was selected from the dataset, and the resulting histogram is shown in Figure 15. In this diagram, two bars representing DSP values appear to be outliers. Examination of the summary statistics also reveals that the data are not normally distributed. Data distributed normally would be indicated by a skewness value close to 0 and a kurtosis value close to 3. Although normal distribution is not required to perform kriging for prediction maps, normal distribution is necessary for producing quantile and probability maps using ordinary, simple, and universal kriging, according to ArcGIS Desktop Help. Therefore, a log transformation is necessary to normalize the distribution for producing such maps (Figure 16). The resulting histogram shows a skewness value of 0.27127, much closer to 0, and a kurtosis value of 3.4623, closer to the desired value of 3. With the data now normally distributed, there are no obvious outliers in the data. It is evident that the application of a log transformation is needed before performing a kriging interpolation method for quantile and probability maps when using ordinary, simple, and universal kriging. For prediction kriging interpolations, the transformation is not necessary, however.

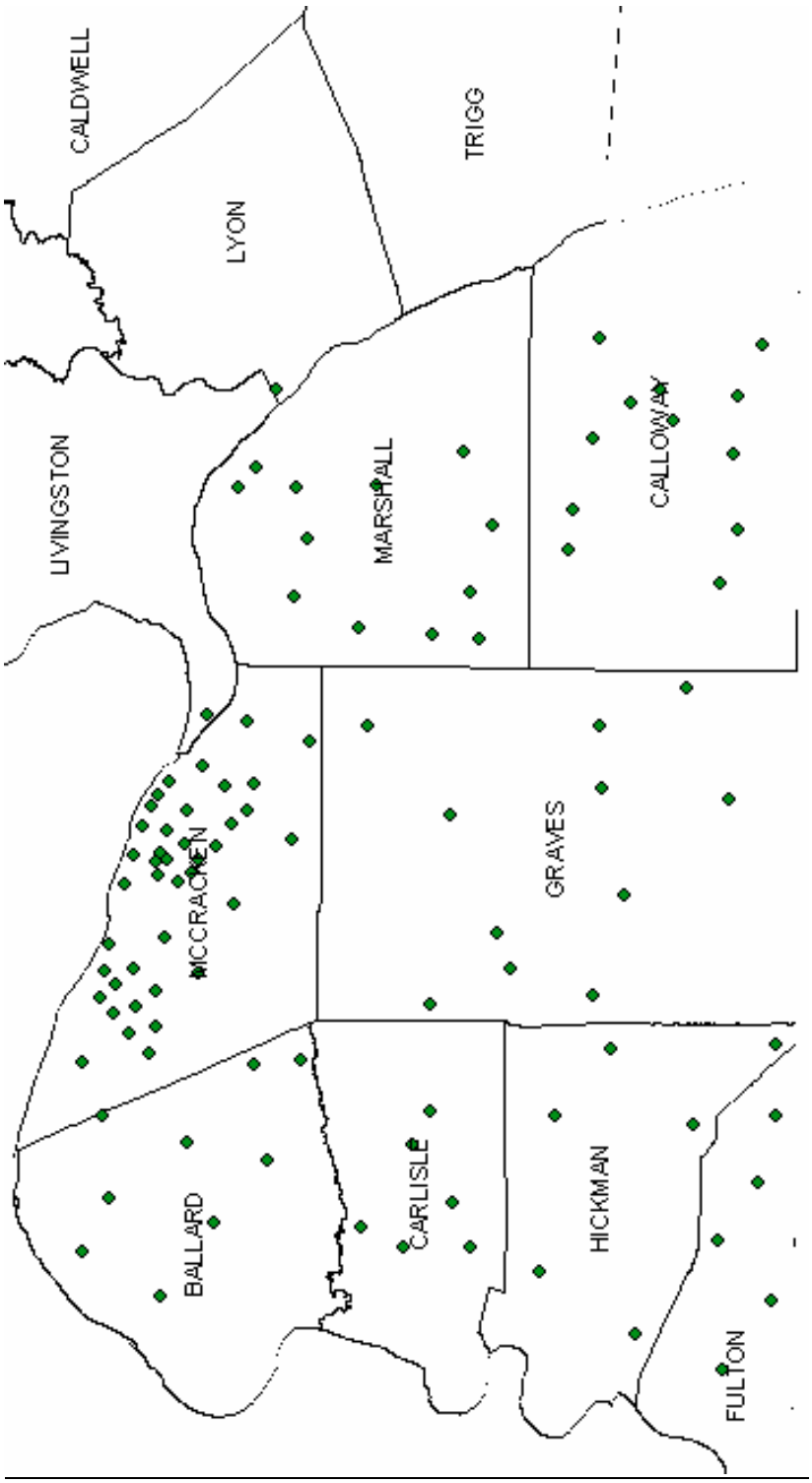

Figure 13. Distribution of the sample locations in the Jackson Purchase area that were used for the interpolations.

Normal Quantile-Quantile (QQ) Plot

The normal QQ plot is constructed by plotting the quantile values for the dataset versus the quantile values for a standard normal distribution (ESRI, 2006). The normal QQ plot without the log transformation is shown in Figure 17. The plot deviates from the straight line, indicating non-normal distribution. When the log transformation is applied, the resulting plot is closer to a straight line but still shows considerable deviation, particularly between standard normal values of 1.05 to 2.6 (Figure 18). A perfect straight line would indicate perfect normal distribution. Thus, the QQ plot confirms the benefit of applying a log transformation to the DSP data to obtain normal distribution.

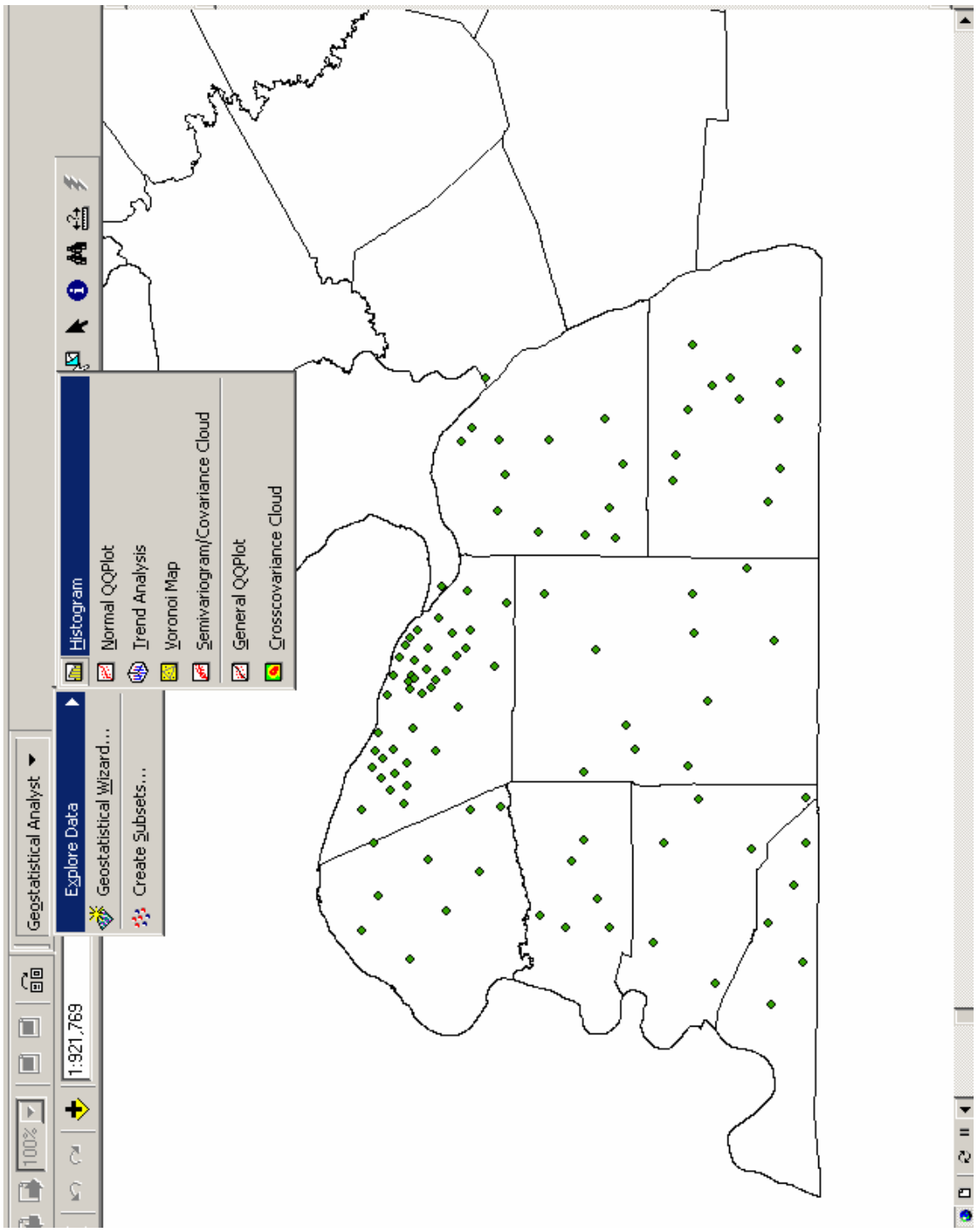

Figure 14. The ESDA options are accessible in Geostatistical Analyst**.**

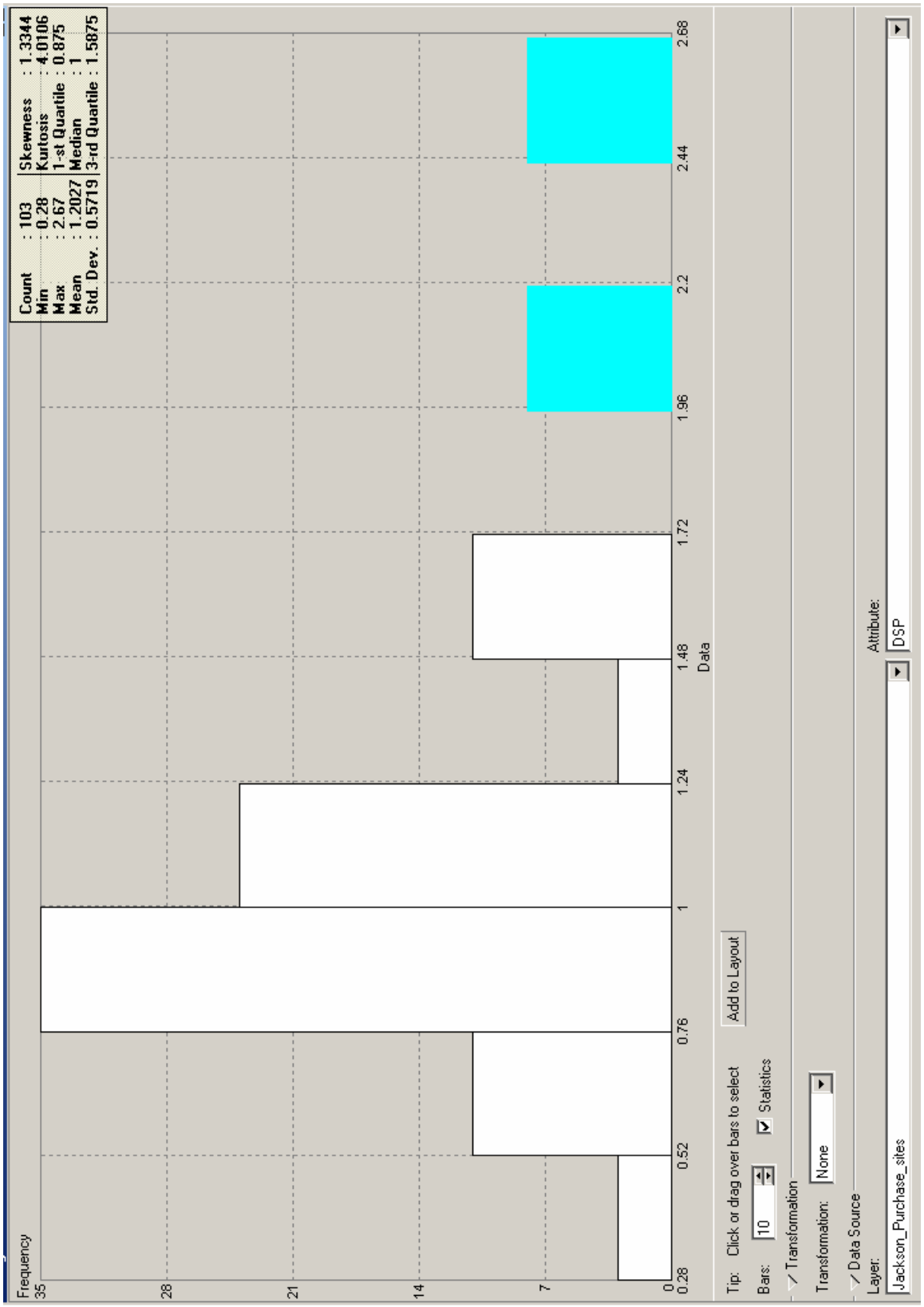

Figure 15. The histogram of Jackson_Purchase_sites DSP data. No transformation has been applied, and summary statistics are found in the upper right of the window.

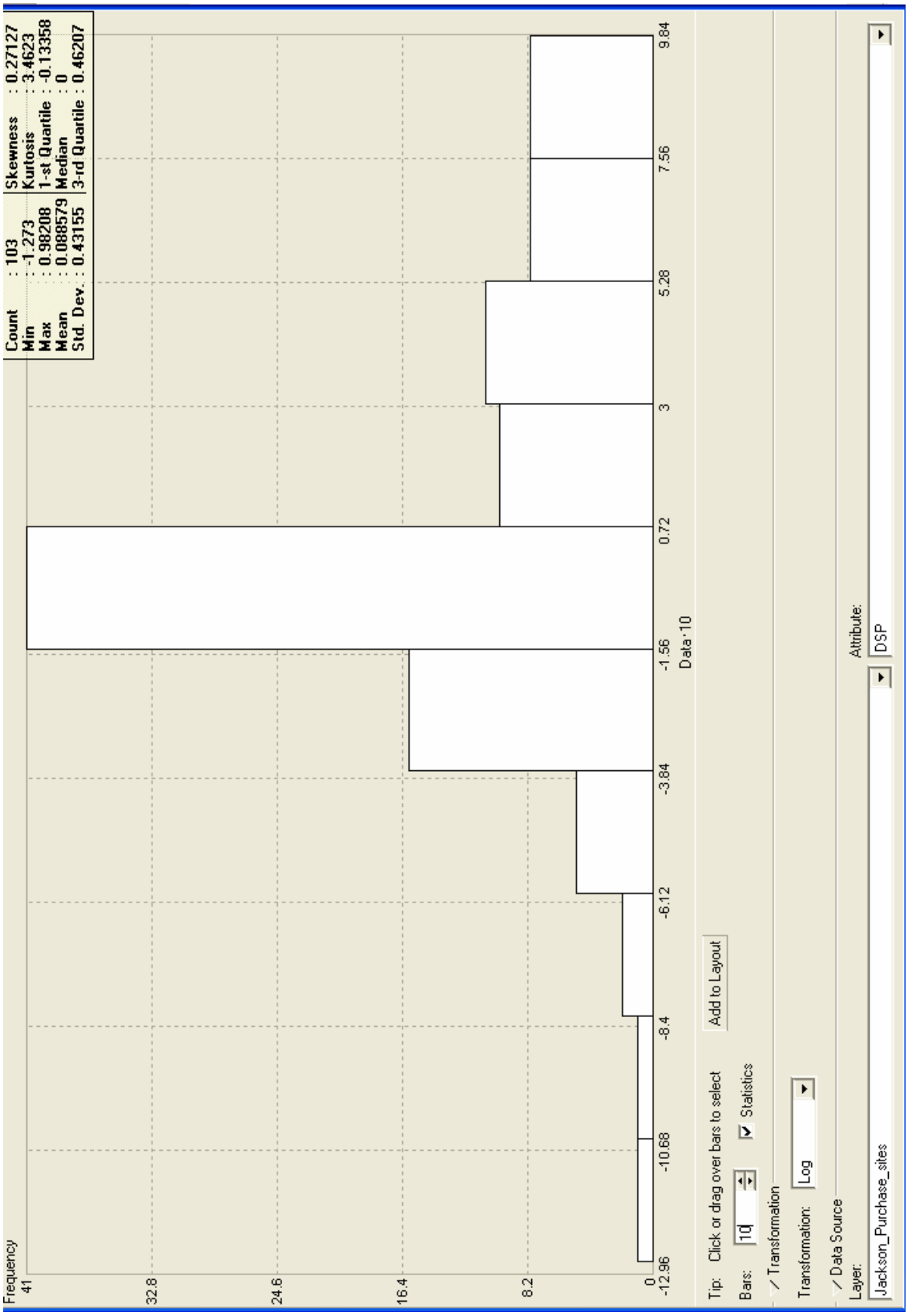

Figure 16. The histogram after the log transformation has been applied. The summary statistics reflect the change.

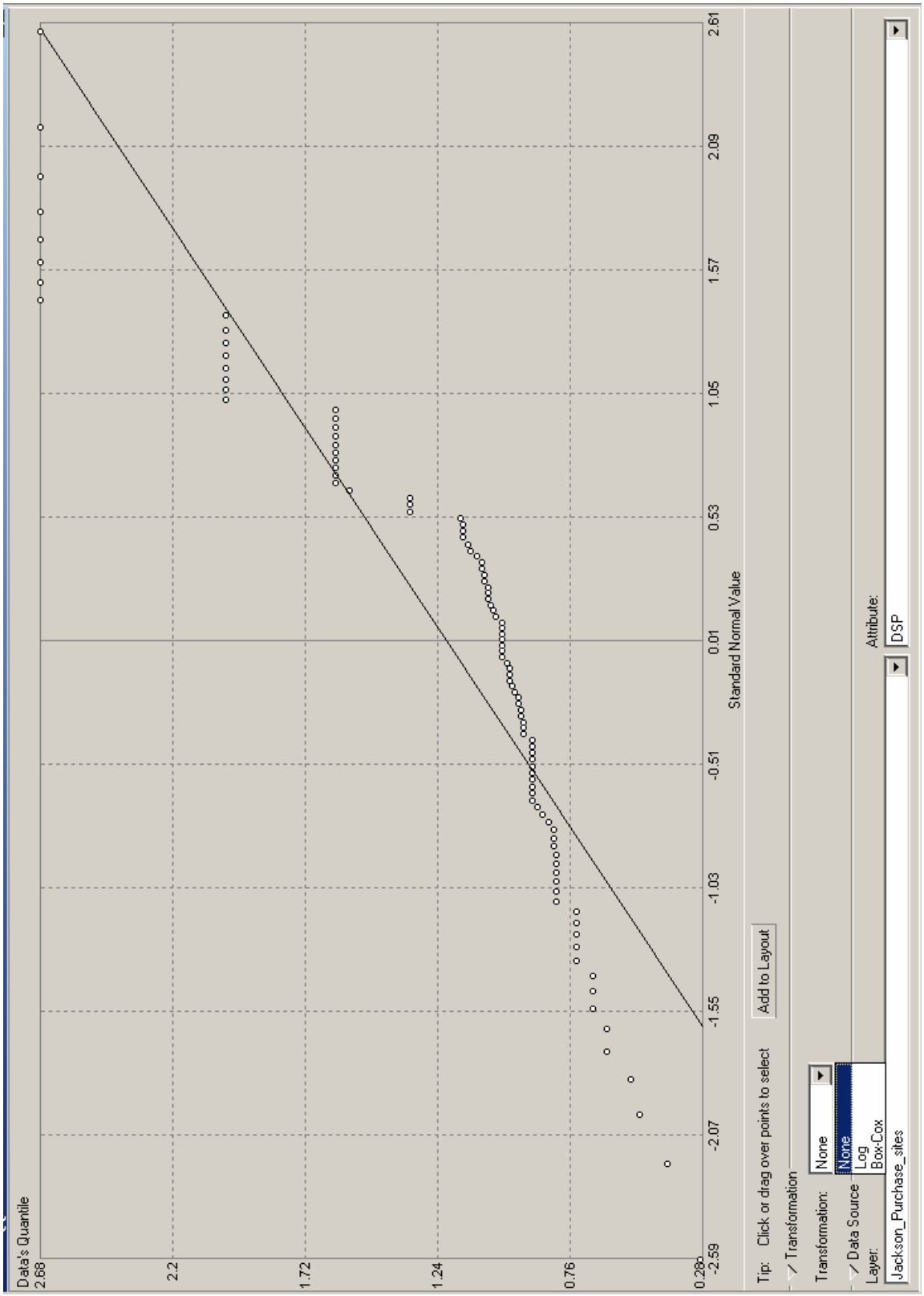

Figure 17. The normal QQ plot with no data transformation.

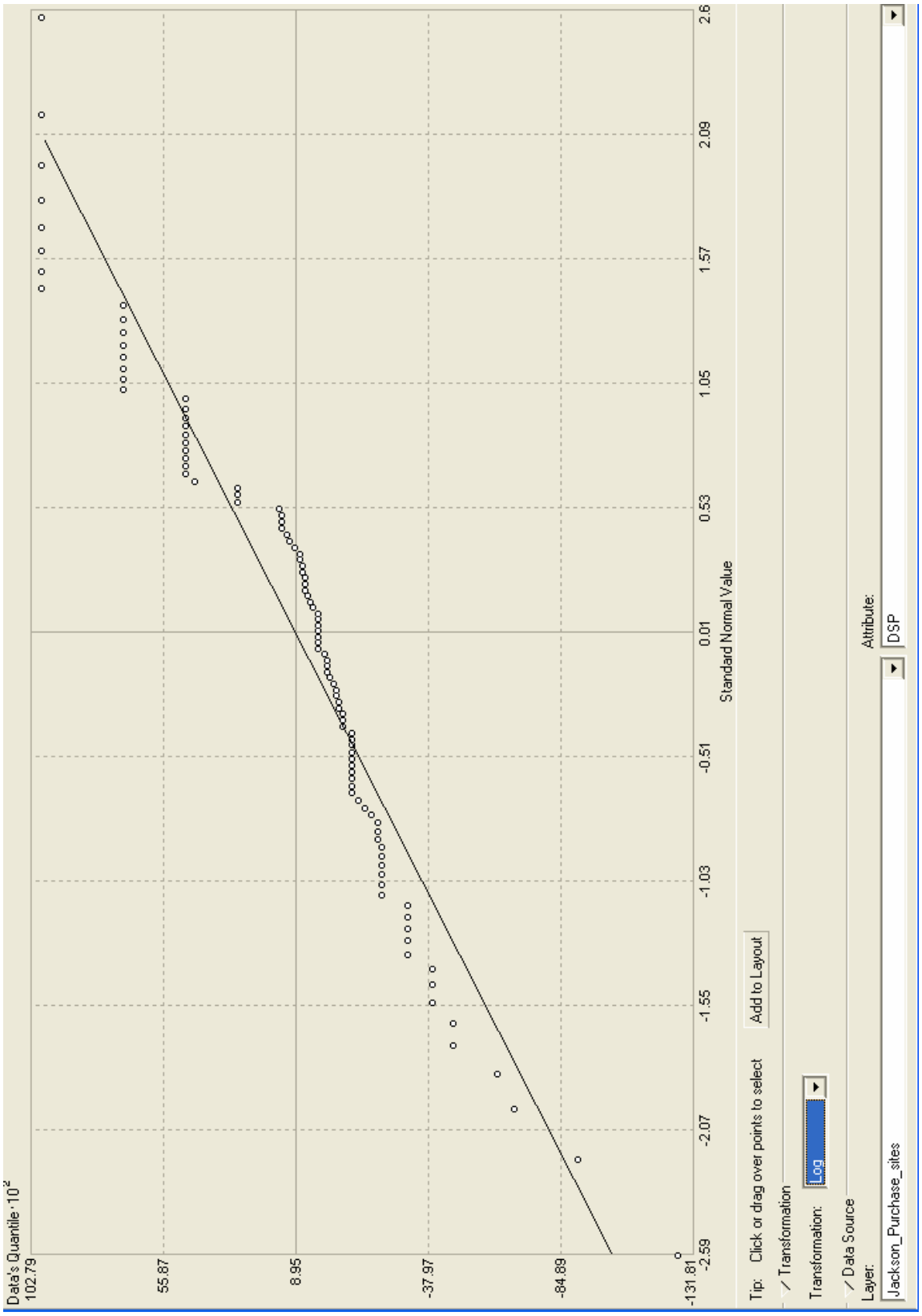

Figure 18. Normal QQ plot with a log transformation applied to the data.

Voronoi Map

The Voronoi map offers multiple insights into the data. Four of the eight different types of map that may be drawn, including simple, mean, cluster, and standard deviation (StDev), were examined.

The first Voronoi map examined was the *simple* map (Figure 19). The simple Voronoi map shows the extent of each sample point's local influence. Each polygon reflects the value of the sample point contained within that polygon, and it is possible to see the distribution of values and the areal extent to which the sample points influence the immediate vicinity during interpolation. For example, a concentration of sample points with values between 0.95507 and 1.3487 is found in the vicinity of Paducah (top center of Figure 19). Sparse sample points are found in the upper right corner of the figure (east of Paducah); dominant values are between 1.8995 and 2.67.

In the mean Voronoi map, the value assigned to a polygon is determined by averaging the value of that polygon and its neighbors (Figure 20). The local smoothing effect of this method emphasizes local trends in the dataset.

The cluster Voronoi map is used to identify local outliers (Figure 21). Each of the polygons is placed into five class intervals. If the class interval of a particular cell is different from each of its neighbors, it is colored gray to distinguish it from its neighbors. Figure 16 shows ten outliers across the extent of the map. When choosing parameters for an interpolation, it may be beneficial to remove these outliers in order to prevent unrealistic influence from these anomalies.

The standard deviation map is shown in Figure 22. Values assigned to polygons are standard deviations calculated from a polygon and its neighbors. From the resulting map, it is possible to examine local variation among the data. It is clear that in areas with sparse sample points there is greater variation in the data values, indicating spatial autocorrelation in the dataset. Examination of the Voronoi maps indicates a trend in the DSP values. In general, the values are higher in the northeast and southwest, and lower in the intervening areas. This information is useful when defining a search neighborhood. Specifically, the search neighborhood was elongated northeast to southwest in order to make predictions based on real measurements that were likely to share similar values.

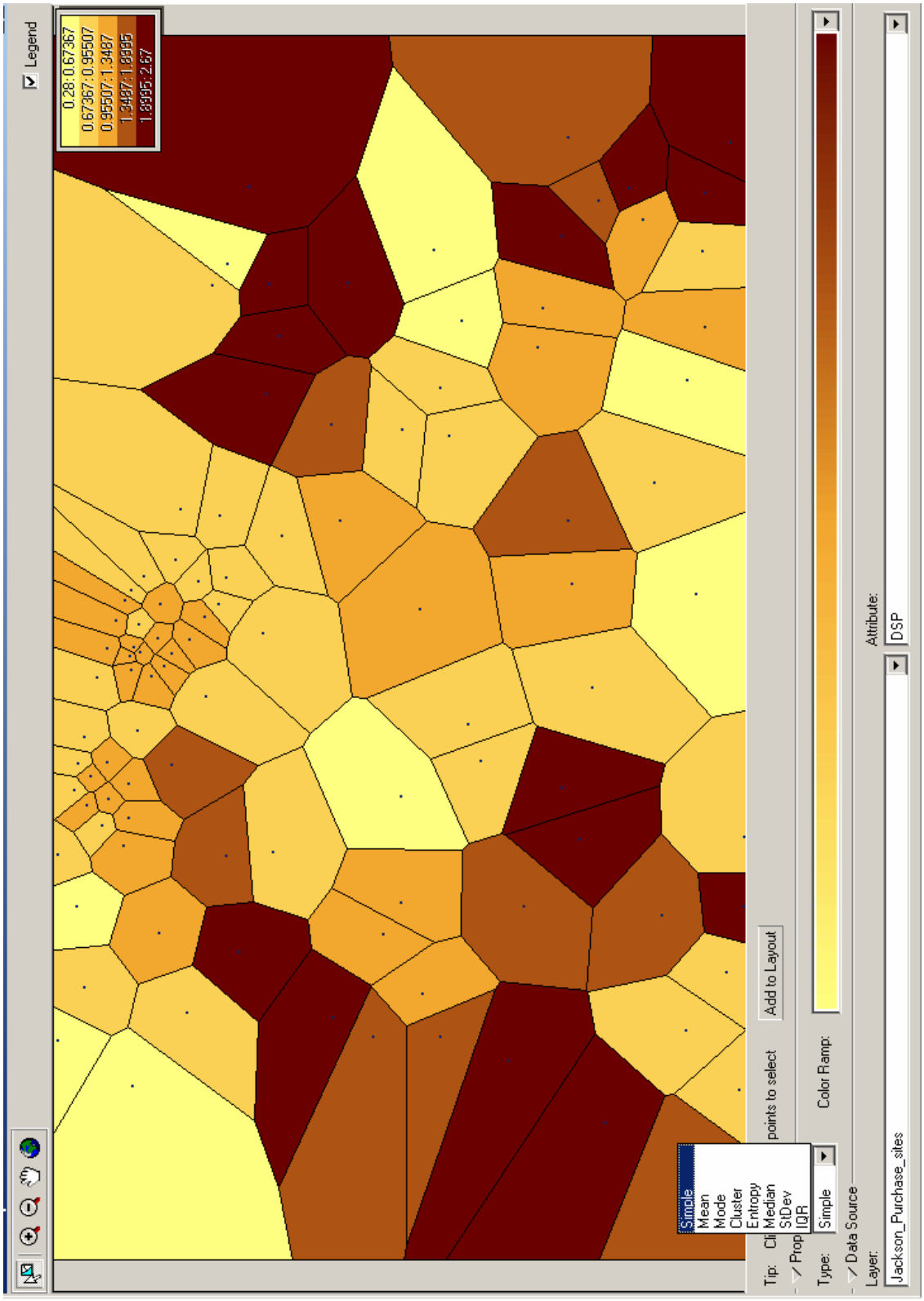

Figure 19. The simple Voronoi map shows that a single sample point has greater local influence where sample locations are sparse. Areas of high sample-point density show less local influence from a single sample point.

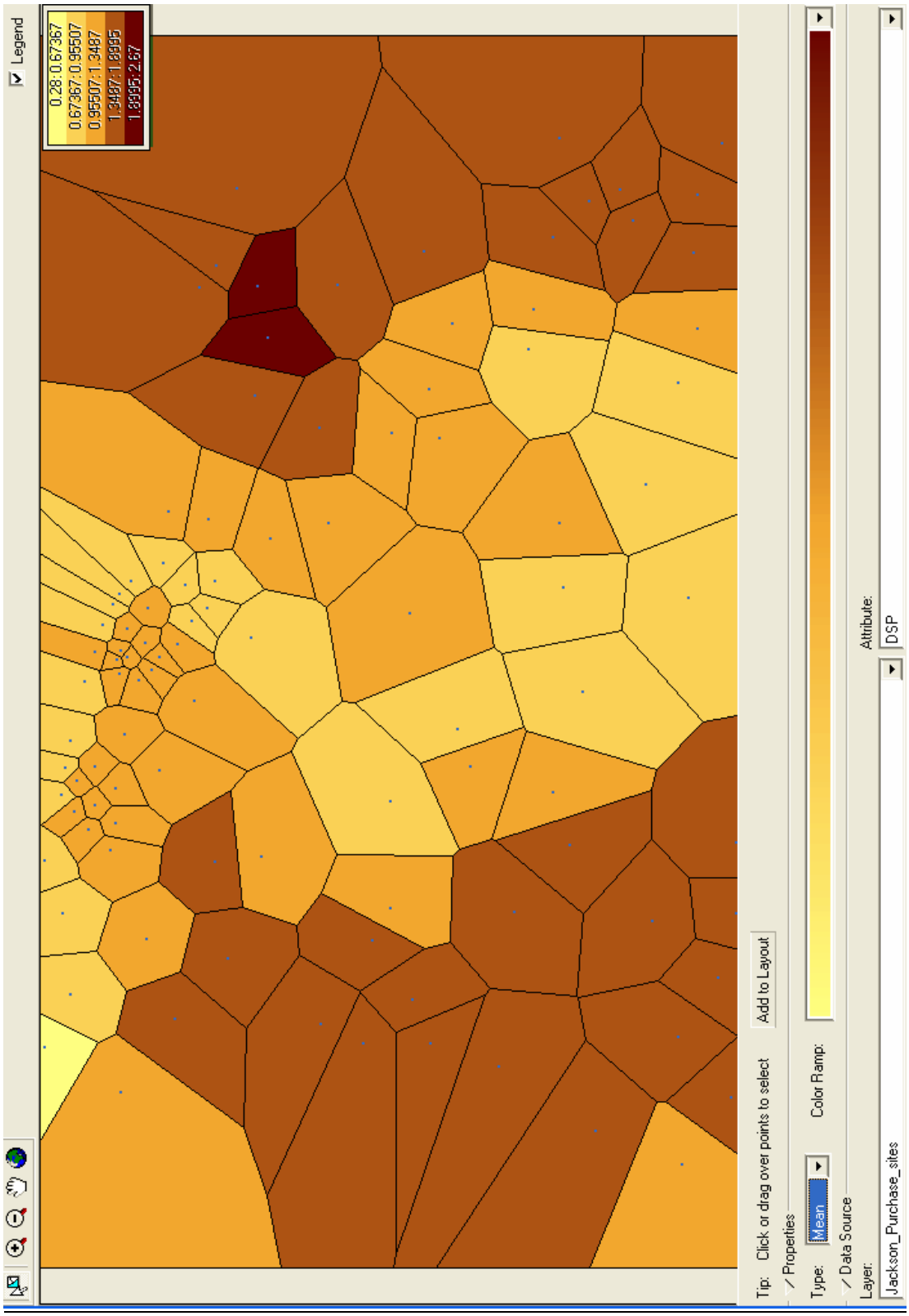

Figure 20. The mean Voronoi map. The value assigned to each polygon is calculated by averaging the sample value with those of neighboring polygons. The smoothing effect emphasizes local trends in the data.

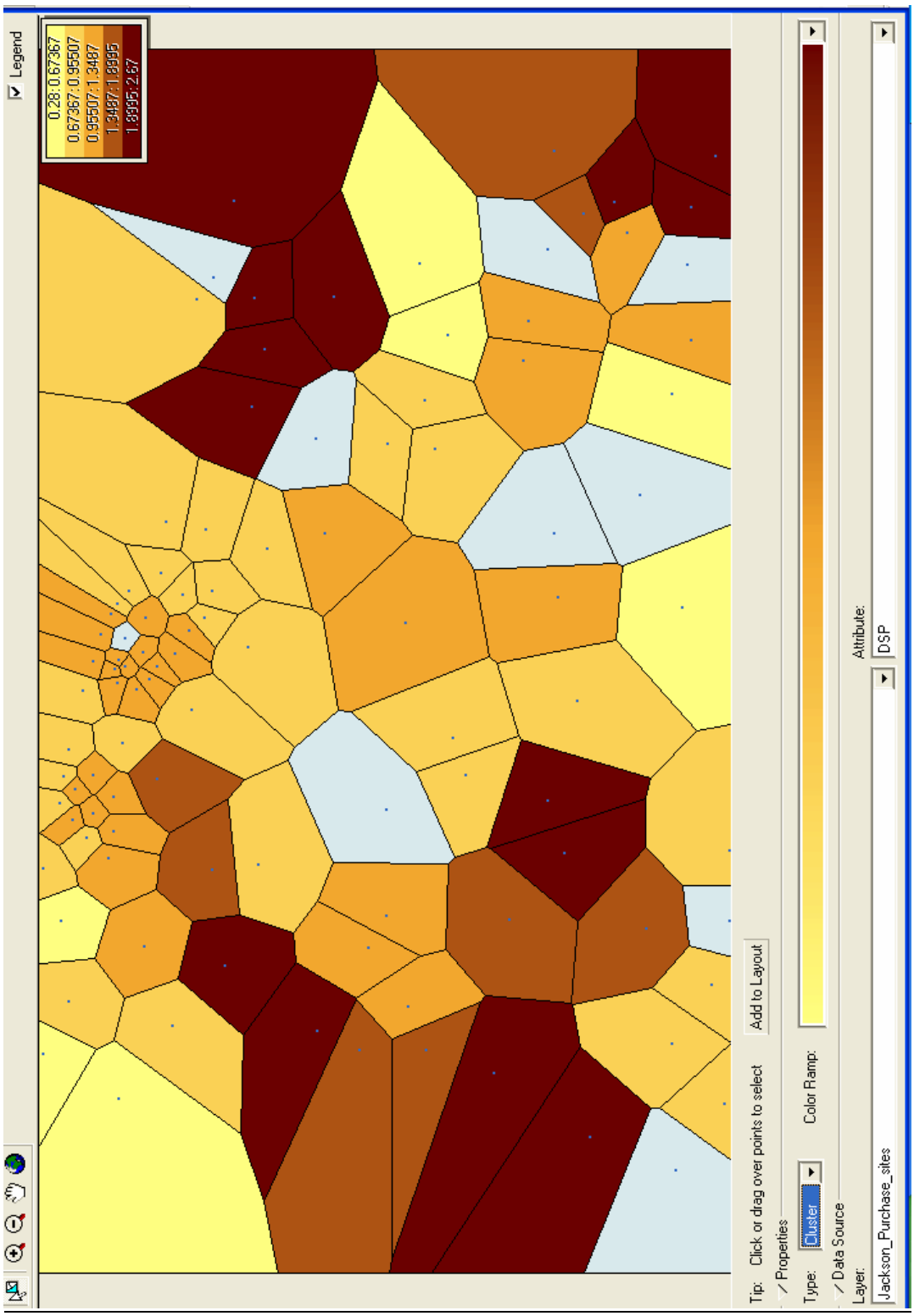

Figure 21. The cluster Voronoi map. Each of the values of the sample points is placed into one of five bins. If the value of a polygon is placed into a bin different from that of its neighbors, the polygon is shown in gray. These sample points are identified as local outliers.

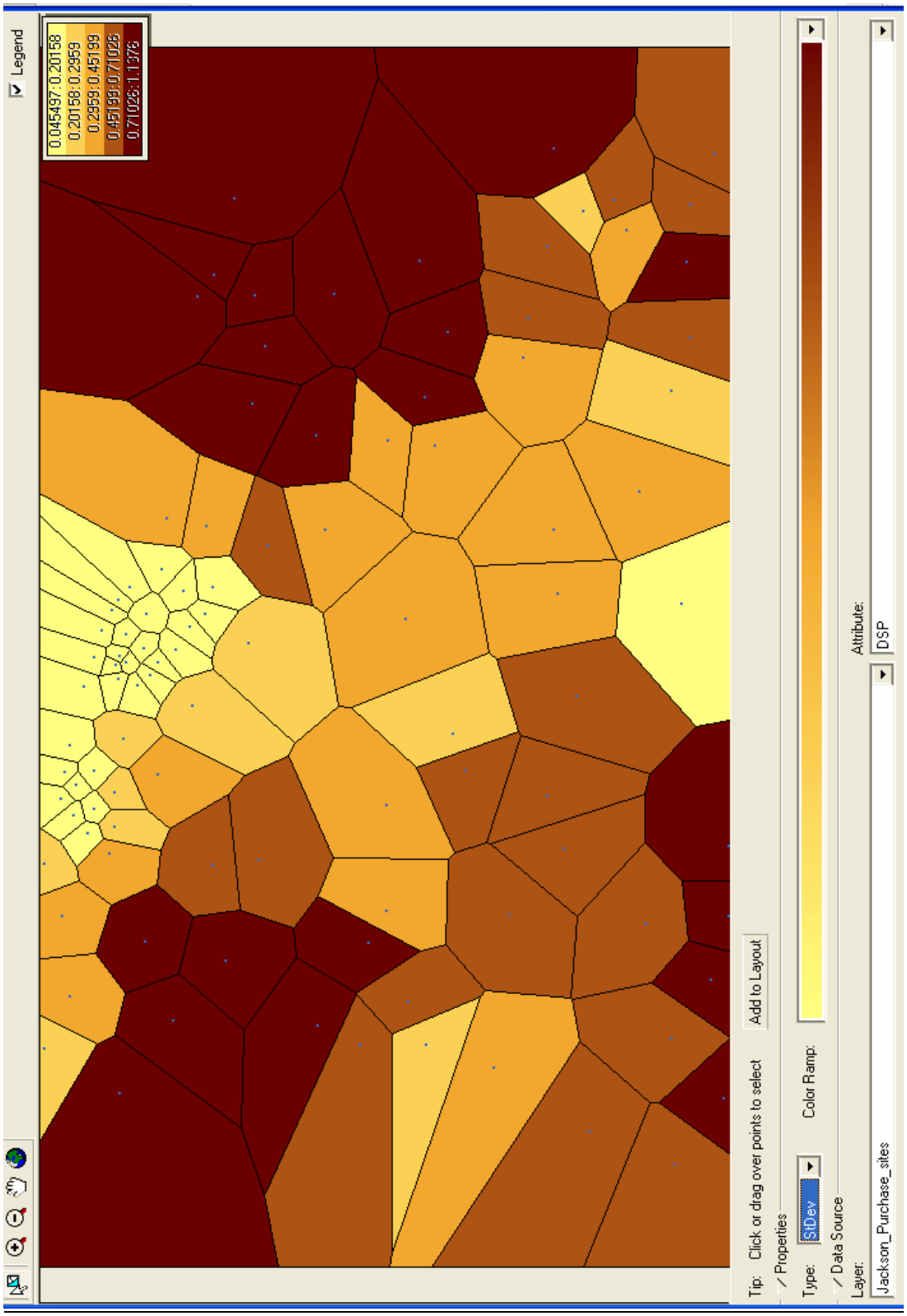

Figure 22. The standard deviation Voronoi map. Values are calculated as standard deviations between a sample location and its neighbors, allowing local variation to be identified.

Semivariogram/Covariance Cloud

The semivariogram is a plot of the difference squared, $(x_1–x_2)^2$, between two points as a function of the distance between them (ESRI, 2006). The term *autocorrelation* refers to the correlation of a variable with itself, as measured at different locations. For instance, if positive spatial autocorrelation exists for a given variable, then the magnitude will be more similar at locations closer together than locations measured farther apart (Schabenberger et al., 2005). If the data are autocorrelated, the difference squared should increase as the distance between a given pair of points increases. In choosing the lag size and number of lags, it is general practice to choose values that, when multiplied together, equal about half the greatest distance between a pair of points (ESRI, 2006).

Construction of a semivariogram of the mean dynamic site periods demonstrates directional influences. In Figure 23, the strongest autocorrelation is apparent when the search direction is oriented 45º. This fact has implications regarding the selection of search direction when performing interpolations. During that process, the search neighborhood can be set to preferentially examine adjacent points in the orientation identified from examination of the semivariogram.

The covariance cloud shows the variance between a pair of data points plotted as a function of distance between the two points. Each pair is represented by one red dot on the covariance graph. Figure 24 shows that there is good covariance in the DSP data, which is necessary for accurate interpolation.

General Quantile-Quantile (QQ) Plot

The formula for calculating dynamic site period, 4H/V, indicates dependence on the depth to bedrock variable, H. For this reason, the general QQ plot is shown with the distribution of the mean dynamic site period quantiles compared to the distribution of depth-to-bedrock quantiles. The result is close to a straight line. The values exceeding approximately 1.5×10^{-2} continue the trend, though DSP data beyond this point predominantly correspond to equal bedrock depth values. The correlation between the two variables is evident from this graph (Figure 25). Correlation of two datasets as demonstrated by the general QQ plot indicates cokriging may be the best-suited interpolation technique. As discussed in later sections, this proved accurate.

Crosscovariance Cloud

When using the cokriging method, the crosscovariance cloud tool can be used to examine the local spatial correlation between two datasets (ESRI, 2006). Figure 26 shows that the crosscovariance of the DSP and bedrock depth datasets remains constant for pairs of data points at increasing distances when the search direction is oriented approximately 45º, indicating the presence of spatial correlation between the two datasets. As with kriging, cokriging assumes the data are spatially correlated. The crosscovariance cloud confirms this assumption.

Figure 23. The semivariogram cloud shows the difference squared between the values of a pair of data points as a function of the distance between them.

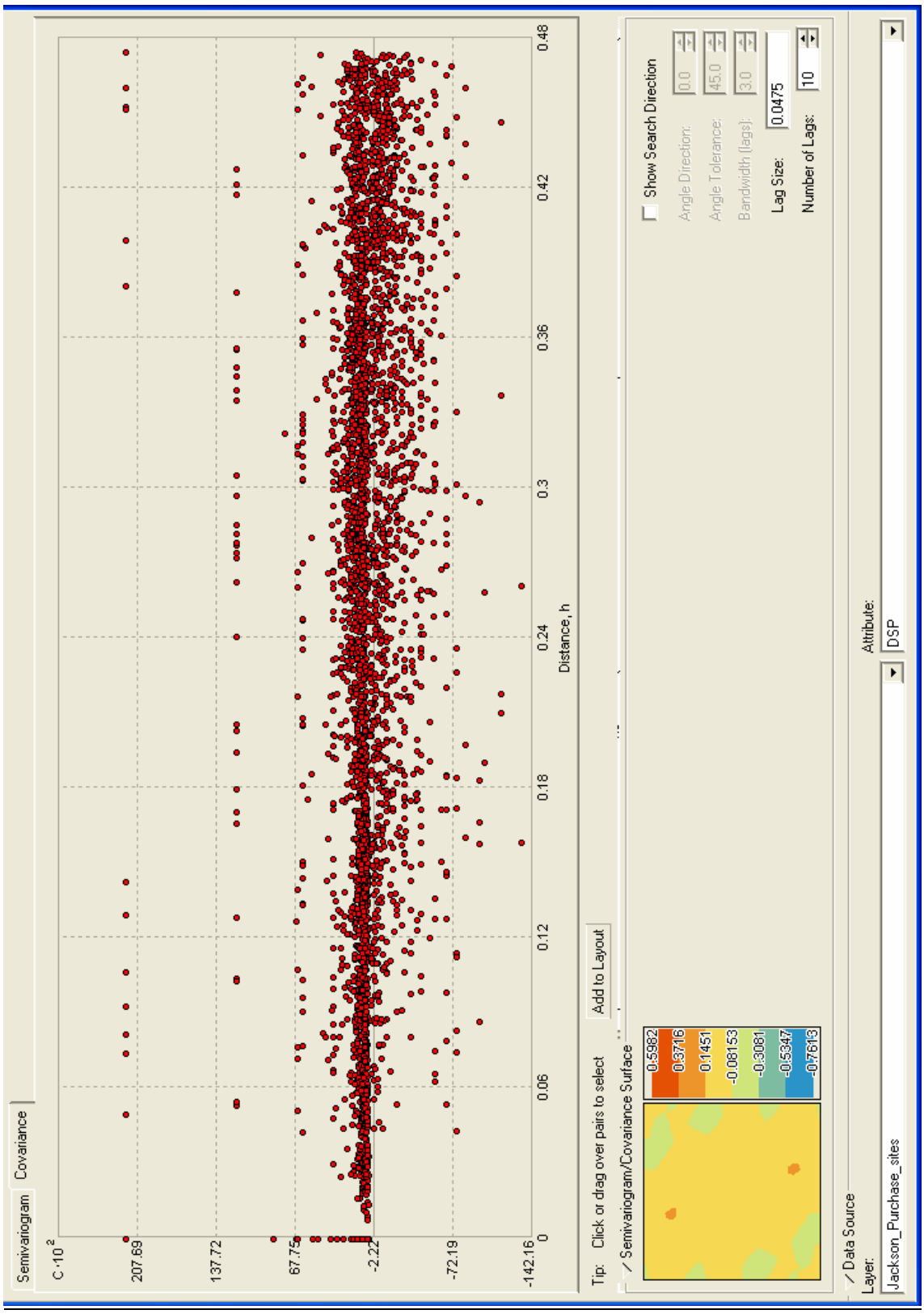

Figure 24. Covariance cloud of the DSP values showing covariance of a pair of points as a function of the distance between them.

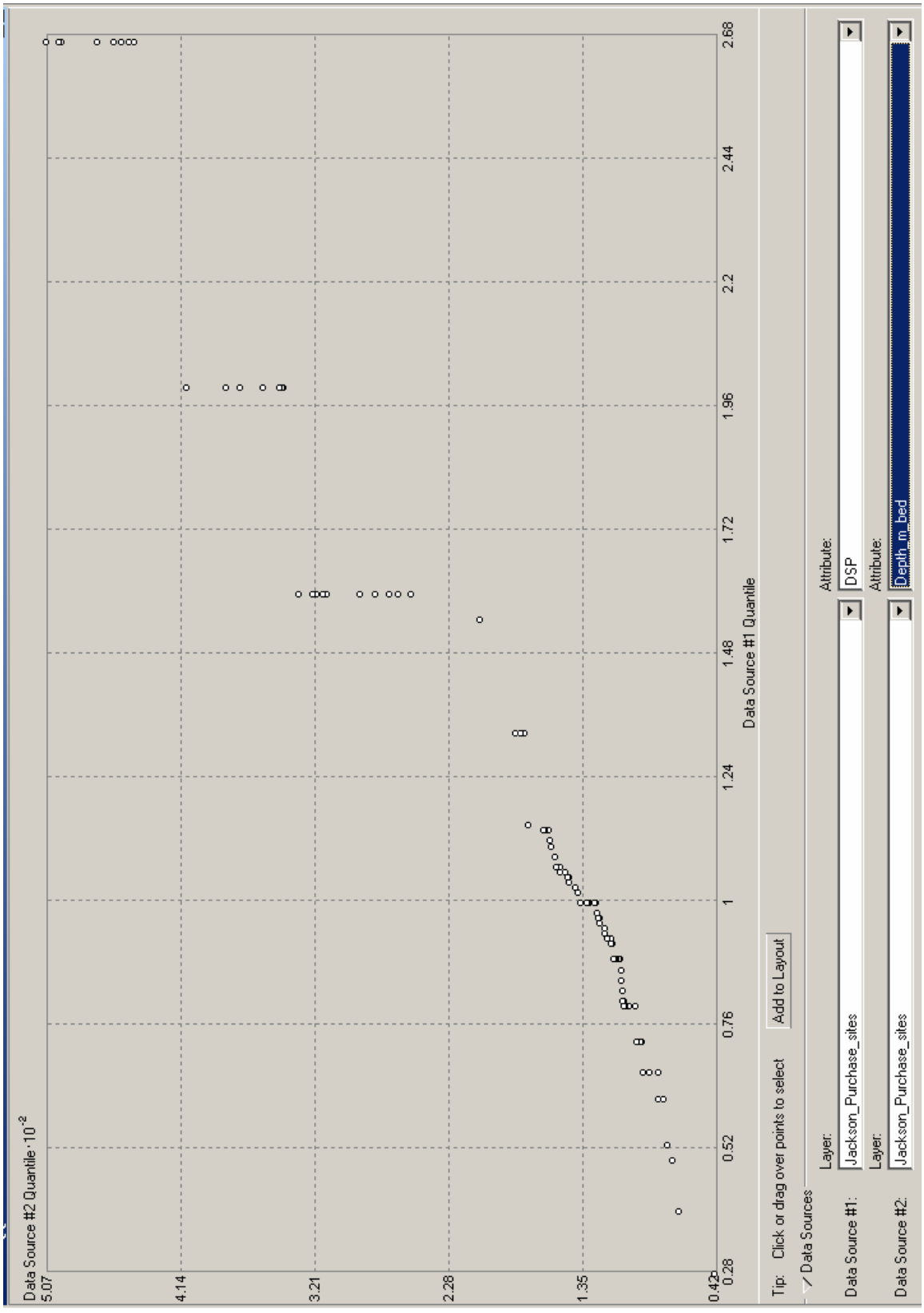

Figure 25. General QQ plot of DSP and bedrock depth data.

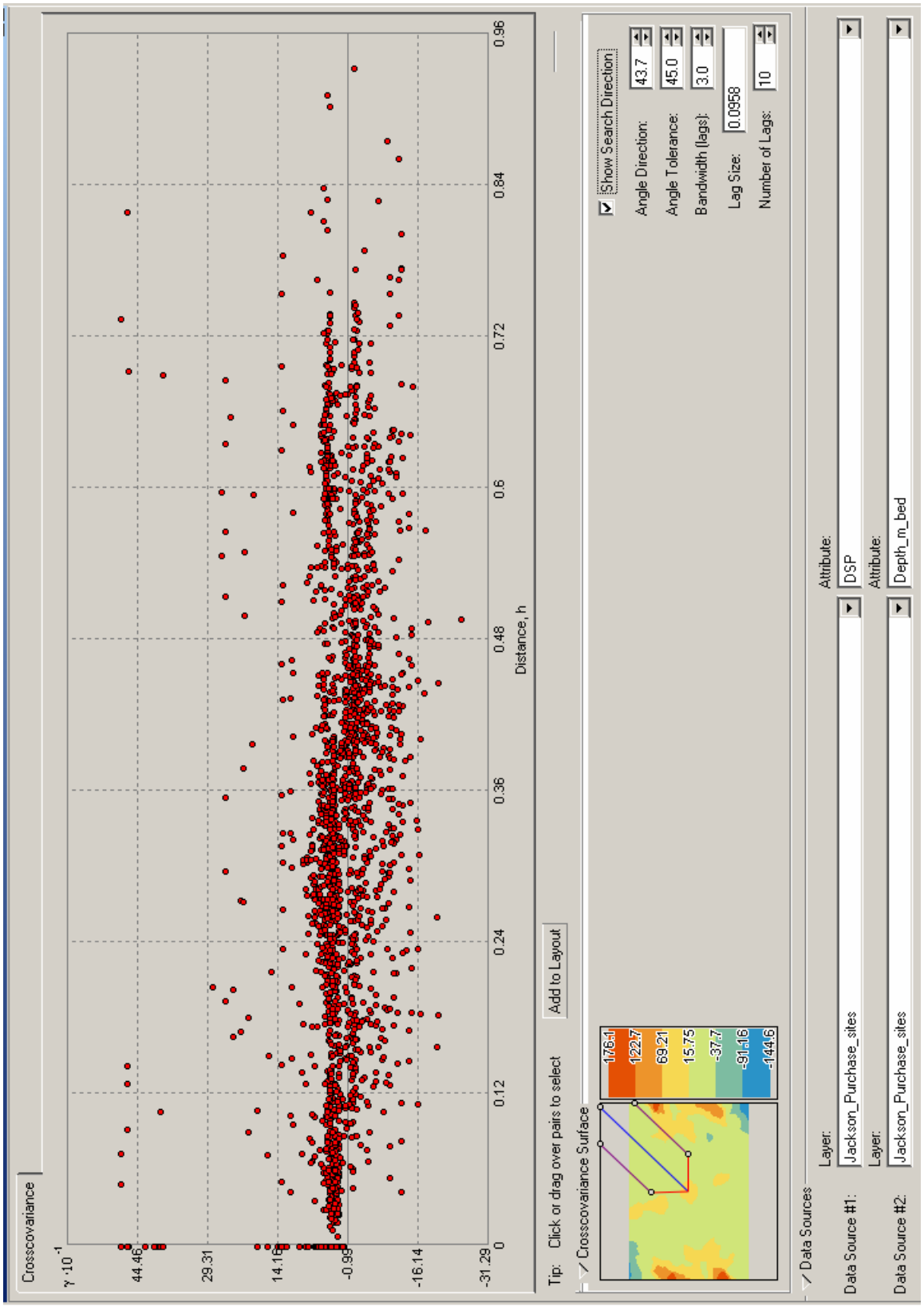

Figure 26. Crosscovariance cloud of DSP and bedrock depth data.

4.2 Stochastic Methods

Also known as *geostatistical methods*, stochastic methods use both mathematical and statistical methods for interpolation and provide measures of uncertainty in the results (ESRI, 2006). Using the Geostatistical Analyst toolbar, the Geostatistical Wizard function is chosen. The input data is selected as "Jackson Purchase sites" and the attribute to be interpolated is the mean dynamic site period (DSP) (Figure 27). In the Methods menu, the interpolation options are listed. Note that a description of each selected method is given to the right of the Methods menu. For the geostatistical methods, the Ordinary Kriging model is the simplest and requires the fewest parameter choices. Each additional parameter that must be selected requires additional estimation, thus potentially introducing more error into the final output surface. Therefore, it is beneficial to select the kriging method that requires the fewest choices of parameters, unless there is sufficient knowledge to select the parameters accurately. Each of the other kriging methods is a derivation of the ordinary kriging model and require more parameter decision-making.

The dynamic site period is calculated according to the equation

$$T_{DSP} = 4H/V$$

where H is the thickness of soil overburden above bedrock, V is the weighted-average seismic shear-wave velocity of the combined soil layers, and T_{DSP} is the dynamic site period. From this equation, it is evident that the DSP is directly proportional to the soil thickness, H. Also, it may be assumed that there is a trend in the data that generally follows the distribution of bedrock depth, though the coefficients of the polynomial that would describe the trend are unknown, accompanied by random autocorrelated errors in measured values. Therefore, the universal cokriging model was chosen as the test method for interpolation of DSP values. The universal kriging interpolation technique is examined in detail, and the results of the remaining methods are subsequently discussed and compared.

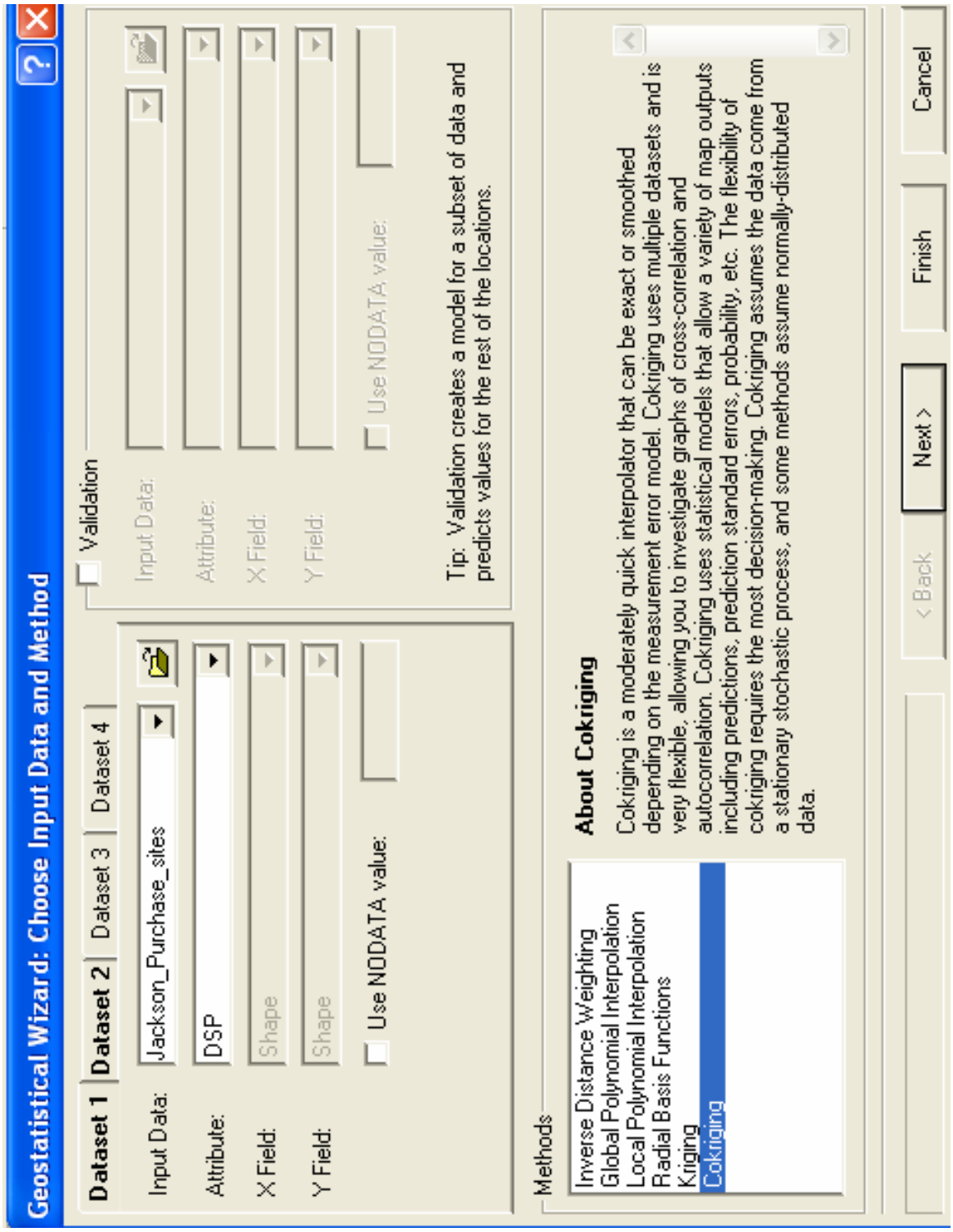

Figure 27. Cokriging is selected as the interpolation method. The DSP and bedrock depth attributes of the Jackson_Purchase_sites feature class are selected as the input datasets.

4.2.1 Universal Cokriging

The procedure chosen for interpolating DSP values across the study area is the universal cokriging method, defined by two equations,

$$Z_1(\mathbf{s}) = \mu_1(\mathbf{s}) + \varepsilon_1(\mathbf{s})$$

$$Z_2(\mathbf{s}) = \mu_2(\mathbf{s}) + \varepsilon_2(\mathbf{s})$$

where Z(s) is any given point to be interpolated, $\mu(\mathbf{s})$ is the deterministic function defining the unknown trend in the data, and $\varepsilon(\mathbf{s})$ is the random autocorrelated error associated with a measured sample point. The first equation represents the first dataset, the dynamic site periods, and the second equation represents the depths-to-bedrock (or soil overburden thicknesses) dataset. Each dataset is actually an attribute of the "Jackson Purchase sites" dataset.

To begin the interpolation process, cokriging is chosen as the method of interpolation using the DSP and bedrock depth attributes of the Jackson Purchase dataset. No transformation is selected for either dataset since normal distribution is not necessary for this type of interpolation, and the order of trend is left as *constant* (Figure 28).

The "detrending" tool is then used to identify and remove trends (Figure 29). Two options are available for detrending. The first is presented as the "Standard Options," in which the search neighborhood can be selected as 100 percent global, 100 percent local, or any combination of the two. The global search neighborhood uses the entire dataset, whereas the local search neighborhood uses a subset of data values, limiting the influence of points used for the detrending calculation to those located within a defined area around a given location. A color ramp is calculated and a map displaying the defined search neighborhood is drawn. If more than one dataset is being examined, detrending options may be selected separately for each dataset. For this interpolation, detrending combinations were examined for both datasets and were set at 50 percent global and 50 percent local, which resulted in the lowest error values. Figure 30 shows the "Advanced Options" parameters, available where parameters may be set to perform more precise detrending.

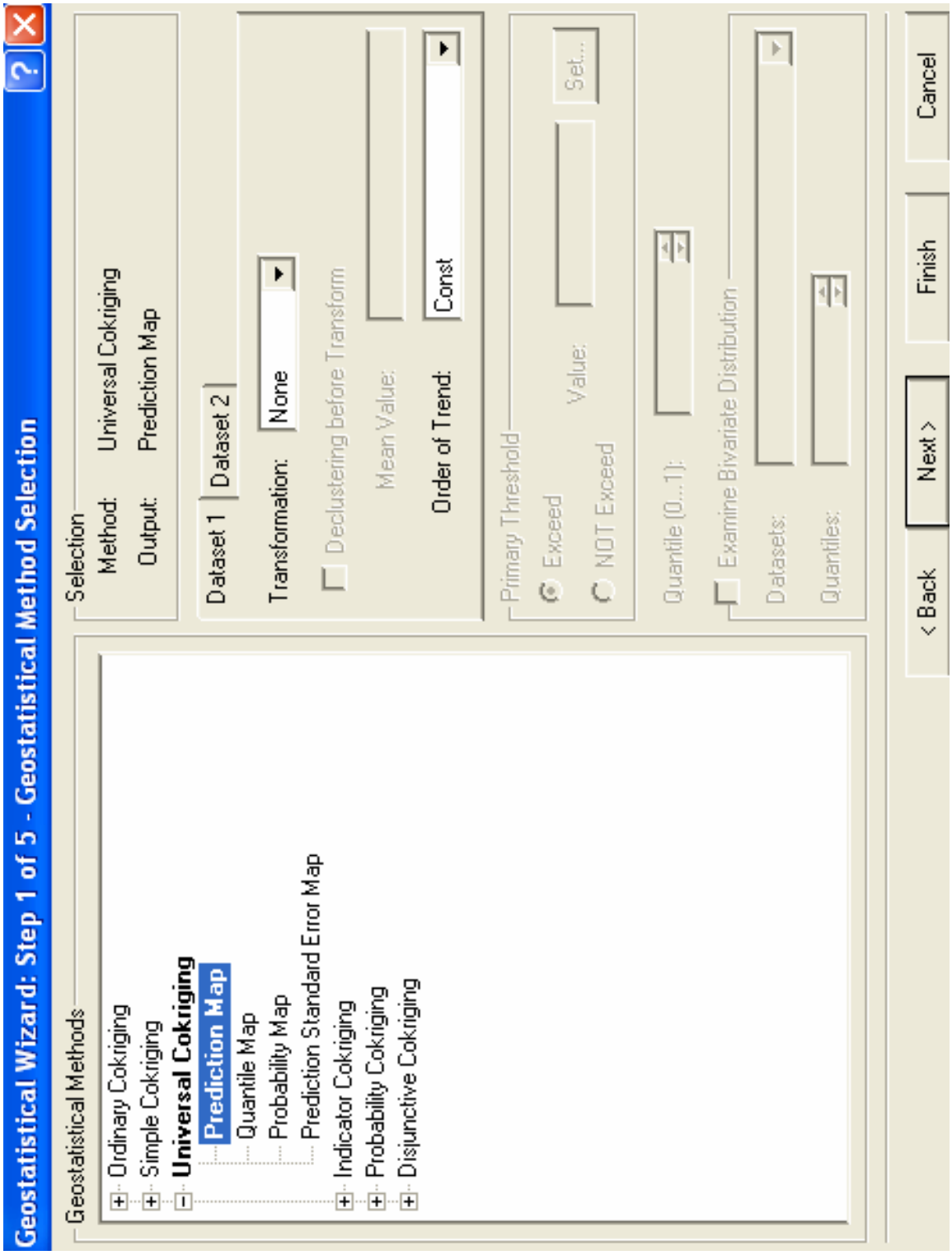

Figure 28. Based on information gained from the ESDA process, the universal cokriging method is selected and the type of output surface to be produced is a map showing predicted values across the study area based on measured values from a limited number of sample locations.

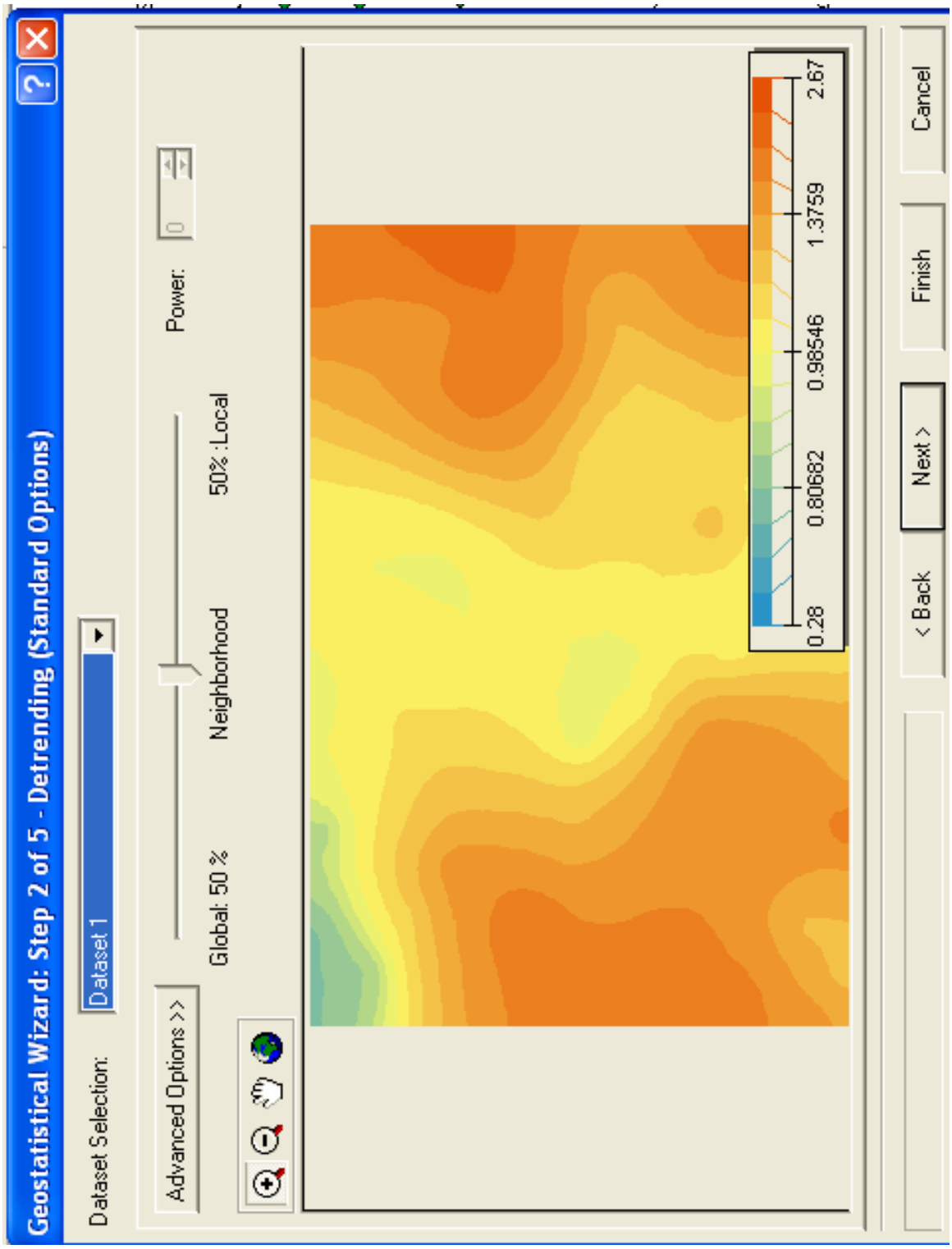

Figure 29. The detrending tool standard options.

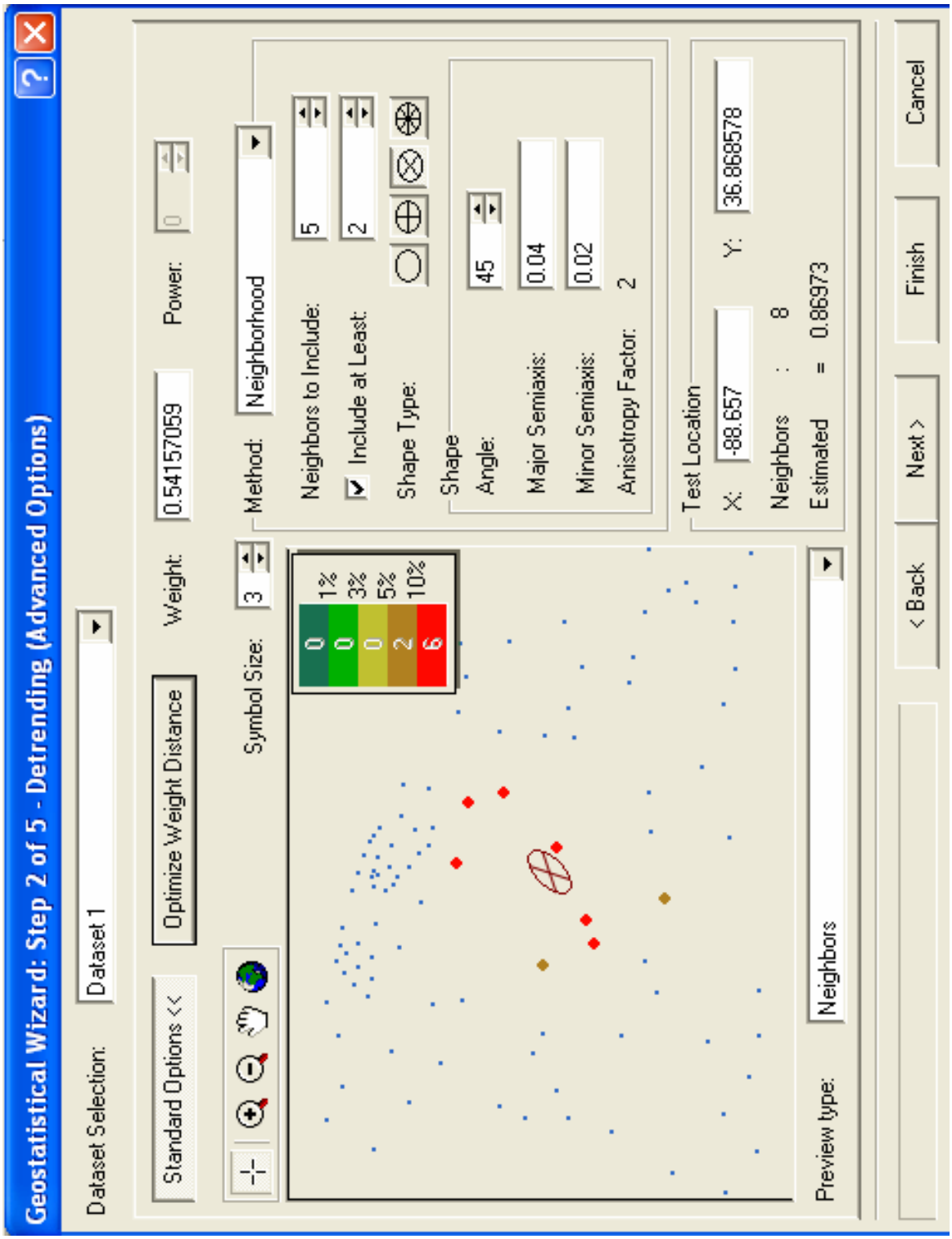

Figure 30. The detrending tool advanced options.

In modeling the semivariogram and covariance, parameters are selected by default by the Geostatistical Wizard, each optimized according to the input dataset (Figure 31). These parameters include the range, partial sill, nugget, lag size, and number of lags, which describe the semivariogram model and may be entered manually. When viewing the semivariogram model, the curve fitted to the plotted points levels out at a particular distance. The distance at which the curve begins to flatten out is the range. Points within the range are autocorrelated, whereas points beyond the range are not autocorrelated. In theory, the value of the semivariogram at zero separation distance is zero. As a result of measurement errors, however, the semivariogram value at infinitely small separation distance is usually greater than zero. This is referred to as the *nugget*. The sill is defined as the value on the y-axis corresponding to the range on the x-axis. The partial sill is then defined as the sill minus the nugget. Construction of the semivariogram involves placing the data into bins of similar values. This is done to reduce the number of points displayed in the semivariogram plot, making the necessary calculations manageable. The lag size determines the size of the bins. Lag size must be chosen carefully, because small-scale variation may be masked by a lag size that is too large, whereas a lag size that is too small may overly smooth the results. Both the semivariogram and covariance clouds can be viewed. A search direction may be defined if directional influences are suspected in the data.

The final selection to be made is a function to define the semivariogram and covariance. Functions available include circular, spherical, tetraspherical, pentaspherical, exponential, Gaussian, rational quadratic, hole effect, K-Bessel, J-Bessel, and stable. The semivariogram/covariance model can be defined by one function, or a combination of up to three functions. After examining the fit of the curves to the semivariogram and the resulting error values, it was determined that the addition of the spherical and exponential functions produced the lowest prediction errors.

The covariance of the dataset was also examined (Figure 32). In the covariance cloud, the covariance is plotted as a function of distance, so data that are closer together should show higher covariance.

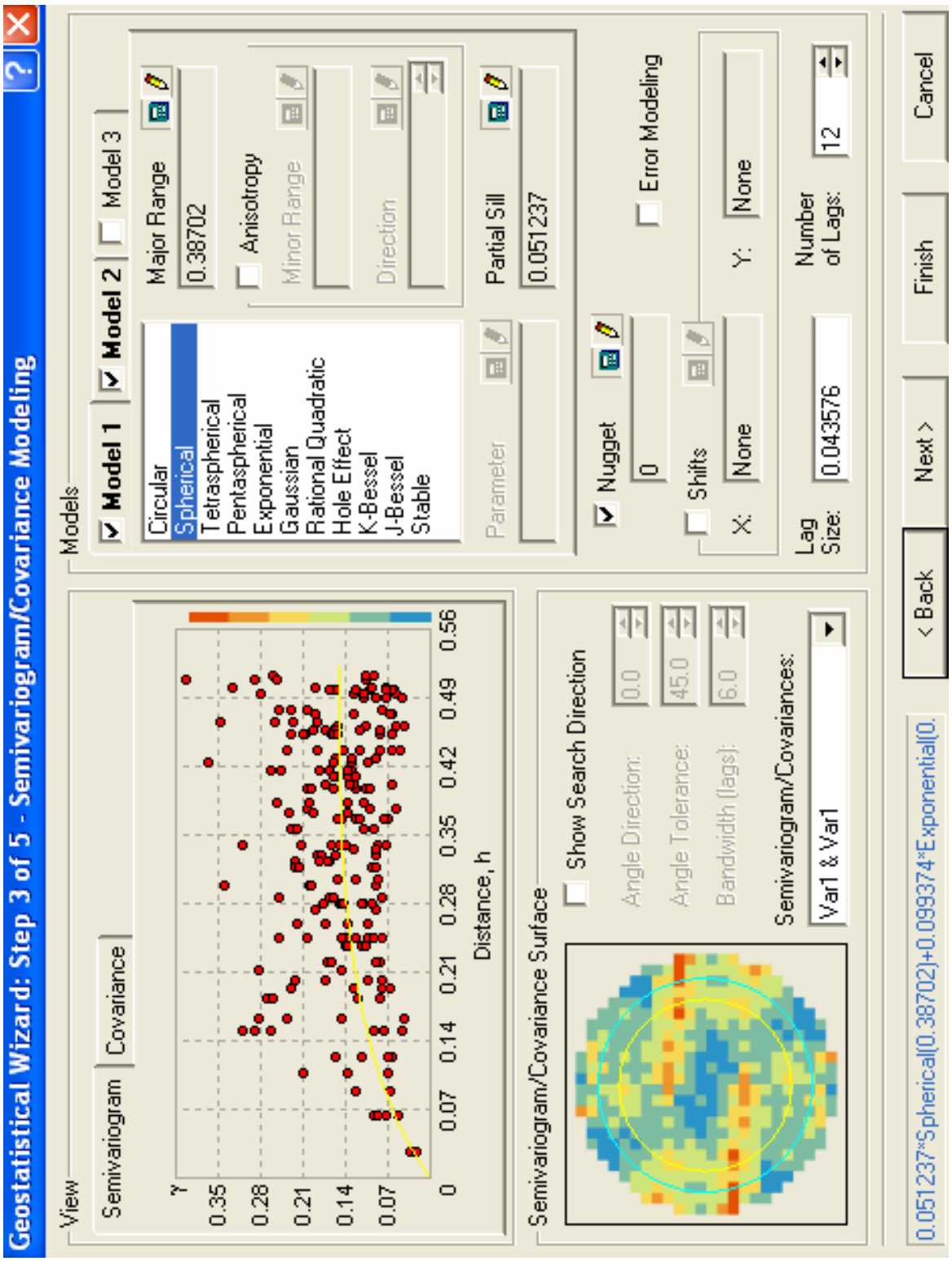

Figure 31. Modeling the semivariogram/covariance.

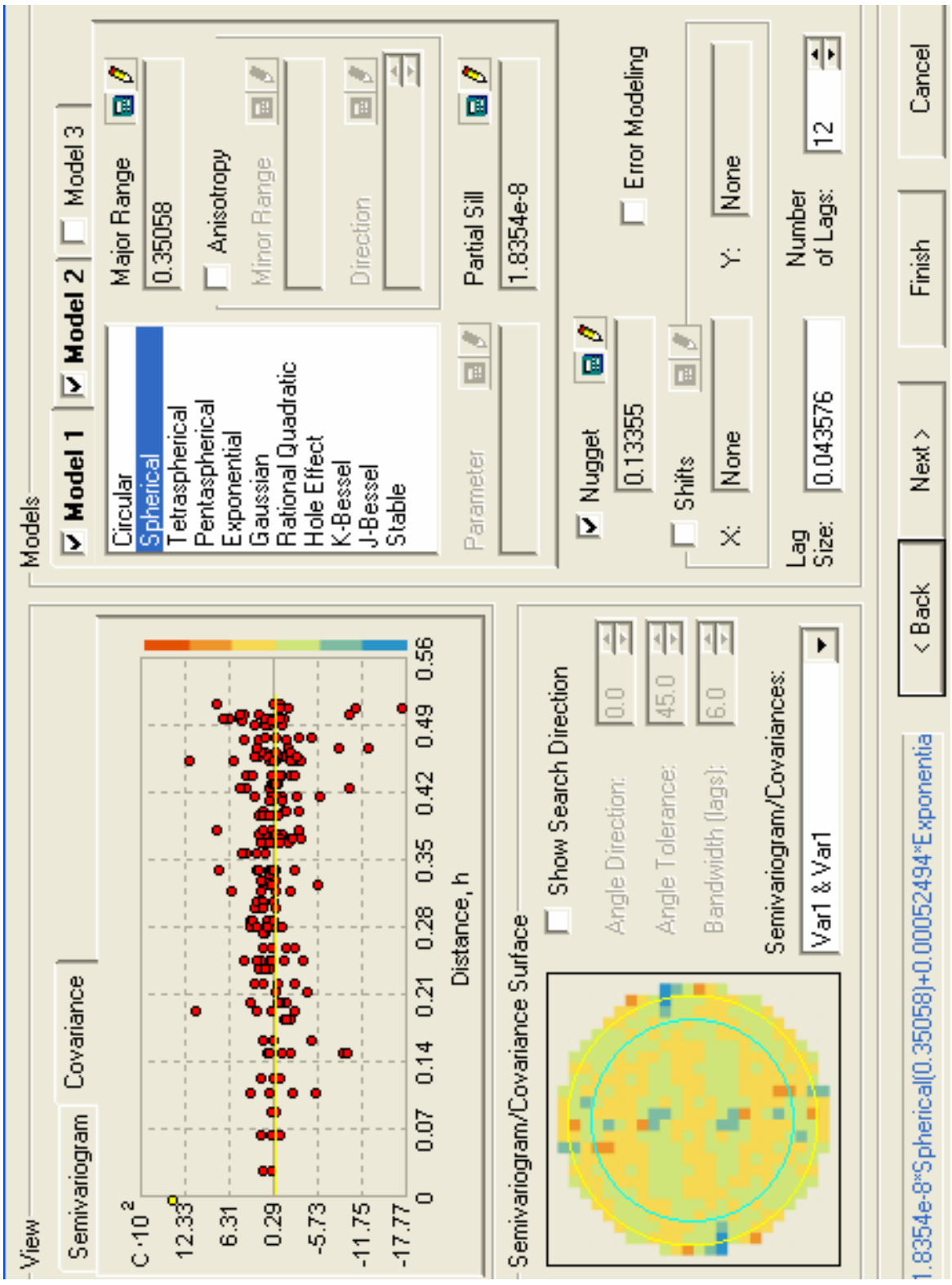

Figure 32. Modeling the covariance.

Search neighborhoods may be defined for both datasets (Figure 33). Parameters to be selected include the number and minimum number of neighbors used, shape type, and details concerning the orientation, shape, and size of the search neighborhood. A preview of the sample points and search neighborhood, and a preview of the output surface can be viewed. In the preview of the search neighborhood, any point on the map may be selected to show which sample points will be included in the calculation of the predicted value at that point. The x- and y-coordinates, number of neighbors, and predicted value at a given location are displayed.

Cross-validation completes the model-fitting process. Multiple options are available for viewing plots of predicted versus measured values (Figure 34), error versus measured values (Figure 35), standardized error versus measured values (Figure 36), and a QQ plot of standardized error versus normal values (Figure 37). A table consisting of the coordinates of each measured sample point along with statistics associated with each point, including measured and predicted values, error, standard error, standardized errors, and normal values, results. In addition, measures of interpolation accuracy are provided in the form of statistics of the prediction errors. These statistics are used to assess and compare the accuracy of one output surface to another.

When cross-validation is complete, a summary of the method and selected parameters is displayed (Figure 38). The resulting derivative map is shown in Figure 39. The new output surface layer is added to the basemap. Summary information and a legend are shown in the map's table of contents. A prediction standard error surface can be produced showing spatially the relative uncertainty in the predictions. A discussion of the results is provided in the following chapter.

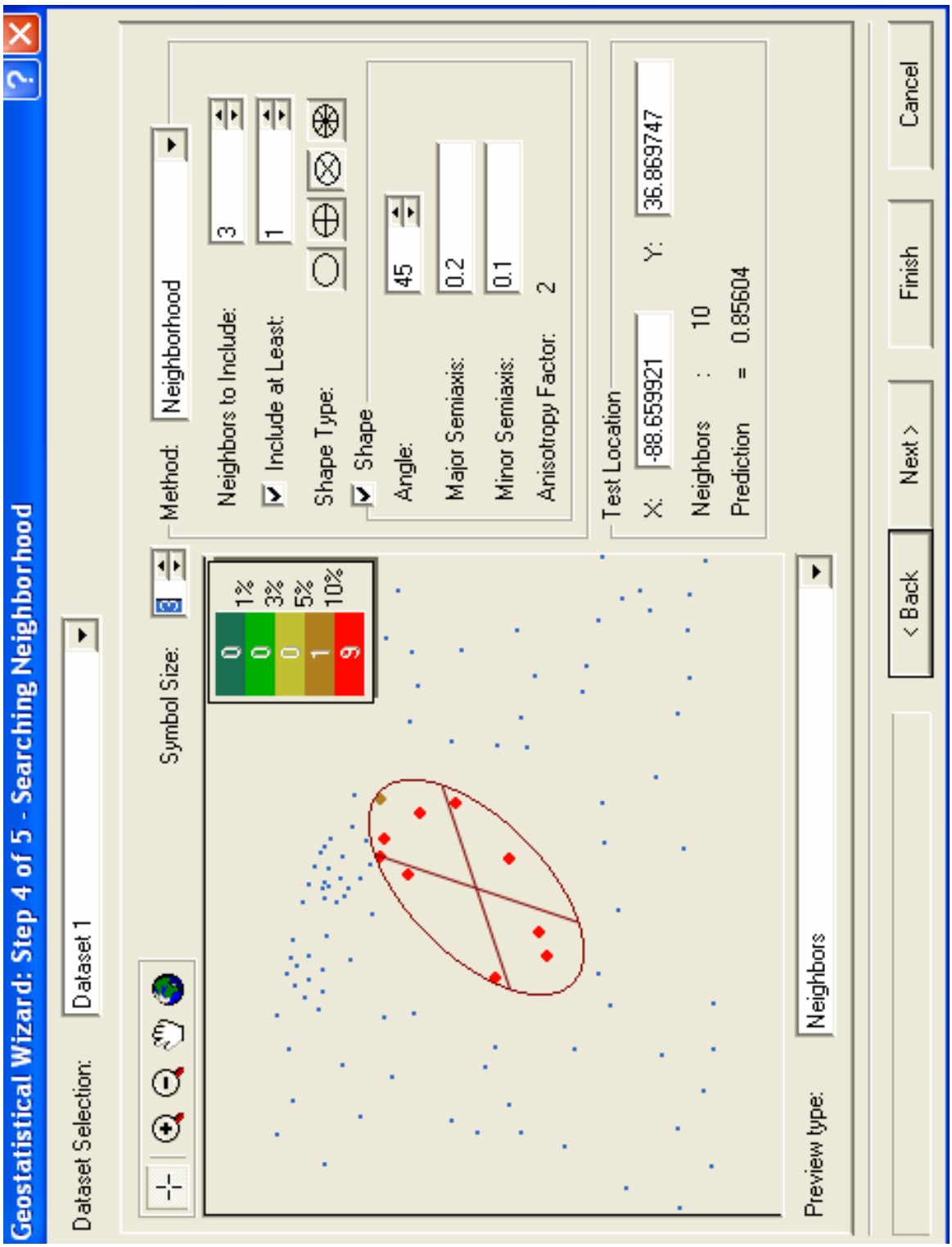

Figure 33. Definition of the search neighborhood for dataset 1. A unique search neighborhood may be defined for dataset 2.

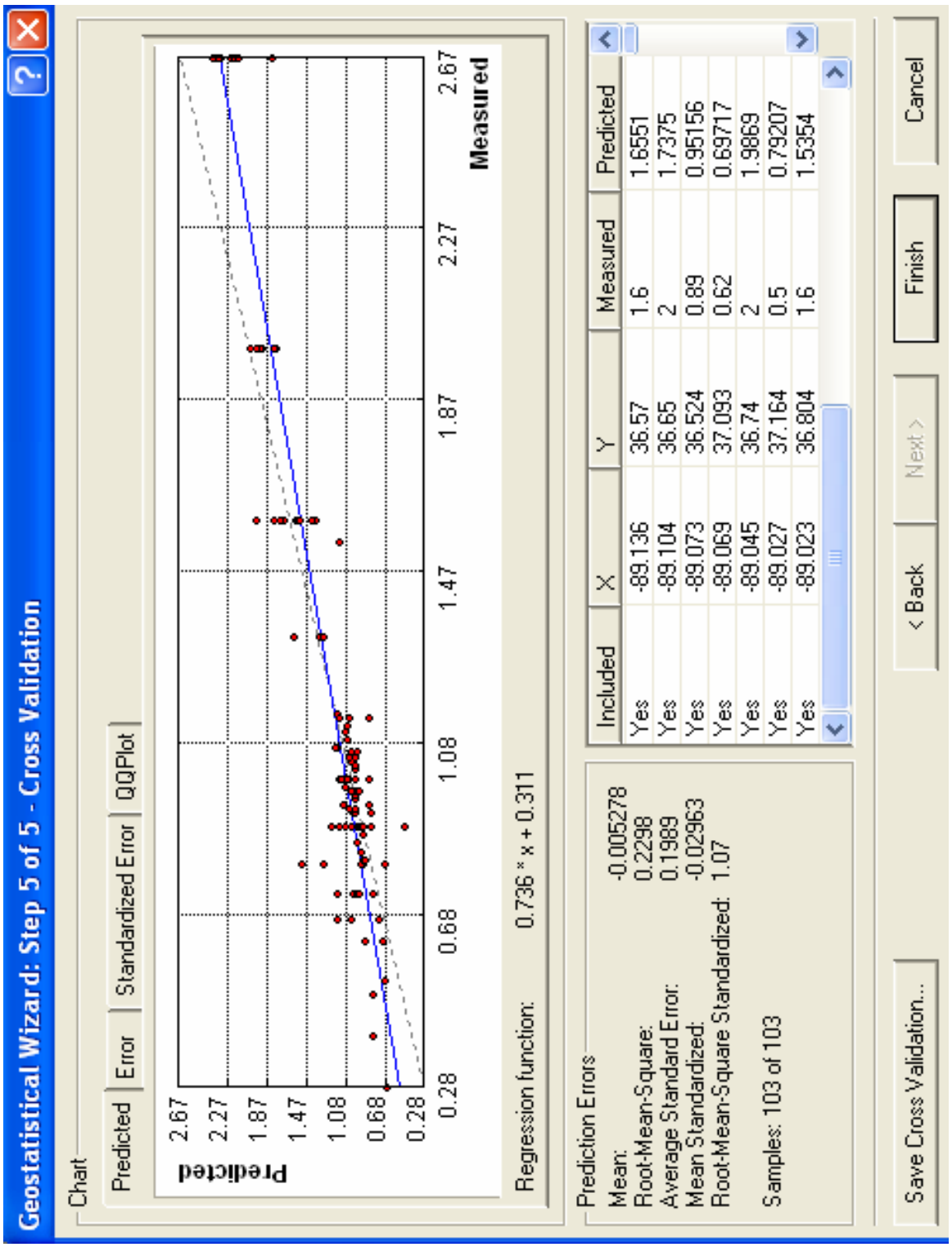

Figure 34. Cross-validation involves the interpretation of prediction error statistics. Shown is the predicted versus measured values plot.

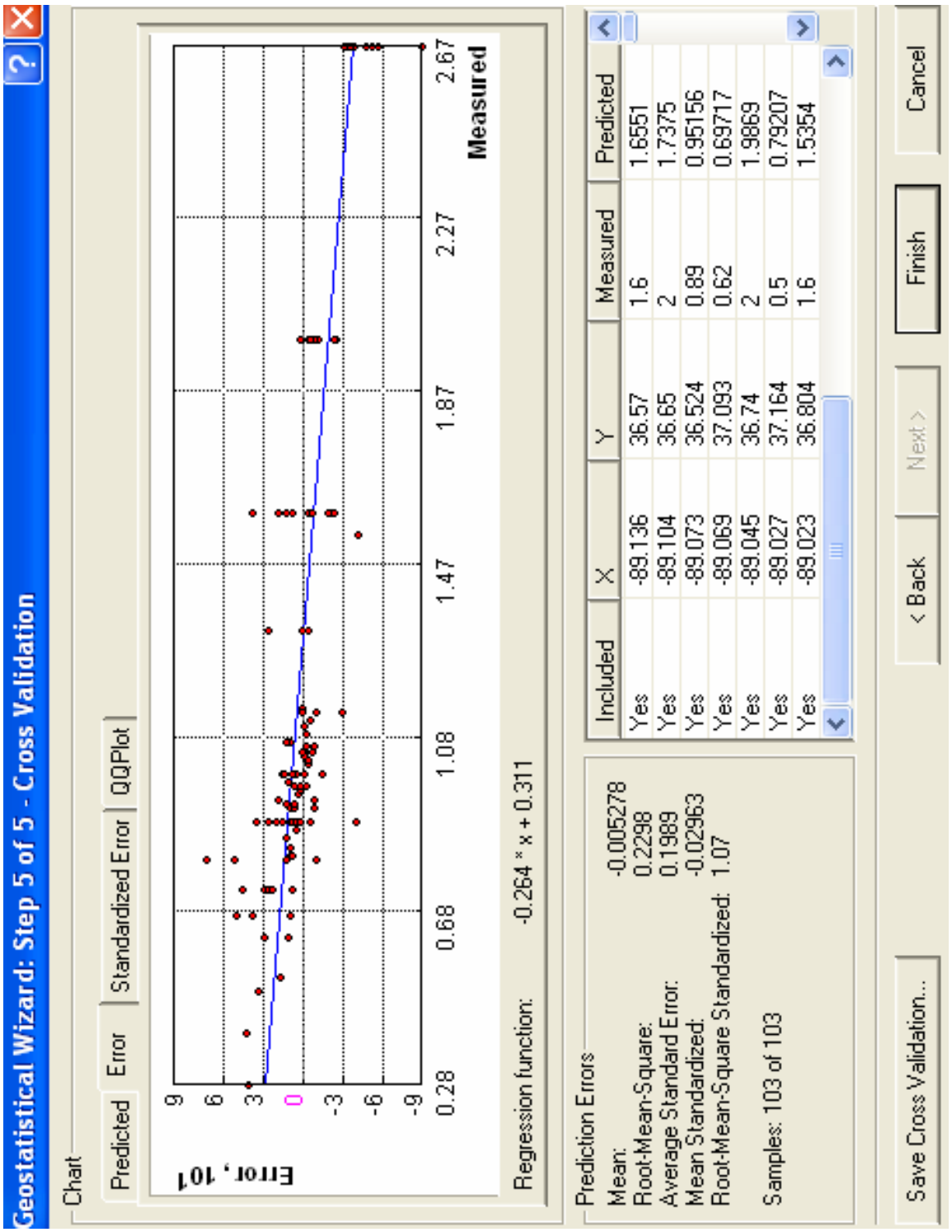

Figure 35. Plot of error versus measured value. The more accurate the predictions, the closer the points should plot to the line.

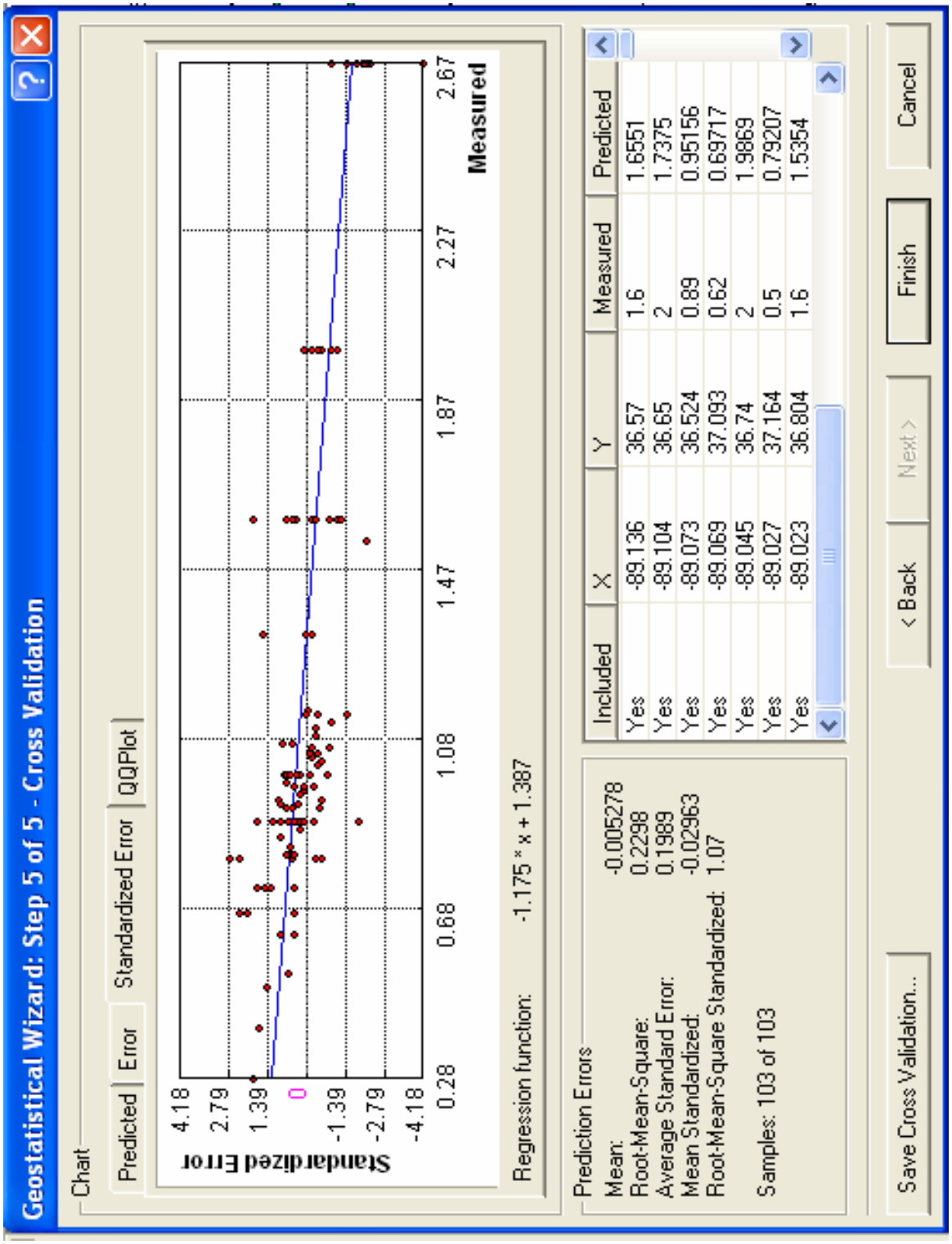

Figure 36. Plot of standardized error versus measured value.

Figure 37. Plot of standardized error versus normal value QQ.

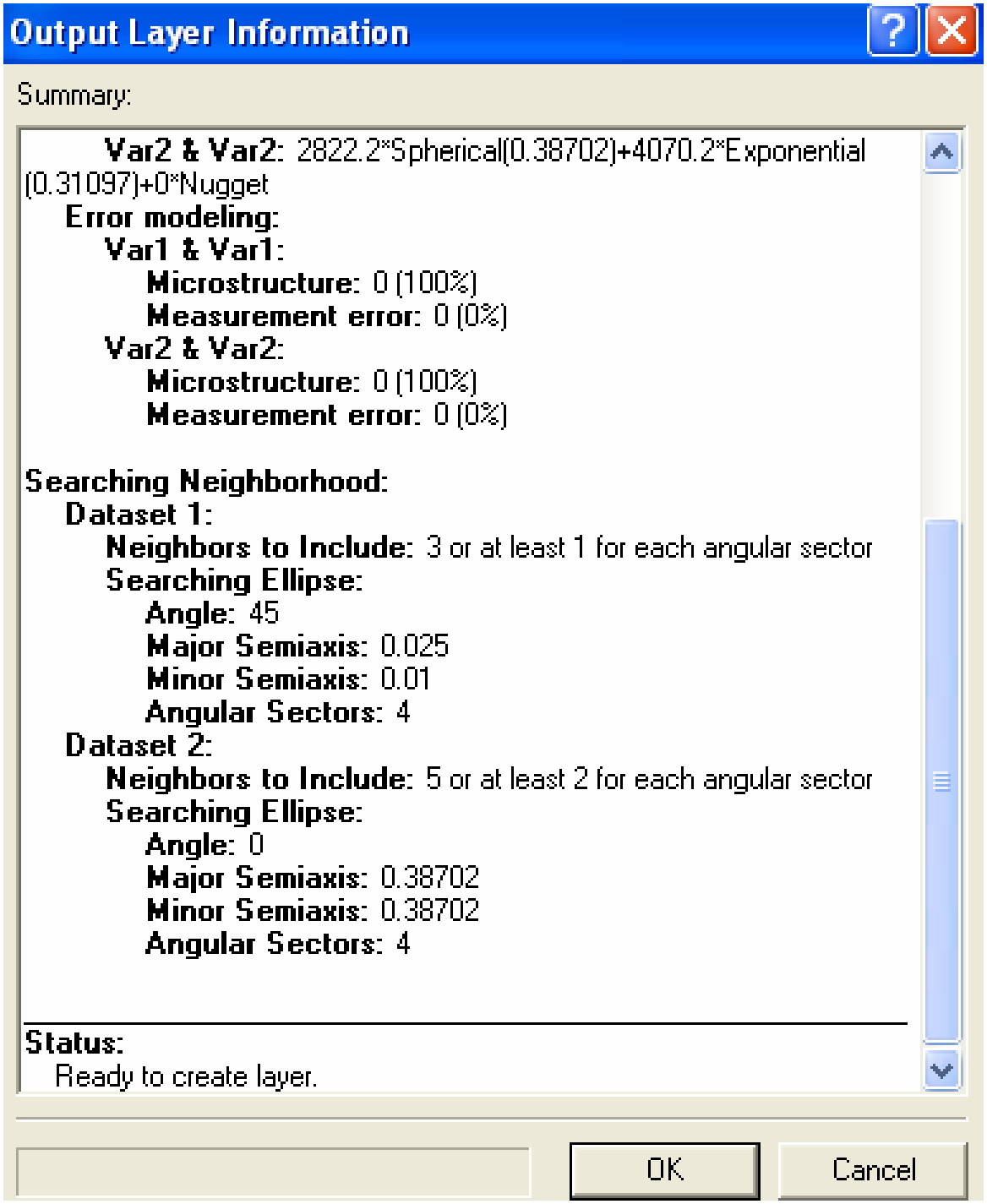

Figure 38. Prior to generation of the output surface, the Geostatistical Wizard displays a summary of the parameters selected for interpolation.

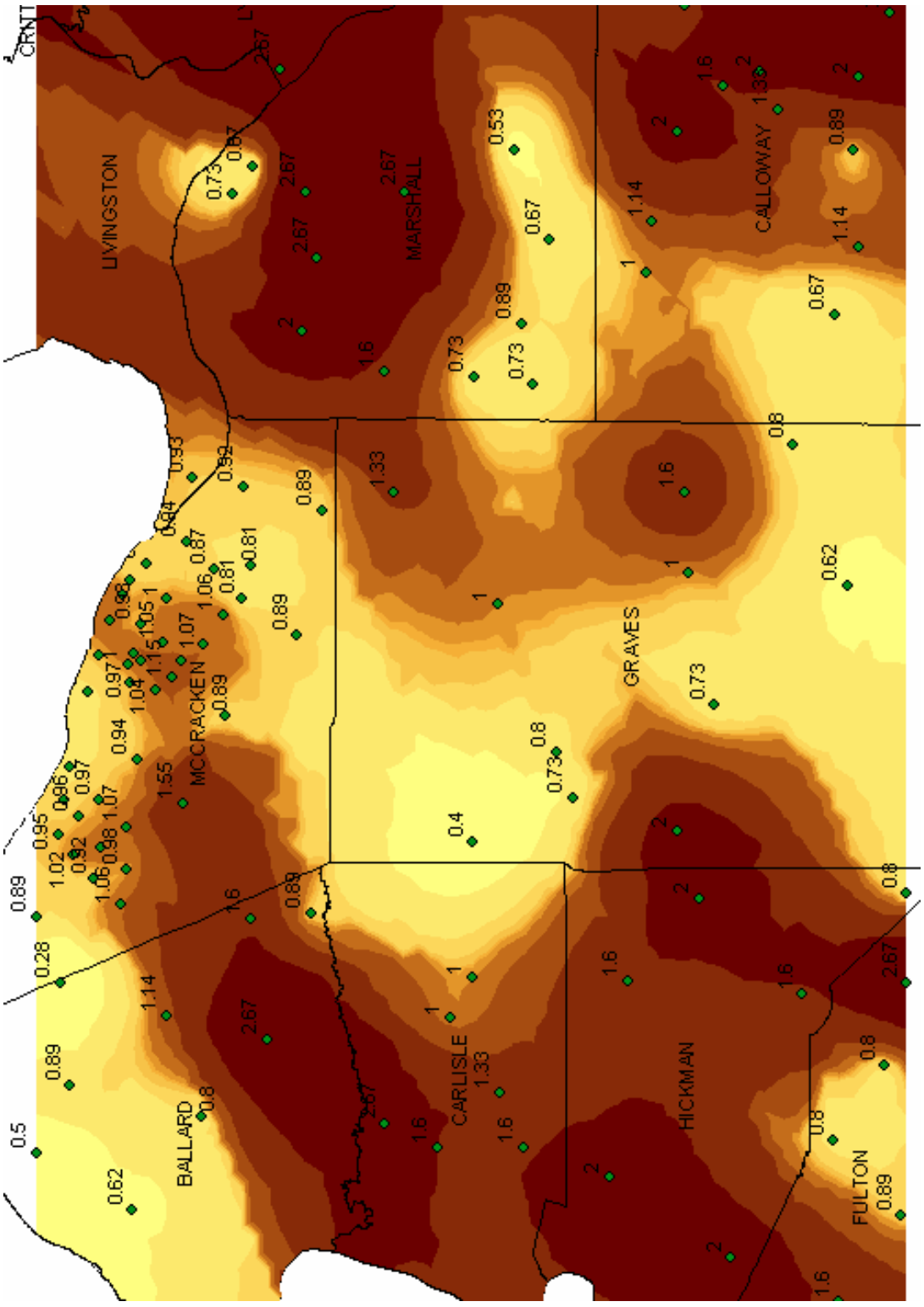

Figure 39. The output surface showing distribution of DSP values. See Appendix B for interpolations of the DSP and V_{30} attributes using other techniques available in ArcMap 9.1.

5.0 Output Surfaces and Prediction Error Statistics

5.1 Prediction accuracy

Measures of prediction accuracy calculated by Geostatistical Analyst are provided during cross-validation and include the mean, root-mean-square, average standard error, mean standardized, and the root-mean-square standardized error. The mean and root-mean-square are available for both geostatistical (kriging) and deterministic (e.g., splines) interpolation methods. The average standard error, mean standardized, and root-mean-square standardized statistics, which provide measures of uncertainty in the predictions (i.e., how good are the predictions) are available only for the geostatistical methods, however.

Parameters may be selected and changed to achieve optimal prediction error statistics. Once the process has been completed, the prediction errors associated with each method can be compared, as well as graphs of the predicted, error, standardized error, and QQ plots from each method (Figure 40).

5.2 Mean Dynamic Site Period (DSP)

5.2.1 Prediction Map

Universal cokriging, using depth-to-bedrock values as a correlating variable, was used to produce the DSP prediction map. The resulting prediction error values suggest this method produced the most accurate results. If the predicted values are unbiased (centered on the true values), the mean should be near zero. For this interpolation, the calculated mean was –0.005278. The root-mean-square error (RMS) measures how close the predicted values are to the measured values, and the RMS should be as small as possible (the closer to zero the better). The RMS was 0.2298.

The remaining measurements detail the validity of the results, describing the uncertainty in the predictions. Average standard error (ASE) is a measure of the variability of the prediction and should be close to the RMS value. Here, the ASE was 0.1989, a difference of 0.0309 from the RMS. If the ASE is greater than the RMS

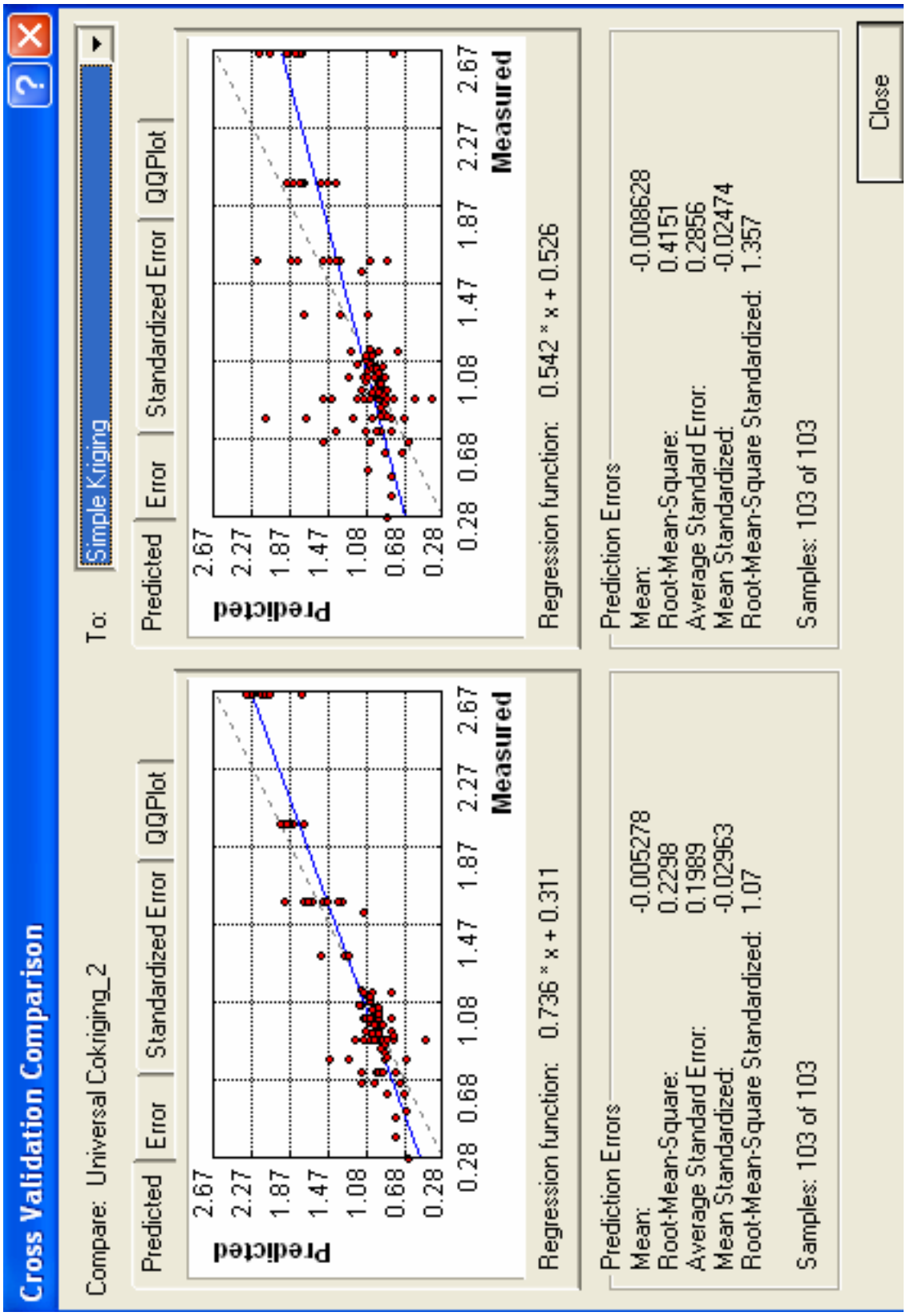

Figure 40. The cross validations from multiple output surfaces can be compared side-by-side.

the variability in prediction is overestimated, and if the ASE is less than the RMS, the prediction variability is underestimated. The mean prediction error depends on the scale of the data, so the mean standardized error is calculated by dividing the prediction errors by the prediction standard errors. The mean standardized error should be as close to zero as possible. In this case, the calculated value was –0.02963. Root-mean-square standardized error is another measure of variability and is calculated by dividing each prediction error by its estimated prediction standard error. These values should be similar, resulting in RMS standardized values close to 1 if the prediction standard errors are valid. If the value is greater than 1, the prediction variability is underestimated. Values less than 1 indicate overestimation of variability. The interpolation of DSP using universal cokriging resulted in an RMS standardized value of 1.07.

Inspection of the DSP output surface allows conclusions to be drawn concerning the geological and geophysical nature of the Jackson Purchase Region. First, trends in the distribution of DSP values are clearly visible. Areas with mean dynamic site periods ranging from 1.0 to 3.0 extend from north to south in parts of McCracken County (predominantly in the central and western sections of the county), Ballard County (predominantly in the southeastern half of the county), Carlisle County (in most areas except in the east), Hickman County (covering the vast majority of the county), and Fulton County (in the northwestern and northeastern sections of the visible study area). Parts of west-central, east-central, and northeastern Graves County show DSP values above 1.0, as well as the northern half of Marshall County and the eastern half of Calloway County.

Figure 41 shows the DSP output surface with bedrock depth distribution. The positive correlation between the two variables is observed graphically where deeper bedrock depths align with higher dynamic site periods.

Caution should be taken when examining areas of the map with few sample points (e.g., the northwestern, south-central, and eastern edges of the map, as well as the north-central and south-central parts of Graves and McCracken Counties, respectively). Two additional areas, central Hickman County and west-central Graves County, also contain few sample points. In these areas, the scarcity of sample points results in less-reliable predictions, sometimes referred to as “edge effects.”

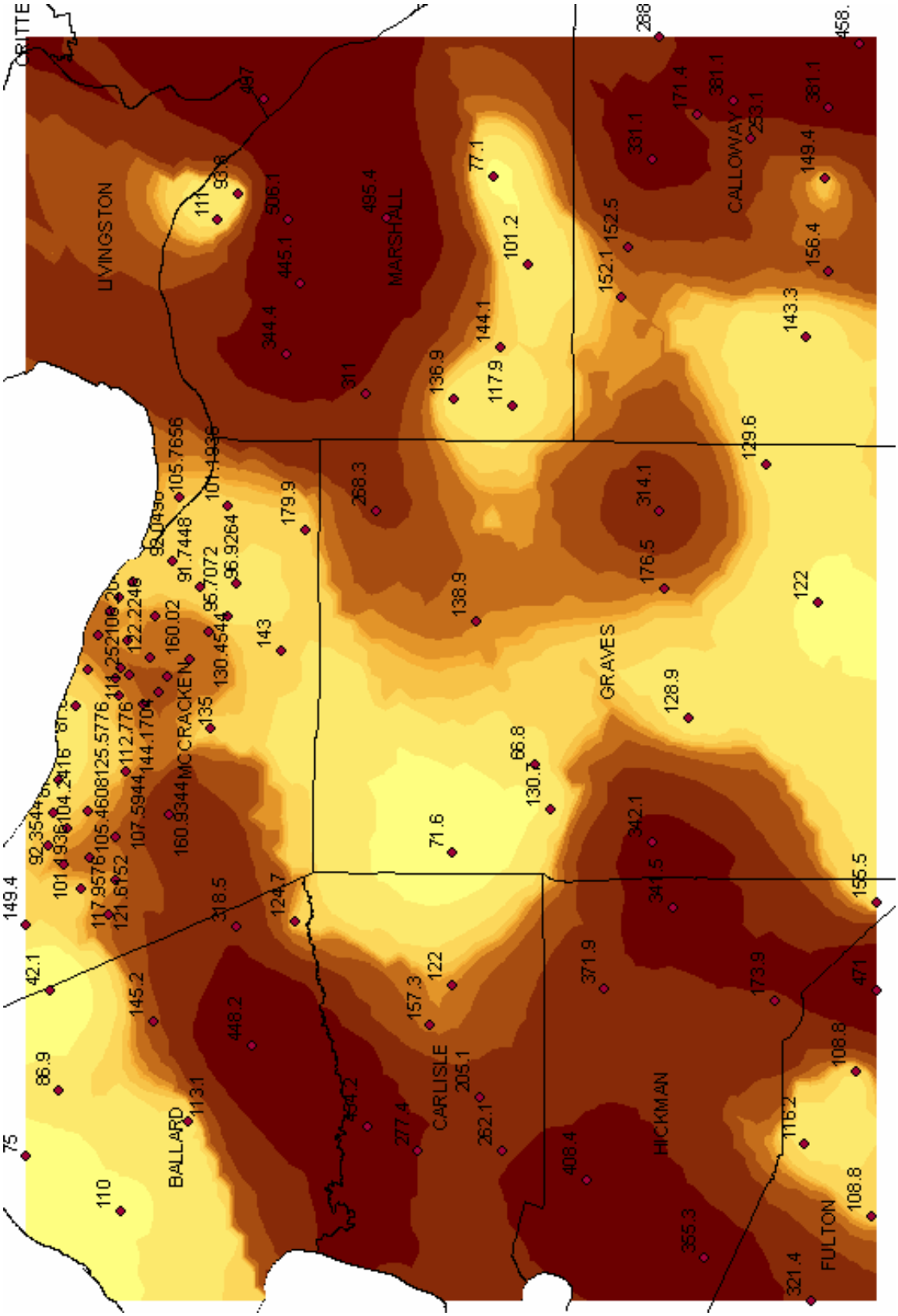

Figure 41. Distribution of bedrock depths over DSP output surface. Higher dynamic site periods correlate with deeper sediments.

5.2.2 Prediction Standard Error Map

The prediction standard error map shows the distribution of prediction standard errors calculated for every point on the output surface (Figure 42). Higher error values are represented by darker colors, and lower error values by lighter colors. As expected, error values are highest in areas with the fewest sample points, such as in north-central Graves County. In this area, errors with values as high as about 0.3 are recorded, whereas in the vicinity of Paducah in McCracken County, where many more sample points are located, providing better control on the distribution of DSP values, error values of about 0.09 are common.

Using the prediction standard error map, areas can be identified where additional field measurements may be necessary. Conversely, areas of high sampling density and, therefore high confidence in the predicted values, can be identified. For example, if knowledge of the mean dynamic site period for locations in north-central Graves County is needed, additional field investigation to determine DSP should be conducted rather than relying completely on the values predicted by Geostatistical Analyst.

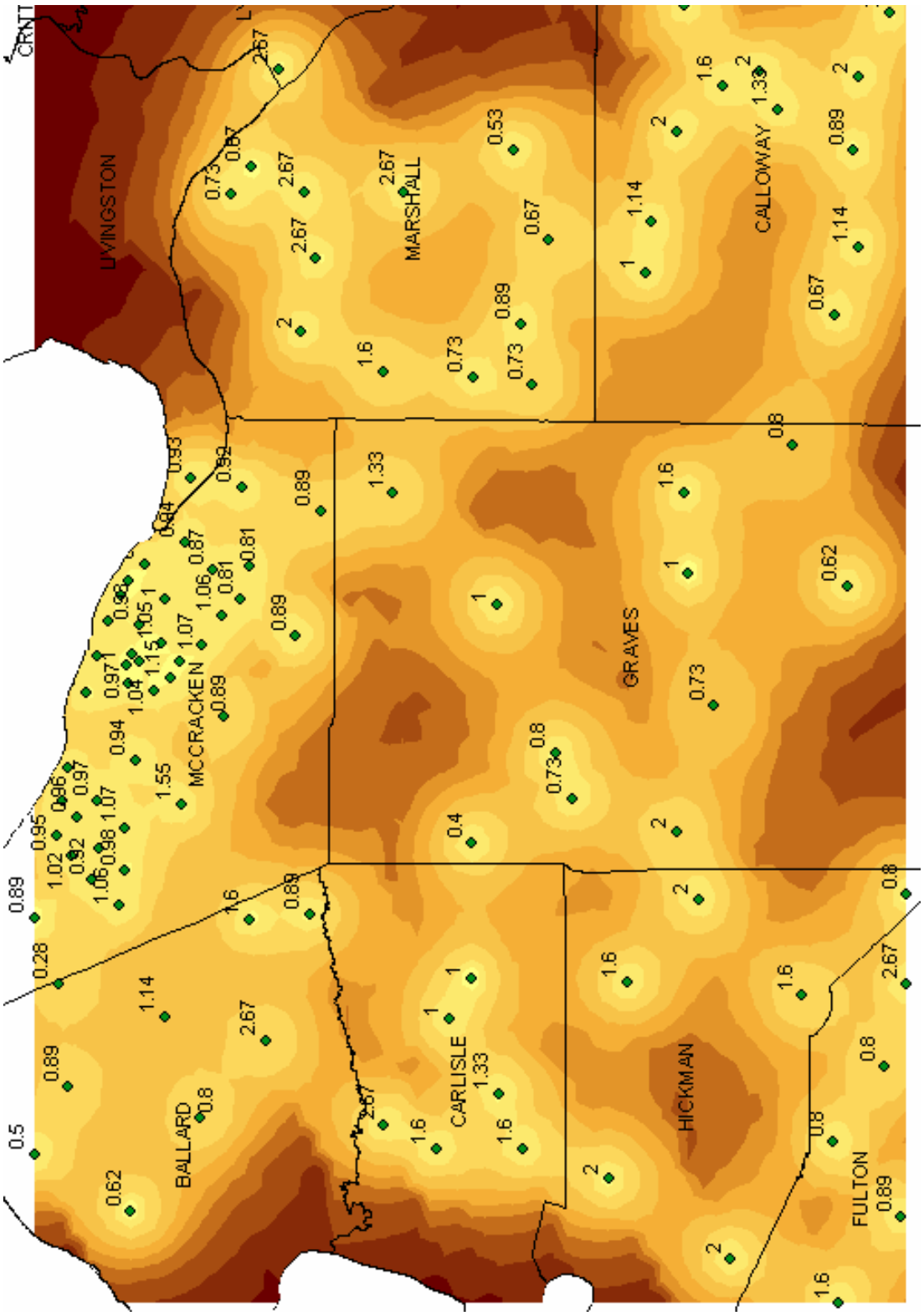

Figure 42. The prediction standard error map derived from the DSP prediction map shows graphically the calculated uncertainty in the predictions. Light colors represent areas of low uncertainty, and dark colors represent high uncertainty as a result of lack of sample locations.

5.3 Weighted Shear-Wave Velocity of the Upper 30 m of Soil (V_{30})

The interpolation techniques used for the DSP output surfaces, other than cokriging**,** were also used to interpolate V_{30} values over the same study area using data collected at the same sample locations (Figure 43). Resulting accuracy statistics indicate that prediction of V_{30} values over the study area was unsuccessful (Figure 44). The prediction error statistics were:

Mean: –0.1273

RMS: 79.7

Average standard error: 73.13

Mean standardized: –0.003095

RMS standardized: 1.078

The RMS error shows that there was a very large discrepancy in the predicted values versus the actual measured values. For this reason, the output surface of interpolated V_{30} values is not considered a true representation of the geophysical reality of the Jackson Purchase Region and should not be used to infer relationships of V_{30} values from one location to another within the study area. Figure 45 is a prediction standard error map derived from the V_{30} prediction map showing areas of high uncertainty in areas with few sample locations.

The difficulty with interpolation of V_{30} arises as a result of the lateral variation in stratigraphy in the Jackson Purchase. Thicknesses of individual soil layers and their s-wave velocities are used for V_{30} calculation. The thickness of a layer determines how much weight is given to its velocity, as shown in the equation $V_{30} = 30/\Sigma^{n}_{i=1}(h_i/v_i)$ (BSSC, 1997). High variation in stratigraphy, thicknesses of individual soil layers, and layer velocities over short distances within the study area cause high interpolation prediction errors. In contrast, DSP values are dependent only on the total thickness of the soil/sediment overburden and the weighted-average velocity of all layers, parameters that are much more consistent over the entire study area than thicknesses and velocities of individual layers. This accounts for the discrepancy in prediction error statistics of DSP and V_{30} values.

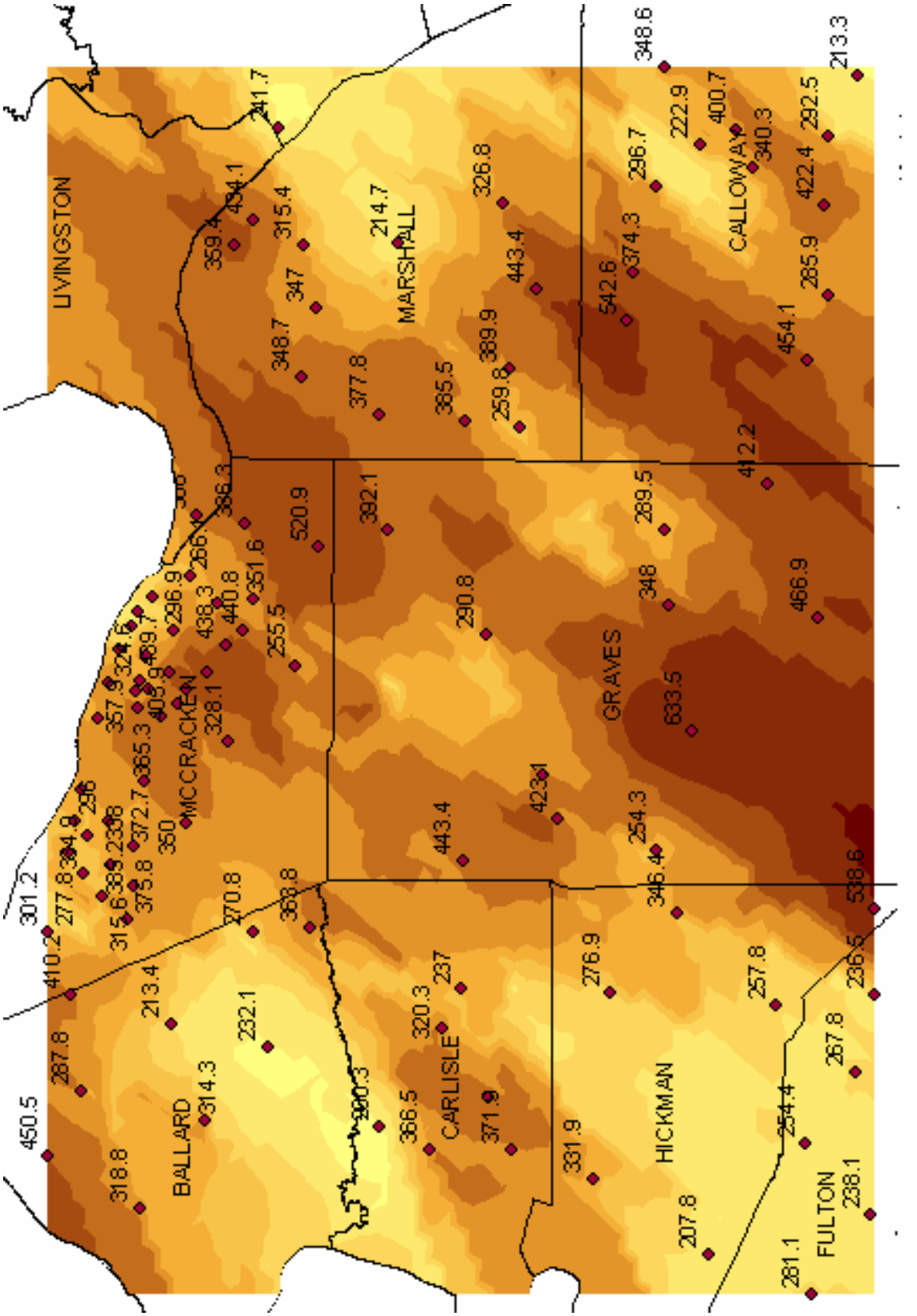

Figure 43. The output surface showing distribution of V_{30} values.

Figure 44. Cross-validation summary statistics of prediction errors for V_{30} output surface.

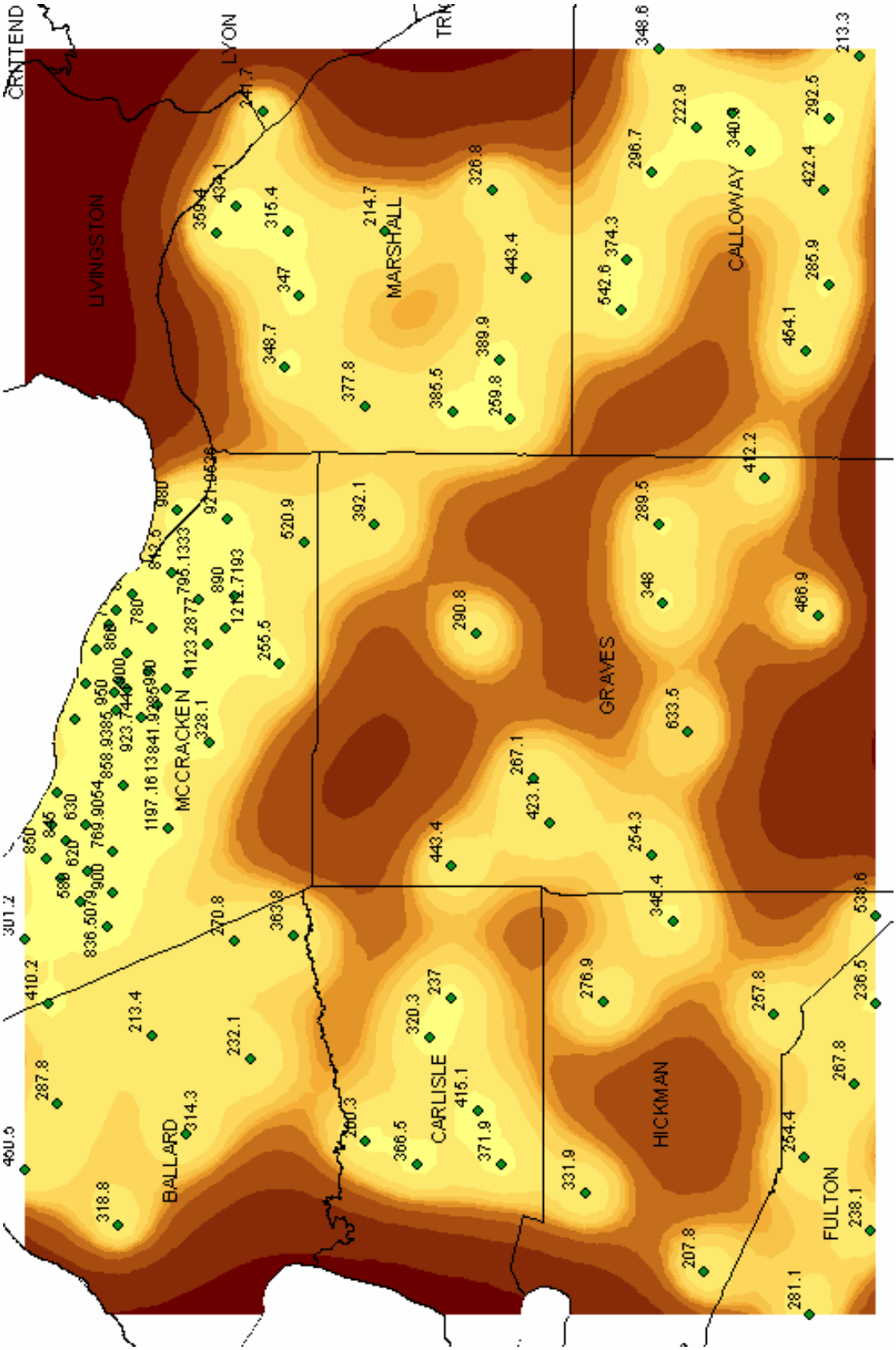

Figure 45. Prediction standard error map derived from V_{30} output surface.

5.4 Deterministic Methods

In addition to the kriging methods, deterministic techniques were considered. Although these methods, including inverse distance weighted (IDW), global and local polynomial, and radial basis functions, including splines, produced surfaces with RMS values approximately 0.45, no means are available for assessment of uncertainty in the predictions. These methods are ideal for fast interpolation and can provide output surfaces for use in general examination of trends in a study area when no detailed uncertainty statistics are necessary.

The surface shown in Figure 46 was produced using a *completely regularized spline.* The RMS error was 0.4412 with mean prediction error of –0.007481. Although the RMS error was smaller using the universal cokriging method, the spline method still produced a relatively accurate result. Though there are no associated measures of uncertainty, and prediction standard error maps cannot be created from deterministic method output surfaces, the spline output surface can be compared with the kriging surface to show the similarities between them. Cokriging clearly produces a more detailed surface, but the spline surface shows agreement with the major trends in DSP distribution across the study area.

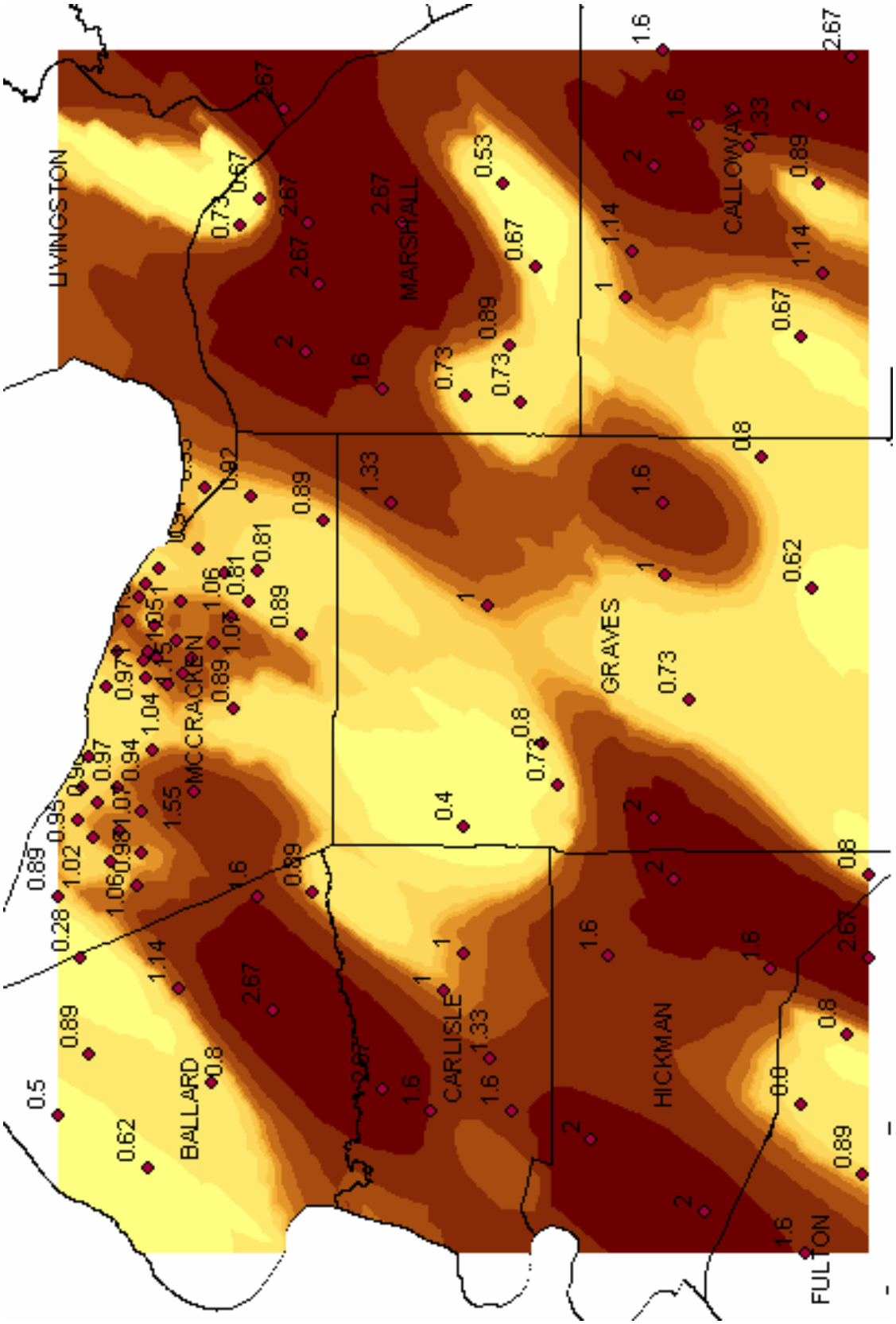

Figure 46. The completely regularized spline surface shows regional DSP trends.

6.0 Conclusion and Considerations

Over the last 20 years, researchers at the University of Kentucky have collected seismic reflection/refraction data for characterization of the seismic velocity models of the soil/sediment overburden throughout the central United States. These data and associated information have been difficult to manage because of the lack of a centralized repository to assist storage, retrieval, and analysis. The goal of this project was to use the ESRI ArcGIS software tools to make these data accessible and manageable and to use some of the tools available with this software for spatial and geostatistical analysis in order to provide a regional assessment of dynamic soil properties used in seismic hazard analysis.

To accomplish this goal, the data were gathered from various journals, publications, theses, and dissertations and digitized and stored in a personal geodatabase using ArcCatalog 9.1. The data were then projected on a digital map in ArcMap, and the data from the Jackson Purchase Region of western Kentucky were used to produce derivative maps in the Geostatistical Analyst extension of ArcMap. Exploratory spatial data analysis was used to examine characteristics of the dataset, particularly the mean dynamic site period and V_{30} attributes associated with each sample site. Based on this information, the universal cokriging method was selected as the optimal technique for interpolation of the DSP data across the study area. Other methods, including deterministic methods and other geostatistical techniques, were considered, but analysis revealed that the kriging methods in general, and the universal cokriging method in particular, produced the most accurate results. Cokriging uses two datasets presumed to be correlated to each other for mathematical and statistical modeling of the output surface. The directly proportional relationship between the dynamic site period and depth-to-bedrock datasets was the basis for the decision to use the cokriging interpolation method.

Interpolation of V_{30} was unsuccessful as a result of the lateral variation in soil layer thicknesses and velocities. Further research is recommended to determine if interpolation of V_{30} is possible over smaller scales.

When using Geostatistical Analyst interpolation capabilities to produce output surfaces, it is advisable to remember that the scale of the surface under investigation may have an effect on the way the results should be interpreted. This, of course, depends on the purpose for which the output surfaces are being created. Although prediction error statistics are calculated by Geostatistical Analyst to quantify the prediction accuracy of the output surfaces, the researcher

must judge, according to the stated aims of the project, the validity of the results. Errors calculated for a surface spanning the Jackson Purchase Region may translate into differences on the order of tens of meters, whereas errors calculated for a study area such as the city of Paducah may represent only a few meters. The implications may be significant, depending on the nature of the project and will compel the researcher to use caution when interpreting the results of output surfaces.

6.1 Future Work

6.1.1 Database Design

The structure used to develop the database is relatively simple. Each of the feature classes are nearly identical and are divided by source and geographic location. Some feature classes contain more attributes than others, depending on the nature of the original research. For this project, the goal was to digitize the data and store it in a common location. The data were used to produce interpolated derivative maps useful in future research related to seismic hazard assessment. The structure of the database allows the addition of new data and data types. As the database grows and the intended use of the data evolves, attention to the structure and design of the database is recommended. It may be necessary to reconfigure the database in order to accommodate new data and data types to maximize the potential of the database. Hernandez (1997) is an excellent resource for database design considerations. The ArcGIS database platform is ideal for storage of multiple interrelated data types. Raster images, such as stacked seismic profiles and photographs from study areas, core data, soil classifications and descriptions, and other geotechnical data should be included in the database.

6.1.2 Field Work

To improve the accuracy and reliability of output surfaces using interpolation techniques available in Geostatistical Analyst, further field sampling of seismic velocities and other geophysical attributes is recommended. More sample locations, particularly in areas where few already exist, would likely improve interpolation accuracy. Several references are available that discuss sampling regimes for optimal interpolation performance, including Laslett (1994), Carver (1997), O'Sullivan and Unwin (2003), Arlinghaus (1996), and Schabenberger and Gotway (2005).

Appendix A

A comprehensive list of data tables included in the database, showing all fields and data.

OBJECTID	SITE	LAT	LONG	DSP (ms)	Shape	V_{30} (m/s)	Depth to Bedrock
1	H-1	37.102	-88.843	1.06	Point	375.8	121.6152
2	H-2	37.116	-88.8	1.05	Point	282.9	113.3856
3	H-3	37.122	-88.824	0.92	Point	315.6	104.5464
4	H-4	37.097	-88.817	0.98	Point	385.2	117.9576
5	H-5	37.097	-88.785	1.07	Point	338	117.9576
6	H-6	37.117	-88.765	0.97	Point	296	105.4608
7	H-7	37.056	-88.768	1.55	Point	350	160.9344
8	J-3	37.136	-88.806	1.02	Point	277.8	104.8512
9	J-4	37.148	-88.791	0.95	Point	309.3	101.1936
10	J-5	37.144	-88.766	0.89	Point	288.8	92.3544
11	J-6	37.133	-88.778	0.96	Point	334.9	104.2416
12	M-1	37.139	-88.741	0.81	Point	322.9	81.0768
13	M-2	37.126	-88.685	0.83	Point	309	81.0768
14	PE-1	37.048	-88.527	0.93	Point	388	105.7656
15	PE-2	37.032	-88.595	0.87	Point	285.6	91.7448
16	PE-3	37.053	-88.575	0.94	Point	266.1	92.0496
17	PE-4	37.011	-88.534	0.92	Point	386.3	101.1936
18	PE-5	37.1	-88.613	1.03	Point	248.9	107.5944
19	PE-6	37.094	-88.603	0.92	Point	235.8	106.9848
20	PE-7	37.083	-88.591	0.85	Point	304.4	106.3752
21	PE-8	37.067	-88.617	1	Point	296.9	113.3856
22	PE-10	37.005	-88.592	0.81	Point	351.6	96.9264
23	PE-11	37.012	-88.617	0.81	Point	440.8	95.7072
24	PW-1	37.092	-88.657	1.12	Point	341.2	110.3376
25	PW-2	37.089	-88.735	0.94	Point	372.7	107.5944
26	PW-3	37.076	-88.684	1.04	Point	365.3	112.776
27	PW-4	37.086	-88.662	1.11	Point	324.1	111.252
28	PW-5	37.109	-88.632	1.05	Point	270	104.8512
29	PW-6	37.094	-88.678	0.97	Point	425.5	125.5776
30	PW-7	37.096	-88.665	1	Point	357.9	111.8616
31	PW-8	37.087	-88.636	0.93	Point	309.7	108.204
32	PW-9	37.057	-88.663	1.09	Point	382.4	123.7488
33	PW-10	37.04	-88.65	1.07	Point	468.6	160.02
34	PW-11	37.064	-88.675	1.15	Point	405.9	144.1704
35	PW-12	37.026	-88.629	1.06	Point	438.3	130.4544
36	PW-13	37.07	-88.649	1.05	Point	439.7	122.2248
37	PW-14	37.117	-88.658	0.97	Point	324.6	93.5736
38	K01	37.164	-88.852	0.89	Point	301.2	149.4
39	K02	37.146	-88.901	0.28	Point	410.2	42.1
40	K03	37.139	-88.977	0.89	Point	287.8	86.9
41	K05	37.164	-89.027	0.5	Point	450.5	75
42	K06	37.019	-88.317	0.73	Point	359.4	111
43	K07	37.004	-88.297	0.67	Point	434.1	93.8
44	K08	37.024	-88.703	0.89	Point	328.1	135
45	K09	37.005	-88.853	1.6	Point	270.8	318.5
46	K10	37.068	-88.925	1.14	Point	213.4	145.2
47	K12	37.042	-89	0.8	Point	314.3	113.1

48	K14	37.093	-89.069	0.62	Point	318.8	110
49	K15	36.984	-88.225	2.67	Point	241.7	497
50	K16	36.891	-88.315	2.67	Point	214.7	495.4
51	K17	36.965	-88.316	2.67	Point	315.4	506.1
52	K18	36.956	-88.365	2.67	Point	347	445.1
53	K19	36.967	-88.419	2	Point	348.7	344.4
54	K20	36.907	-88.448	1.6	Point	377.8	311
55	K21	36.899	-88.538	1.33	Point	392.1	268.3
56	K22	36.953	-88.552	0.89	Point	520.9	179.9
57	K24	36.971	-88.644	0.89	Point	255.5	143
58	K28	36.961	-88.849	0.89	Point	363.8	124.7
59	K31	36.993	-88.943	2.67	Point	232.1	448.2
60	K32	36.906	-89.005	2.67	Point	200.3	454.2
61	K34	36.81	-88.284	0.53	Point	326.8	77.1
62	K35	36.784	-88.351	0.67	Point	443.4	101.2
63	K36	36.805	-88.413	0.89	Point	389.9	144.1
64	K37	36.84	-88.453	0.73	Point	385.5	136.9
65	K38	36.796	-88.458	0.73	Point	259.8	117.9
66	K40	36.823	-88.621	1	Point	290.8	138.9
67	K41	36.779	-88.73	0.8	Point	267.1	66.8
68	K42	36.841	-88.797	0.4	Point	443.4	71.6
69	K43	36.767	-88.764	0.73	Point	423.1	130.7
70	K44	36.842	-88.897	1	Point	237	122
71	K46	36.858	-88.927	1	Point	320.3	157.3
72	K47	36.821	-88.982	1.33	Point	415.1	205.1
73	K48	36.867	-89.023	1.6	Point	366.5	277.4
74	K49	36.804	-89.023	1.6	Point	371.9	262.1
75	K50	36.684	-88.178	1.6	Point	348.6	288.1
76	K51	36.628	-88.226	2	Point	400.7	381.1
77	K52	36.656	-88.237	1.6	Point	222.9	171.4
78	K53	36.69	-88.271	2	Point	296.7	331.1
79	K54	36.708	-88.338	1.14	Point	374.3	152.5
80	K55	36.713	-88.375	1	Point	542.6	152.1
81	K57	36.684	-88.538	1.6	Point	289.5	314.1
82	K58	36.681	-88.597	1	Point	348	176.5
83	K59	36.662	-88.695	0.73	Point	633.5	128.9
84	K60	36.69	-88.789	2	Point	254.3	342.1
85	K61	36.674	-88.838	2	Point	346.4	341.5
86	K62	36.726	-88.9	1.6	Point	276.9	371.9
87	K64	36.74	-89.045	2	Point	331.9	408.4
88	K65	36.65	-89.104	2	Point	207.8	355.3
89	K66	36.57	-89.136	1.6	Point	281.1	321.4
90	K67	36.533	-88.183	2.67	Point	213.3	458.8
91	K68	36.556	-88.231	2	Point	292.5	381.1
92	K69	36.615	-88.255	1.33	Point	340.3	253.1
93	K70	36.559	-88.285	0.89	Point	422.4	149.4
94	K71	36.556	-88.356	1.14	Point	285.9	156.4
95	K72	36.573	-88.406	0.67	Point	454.1	143.3

96	K73	36.604	-88.502	0.8	Point	412.2	129.6
97	K74	36.564	-88.607	0.62	Point	466.9	122
98	K78	36.52	-88.835	0.8	Point	538.6	155.5
99	K79	36.52	-88.901	2.67	Point	236.5	471
100	K80	36.597	-88.909	1.6	Point	257.8	173.9
101	K81	36.536	-88.962	0.8	Point	267.8	108.8
102	K82	36.574	-89.017	0.8	Point	254.4	116.2
103	K83	36.524	-89.073	0.89	Point	238.1	108.8

Jackson Purchase sites (includes Harris–Paducah and Street–Jackson Purchase).

OBJECTID	SITE	LAT	LONG_	AVESED_SH_	V30	BED_VEL__M
1	E-01	37.876	-87.545	328	480.66	1372
2	E-02	37.883	-87.548	366	489.4	1067
3	E-03	37.884	-87.57	225	290.12	800
4	H-01	37.829	-87.516	217	451.91	823
5	H-02	37.85	-87.541	174	303.6	813
6	H-03	37.808	-87.554	211	436.42	863
7	H-04	37.844	-87.562	157	308.23	958
8	H-05	37.821	-87.568	259	399.4	1341
9	H-06	37.835	-87.568	250	405.9	853
10	H-07	37.83	-87.57	370	466.69	1168
11	H-08	37.853	-87.571	245	301.85	884
12	H-09	37.812	-87.581	241	368.08	1270
13	H-10	37.834	-87.588	151	250.67	1618
14	H-11	37.797	-87.591	211	236.9	1418
15	H-12	37.786	-87.592	191	215.08	1778
16	H-13	37.841	-87.594	240	280.1	1674
17	H-14	37.825	-87.594	249	310.1	1676
18	H-15	37.822	-87.601	221	0	1676
19	H-16	37.814	-87.607	221	221.89	1372
20	H-17	37.806	-87.612	169	245.91	1707
21	H-18	37.779	-87.612	192	394.61	1158
22	H-19	37.817	-87.62	251	241.52	1524
23	W-01	37.804	-87.629	197	277.91	1524
24	W-02	37.795	-87.642	151	283.45	1168
25	W-03	37.806	-87.656	214	245.5	1143
26	W-04	37.814	-87.674	215	224.11	1663

OBJECTID	THICK_SED_	SITE_CLASS	Shape
1	17.5	SC-III	Point
2	18.5	SC-III	Point
3	20.6	SC-III	Point
4	8.8	SC-III	Point
5	13.7	SC-IV	Point
6	9.5	SC-III	Point
7	12.6	SC-IV	Point
8	16.9	SC-III	Point
9	13.7	SC-III	Point
10	20.9	SC-III	Point
11	22.2	SC-III	Point
12	17.2	SC-III	Point
13	16.8	SC-IV	Point
14	26.2	SC-III	Point
15	27.4	SC-IV	Point
16	25	SC-III	Point
17	23.1	SC-III	Point
18	23.8	SC-III	Point
19	29	SC-III	Point
20	19.6	SC-IV	Point

21	11.5	SC-IV	Point
22	44.8	SC-III	Point
23	20	SC-IV	Point
24	13.9	SC-IV	Point
25	30.8	SC-III	Point
26	28.6	SC-III	Point

Higgins–Henderson, KY, sites.

OBJECTID	SITE	LAT	LONG_	V30	ARRAY	OFFSET_1__
1	701	35.883	-89.949	671	B	20
2	702	35.931	-89.98	663	B	400
3	703	35.887	-90.029	686	B	20
4	704	35.985	-90.042	674	B	400
5	705	35.857	-89.979	647	B	400
6	706	35.796	-89.942	657	B	400
7	707	35.785	-90.036	631	B	400
8	708	35.858	-90.074	679	B	400
9	709	35.956	-90.165	628	B	400
10	710	35.911	-90.225	638	B	400
11	711	35.836	-90.176	658	B	400
12	712	35.76	-90.149	698	B	400
13	713	35.895	-89.86	623	B	400
14	714	35.965	-89.819	592	B	400
15	715	35.859	-89.829	707	B	400
16	716	35.792	-89.846	658	B	400
17	717	35.917	-90.917	684	B	400
18	718	35.982	-90.361	701	B	400
19	719	35.847	-90.357	710	B	400
20	720	35.861	-90.404	632	B	400
21	721	35.797	-90.429	676	B	400
22	722	35.907	-90.469	696	B	400
23	723	35.985	-90.487	785	B	400
24	724	35.977	-90.533	859	B	400
25	725	35.903	-90.55	685	B	400
26	726	35.912	-90.711	675	B	400
27	727	35.989	-90.709	1503	B	400
28	728	35.981	-90.8	713	B	400
29	729	35.924	-90.854	751	B	400
30	730	35.84	-90.856	833	B	400
31	731	35.767	-90.786	950	B	400
32	732	35.777	-90.763	756	B	400
33	733	35.767	-90.553	0	B	400
34	734	35.672	-89.964	700	C	20
35	735	35.695	-90.035	595	C	20
36	736	35.726	-90.157	603	C	20
37	737	35.684	-90.22	664	C	20
38	738	35.722	-90.344	698	C	20
39	739	35.659	-90.322	665	C	20
40	740	35.57	-90.341	713	C	20
41	741	35.145	-90.103	626	B	20
42	742	35.193	-90.23	596	B	20
43	743	35.081	-90.222	602	B	20
44	744	35.693	-90.486	743	B	0
45	745	35.706	-90.554	688	B	0
46	746	35.671	-90.606	697	B	0
47	747	35.657	-90.648	782	B	0

48	748	35.655	-90.713	845	B	0
49	749	35.695	-90.833	0	B	0
50	750	35.565	-90.797	840	B	0
51	751	35.402	-90.785	923	B	0
52	752	35.325	-90.812	919	B	0
53	753	35.167	-90.847	883	B	0
54	754	35.067	-90.843	844	B	0
55	755	35.581	-90.972	586	C	20
56	756	35.53	-90.087	612	C	20
57	757	35.575	-90.2	660	C	20
58	758	35.567	-90.384	633	C	20
59	759	35.569	-90.558	695	C	20
60	760	35.583	-90.732	928	C	20
61	761	35.555	-90.948	923	C	20
62	762	35.55	-91.057	751	C	20
63	763	35.518	-91.201	682	C	20
64	764	35.446	-91.199	614	C	20
65	765	35.327	-91.193	761	C	20
66	766	35.582	-91.557	3899	C	20
67	767	35.57	-91.612	1176	C	20
68	768	35.599	-91.324	737	C	20
69	769	35.714	-91.202	725	C	20
70	770	35.815	-91.169	782	C	20
71	771	35.145	-90.686	652	C	20
72	772	35.204	-90.56	684	C	20
73	773	35.551	-90.554	740	C	20
74	774	35.287	-90.706	1152	C	20
75	775	35.354	-90.571	726	C	20
76	776	35.268	-90.447	753	C	20
77	777	35.34	-90.321	649	C	20
78	778	35.264	-90.321	696	C	20
79	779	35.266	-90.202	614	C	20
80	788	35.196	-90.91	895	B	0
81	789	35.193	-91.087	821	B	0
82	790	35.936	-90.663	752	B	0
83	791	35.471	-90.465	720	B	0
84	792	35.451	-90.52	767	B	0
85	793	35.397	-90.417	780	B	0
86	794	35.463	-90.359	774	B	0
87	795	35.453	-90.274	720	B	0
88	796	35.435	-90.208	644	B	0

OBJECTID	OFFSET_2__	OFFSET_3__	OFFSET_4__	ELE___FT_	Shape
1	400	20	400	245	Point
2	20	20	400	248	Point
3	400	20	400	240	Point
4	20	20	400	240	Point
5	20	20	400	239	Point
6	20	20	400	240	Point

7	20	20	400	232	Point
8	20	20	400	239	Point
9	20	20	400	239	Point
10	20	20	400	237	Point
11	20	400	20	231	Point
12	20	400	20	231	Point
13	20	20	400	250	Point
14	20	20	400	256	Point
15	20	400	20	254	Point
16	20	400	20	248	Point
17	20	400	20	236	Point
18	400	20	20	238	Point
19	20	400	20	233	Point
20	20	400	20	229	Point
21	400	20	20	224	Point
22	400	20	20	233	Point
23	400	20	20	247	Point
24	20	400	20	280	Point
25	20	400	20	248	Point
26	20	400	20	311	Point
27	400	20	20	373	Point
28	400	20	20	253	Point
29	400	20	20	248	Point
30	400	20	20	259	Point
31	400	20	20	255	Point
32	400	20	20	237	Point
33	400	20	0	226	Point
34	0	20	0	244	Point
35	0	20	0	235	Point
36	0	20	0	232	Point
37	0	20	0	228	Point
38	0	20	0	223	Point
39	0	20	0	222	Point
40	0	20	0	218	Point
41	20	400	0	210	Point
42	400	20	400	220	Point
43	20	400	0	214	Point
44	240	0	240	221	Point
45	240	0	240	223	Point
46	240	0	240	223	Point
47	240	0	240	225	Point
48	230	0	240	248	Point
49	240	0	240	247	Point
50	240	0	240	245	Point
51	240	0	240	255	Point
52	240	0	240	244	Point
53	240	0	240	224	Point
54	240	0	240	218	Point

55	0	20	0	236	Point
56	0	20	0	225	Point
57	0	20	0	224	Point
58	0	20	0	216	Point
59	0	20	0	214	Point
60	0	20	0	257	Point
61	0	20	0	230	Point
62	0	20	0	230	Point
63	0	20	0	220	Point
64	0	20	0	225	Point
65	0	20	0	208	Point
66	0	20	0	590	Point
67	0	20	0	220	Point
68	0	20	0	222	Point
69	0	20	0	242	Point
70	0	20	0	247	Point
71	0	20	0	220	Point
72	0	20	0	207	Point
73	0	20	0	217	Point
74	0	20	0	255	Point
75	0	20	0	213	Point
76	0	20	0	213	Point
77	0	20	0	216	Point
78	0	20	0	224	Point
79	0	20	0	220	Point
80	240	0	240	219	Point
81	240	0	240	218	Point
82	240	0	240	224	Point
83	240	0	240	213	Point
84	240	0	240	212	Point
85	240	0	240	220	Point
86	240	0	240	220	Point
87	240	0	240	219	Point
88	240	0	240	230	Point

Street–Arkansas sites.

OBJECTID	SITE	LAT	LONG_	V30	ELEVATION_
1	301	36.971	-89.208	572	315
2	302	36.892	-89.221	658	315
3	303	36.897	-89.266	643	315
4	304	36.956	-89.331	606	317
5	305	36.886	-89.484	679	317
6	306	36.958	-89.392	703	326
7	307	36.917	-89.52	707	315
8	308	36.95	-89.608	676	335
9	309	37.054	-89.585	662	330
10	310	37.054	-89.526	819	310
11	311	37.04	-89.457	641	322
12	312	36.903	-89.653	695	305
13	313	36.947	-89.725	591	305
14	314	37.024	-89.701	707	315
15	315	37.096	-89.717	972	325
16	316	37.126	-89.697	972	330
17	317	37.196	-89.705	656	330
18	318	37.126	-89.803	571	325
19	319	37.034	-89.781	558	315
20	320	36.961	-89.814	667	310
21	321	36.89	-89.745	700	305
22	322	36.9	-89.982	983	390
23	323	36.848	-89.351	0	315
24	324	36.849	-89.246	563	305
25	325	36.592	-89.562	665	300
26	326	36.629	-89.596	631	300
27	327	36.716	-89.596	607	300
28	328	36.821	-89.588	754	315
29	329	36.835	-89.538	693	305
30	330	36.483	-89.588	628	290
31	331	36.413	-89.56	550	283
32	332	36.863	-89.705	670	299
33	333	36.786	-89.708	674	291
34	334	36.71	-89.693	653	288
35	335	36.657	-89.71	651	284
36	336	36.67	-89.795	681	285
37	337	36.715	-89.838	683	290
38	338	36.715	-89.921	685	291
39	339	36.764	-89.917	784	295
40	340	36.806	-89.791	704	294
41	341	36.76	-89.47	660	295
42	342	36.848	-89.441	667	310
43	343	36.986	-89.145	618	315

44	344	36.213	-89.7	629	267
45	345	36.14	-89.704	594	265
46	346	36.519	-89.665	606	280
47	347	36.594	-89.798	671	280
48	348	36.603	-89.784	660	280
49	349	36.51	-89.804	565	275
50	350	36.6	-89.951	588	280
51	351	36.514	-89.914	637	270
52	352	36.608	-90.04	738	300
53	353	36.484	-90.022	672	290
54	354	36.392	-90.051	734	280
55	355	36.411	-89.96	642	275
56	356	36.421	-89.659	656	280
57	357	36.482	-89.708	681	275
58	358	36.481	-89.795	694	270
59	359	36.416	-89.821	679	265
60	360	36.481	-89.898	609	270
61	361	36.345	-90.05	692	275
62	362	36.276	-90.042	685	260
63	363	36.273	-89.935	710	255
64	364	36.355	-89.879	643	260
65	365	36.335	-89.769	677	270
66	366	36.236	-89.844	710	260
67	367	36.21	-89.942	667	250
68	368	36.139	-89.83	665	260
69	369	36.096	-89.692	578	260
70	370	36.036	-89.789	621	260
71	371	36.102	-89.822	653	260
72	372	36.046	-89.902	648	250
73	373	36.103	-89.963	661	250
74	374	36.154	-89.983	679	250
75	375	36.289	-90.016	616	250
76	376	36.134	-90.07	711	255
77	377	36.149	-90.165	633	255
78	378	36.103	-90.245	688	250
79	379	36.025	-90.287	650	245
80	380	36.04	-90.213	650	245
81	381	36.085	-90.114	667	250
82	382	36.063	-90.031	646	243
83	383	36.35	-89.693	685	275
84	384	36.274	-89.791	651	265
85	385	36.598	-89.449	585	290
86	386	36.677	-89.445	638	295
87	387	36.726	-89.387	649	295

88	388	36.675	-89.303	624	300
89	389	36.611	-89.52	689	295
90	390	37.157	-89.53	1045	385
91	391	37.015	-89.617	842	370
92	392	37.093	-89.895	842	360
93	393	36.776	-90.041	807	340
94	394	36.71	-90.079	693	325
95	395	36.562	-90.088	794	340
96	396	36.214	-90.112	674	260
97	397	36.766	-89.176	667	310
98	398	36.772	-89.274	661	300
99	399	36.667	-89.207	600	300
100	400	36.946	-89.221	0	316

OBJECTID	DATE_	TOPO	ARRAY	OFFSET_1	OFFSET_2
1	21-May-96	Wyatt	A	20	220
2	21-May-96	Wyatt	A	20	220
3	21-May-96	Charleston	A	20	200
4	21-May-96	Charleston	A	20	200
5	21-May-96	Bertrand	A	20	200
6	21-May-96	Bertrand	A	20	200
7	21-May-96	Sikeston N	A	20	200
8	21-May-96	Sikeston N	A	20	200
9	22-May-96	Morley	A	20	200
10	22-May-96	Morley	A	20	200
11	22-May-96	Thebes	A	20	200
12	27-Jun-96	Vanduser	A	20	200
13	27-Jun-96	Vanduser	A	20	200
14	28-Jun-96	Oran	A	20	200
15	28-Jun-96	Oran	A	20	200
16	28-Jun-96	Chaffee	A	20	200
17	28-Jun-96	Chaffee	A	20	200
18	28-Jun-96	White Water	A	20	200
19	28-Jun-96	Bell City	A	20	200
20	28-Jun-96	Clines Island	A	20	200
21	28-Jun-96	Clines Island	A	20	200
22	28-Jun-96	Bloomfield	A	20	200
23	29-Jun-96	Anniston	A	20	200
24	29-Jun-96	Wickliffe SW	A	20	200
25	16-Jul-96	New Madrid	A	20	200
26	16-Jul-96	Kewanee	A	20	200
27	16-Jul-96	Kewanee	A	20	240
28	16-Jul-96	Sikeston S	A	20	200
29	16-Jul-96	Sikeston S	A	20	200
30	17-Jul-96	Point	A	20	200

		Pleasant			
31	17-Jul-96	Point Pleasant	A	20	200
32	31-Jul-96	Morehouse	A	20	200
33	31-Jul-96	Morehouse	A	20	200
34	31-Jul-96	Charter Oak	A	20	200
35	31-Jul-96	Charter Oak	A	20	200
36	31-Jul-96	Hills Store	A	20	200
37	31-Jul-96	Hills Store	A	20	200
38	31-Jul-96	Bernie	A	20	200
39	31-Jul-96	Dexter	A	20	200
40	31-Jul-96	Essex	A	20	200
41	01-Aug-96	East Prairie	A	20	200
42	01-Aug-96	East Prairie	A	20	200
43	01-Aug-96	Wyatt	A	20	200
44	05-Aug-96	Caruthersville	A	20	200
45	05-Aug-96	Caruthersville	A	20	200
46	06-Aug-96	Catron	A	20	200
47	06-Aug-96	Catron	A	20	200
48	06-Aug-96	Parma	A	20	200
49	06-Aug-96	Parma	A	20	200
50	06-Aug-96	Malden	A	20	200
51	06-Aug-96	Malden	A	20	200
52	06-Aug-96	Valley Ridge	A	20	200
53	06-Aug-96	Campbell	A	20	200
54	06-Aug-96	Campbell	A	20	200
55	06-Aug-96	Gideon	A	20	200
56	07-Aug-96	Portageville	A	20	200
57	07-Aug-96	Portageville	A	20	200
58	07-Aug-96	Boekerton	A	20	200
59	07-Aug-96	Boekerton	A	20	200
60	07-Aug-96	Gideon	A	20	200
61	07-Aug-96	Kenneth N	A	20	200
62	07-Aug-96	Kenneth N	A	20	200
63	07-Aug-96	Bragg City	A	20	200
64	07-Aug-96	Bragg City	A	20	200
65	07-Aug-96	Wardell	A	20	200
66	08-Aug-96	Hayti Heights	A	20	200
67	08-Aug-96	Deering	A	20	200
68	08-Aug-96	Hayti Heights	A	20	200
69	12-Aug-96	Cottonwood Point	A	20	200
70	12-Aug-96	Steele	A	20	200
71	12-Aug-96	Steele	A	20	200
72	12-Aug-96	Denton	A	20	200

73	12-Aug-96	Denton	A	20	200
74	12-Aug-96	Deering	A	20	200
75	13-Aug-96	Kennett S	A	20	200
76	13-Aug-96	Kennett S	A	20	200
77	13-Aug-96	Senath	A	20	200
78	13-Aug-96	Arbyrd	A	20	200
79	13-Aug-96	Cardwell	A	20	200
80	13-Aug-96	Arbyrd	A	20	200
81	13-Aug-96	Homersville	A	20	200
82	13-Aug-96	Homersville	A	20	200
83	13-Aug-96	Stanley	A	20	200
84	13-Aug-96	Wardell	A	20	200
85	14-Aug-96	Hubbard Lake	A	20	200
86	14-Aug-96	Henderson Mound	A	20	200
87	14-Aug-96	Henderson Mound	A	20	200
88	14-Aug-96	Bayouville	A	20	200
89	26-Aug-96	New Madrid	A	20	200
90	26-Aug-96	Scott City	A	20	200
91	26-Aug-96	Scott City	A	20	200
92	26-Aug-96	Advance	A	20	200
93	27-Aug-96	Dudley	A	20	200
94	27-Aug-96	Powe	A	20	200
95	27-Aug-96	Valley Ridge	A	20	200
96	27-Aug-96	Kennett S	A	20	200
97	26-Aug-96	Wickliffe SW	A	20	200
98	26-Aug-96	Anniston	A	20	200
99	26-Aug-96	Wolf Island	A	20	200
100	02-Jul-98	Wyatt	A	20	200

OBJECTID	OFFSET_3	OFFSET_4	OFFSET_5	Shape
1	420			Point
2	420	620	820	Point
3	400	600	800	Point
4	400	600	800	Point
5	400	600	800	Point
6	400	600	800	Point
7	400	600	800	Point
8	400	600	800	Point
9	400	600	800	Point
10	400	600	800	Point
11	400	600	800	Point
12	400	600	800	Point
13	400	600	800	Point

14	400	600		Point
15	400	600		Point
16	400	600		Point
17	400	600		Point
18	400	600		Point
19	400	600		Point
20	400	600		Point
21	400	600		Point
22	400			Point
23	400	600		Point
24	400	600	800	Point
25	400	600	800	Point
26	400	600	800	Point
27	460	680		Point
28	400	600	800	Point
29	400	600	800	Point
30	400	600	800	Point
31	400	600	800	Point
32	400	600	800	Point
33	400	600	800	Point
34	400	600	800	Point
35	400	600	800	Point
36	400	600	800	Point
37	400	600	800	Point
38	400	600	800	Point
39	400	600	800	Point
40	400	600	800	Point
41	400	600	800	Point
42	400	600	800	Point
43	400	600	800	Point
44	400	600	800	Point
45	400	600	800	Point
46	400	600	800	Point
47	400	600	800	Point
48	400	600	800	Point
49	400	600	800	Point
50	400	600	800	Point
51	400	600	800	Point
52	400	600	800	Point
53	400	600	800	Point
54	400	600	800	Point
55	400	600	800	Point
56	400	600	800	Point
57	400	600	800	Point

58	400	600	800	Point
59	400	600	800	Point
60	400	600	800	Point
61	400	600	800	Point
62	400	600	800	Point
63	400	600	800	Point
64	400	600	800	Point
65	400	600	800	Point
66	400	600	800	Point
67	400	600	800	Point
68	400	600	800	Point
69	400	600	800	Point
70	400	600	800	Point
71	400	600	800	Point
72	400	600	800	Point
73	400	600	800	Point
74	400	600	800	Point
75	400	600	800	Point
76	400	600	800	Point
77	400	600	800	Point
78	400	600	800	Point
79	400	600	800	Point
80	400	600	800	Point
81	400	600	800	Point
82	400	600	800	Point
83	400	600	800	Point
84	400	600	800	Point
85	400	600	800	Point
86	400	600	800	Point
87	400	600	800	Point
88	400	600	800	Point
89	400	600	800	Point
90	400	600	800	Point
91	400	600	800	Point
92	400	600	800	Point
93	400	600		Point
94	400	600	800	Point
95	400	600	800	Point
96	400	600	800	Point
97	400	600	800	Point
98	400	600	800	Point
99	400	600	800	Point
100	400	600	800	Point

Street–Missouri sites.

OBJECTID	SITE	LAT	LONG_	V30	DATE_	TOPO
1	501	36.482	-89.233	610	13-May-96	Clayton
2	502	36.391	-89.136	853	13-May-96	Clayton
3	503	36.191	-89.439	614	14-Oct-96	Miston
4	504	36.315	-89.417	707	14-Oct-96	Ridgely
5	505	36.466	-89.083	771	03-Jan-97	Union City
6	506	36.467	-88.951	1173	03-Jan-97	Harris
7	507	36.417	-88.891	983	03-Jan-97	Harris
8	508	36.382	-89.092	873	31-Jan-97	Union City
9	509	36.446	-88.836	983	01-Feb-97	McConnell
10	510	36.398	-88.79	786	01-Feb-97	McConnell
11	511	36.465	-88.744	1134	01-Feb-97	Latham
12	512	36.441	-88.666	1107	01-Feb-97	Latham
13	513	36.469	-88.556	867	01-Feb-97	Palmersville
14	514	36.393	-88.344	1108	19-Mar-97	Puryear
15	515	36.433	-88.446	0	19-Mar-97	Cottage Grove
16	516	36.385	-88.571	0	19-Mar-97	Palmersville
17	517	36.36	-88.655	999	19-Mar-97	Dresden
18	518	36.345	-88.21	1138	20-Mar-97	Obion
19	519	36.29	-89.166	784	20-Mar-97	Obion
20	520	36.427	-89.028	644	20-Mar-97	Rives
21	521	36.354	-89.016	773	20-Mar-97	Rives
22	522	36.335	-88.883	923	20-Mar-97	Gardner
23	523	36.284	-88.967	723	20-Mar-97	Gardner
24	524	36.23	-88.926	743	20-Mar-97	Rutherford
25	525	36.216	-89.167	950	21-Mar-97	Trimble
26	526	36.145	-89.219	680	21-Mar-97	Trimble
27	527	36.154	-89.088	751	21-Mar-97	Kenton
28	528	36.23	-89.073	631	21-Mar-97	Kenton
29	530	36.34	-88.19	961	11-Jun-97	W Sandy Dike
30	531	36.29	-88.21	1243	11-Jun-97	W Sandy Dike
31	532	36.23	-88.16	991	11-Jun-97	Manleyville
32	533	36.17	-88.18	897	11-Jun-97	Manleyville
33	534	36.12	-88.152	1011	12-Jun-97	Bruceton
34	535	36.338	-88.3	964	12-Jun-97	Paris
35	536	36.267	-88.37	1173	12-Jun-97	Paris
36	537	36.298	-88.4	1119	12-Jun-97	Osage
37	538	36.349	-88.468	981	12-Jun-97	Osage
38	539	36.365	-88.539	1075	12-Jun-97	Como
39	540	36.268	-88.61	814	12-Jun-97	Como
41	542	36.26	-88.77	918	12-Jun-97	Martin
42	543	36.34	-88.83	879	12-Jun-97	Martin

43	544	36.23	-88.86	831	12-Jun-97	Greenfield
44	545	36.167	-88.917	707	12-Jun-97	Rutherford
45	546	36.163	-88.82	1093	13-Jun-97	Greenfield
46	547	36.234	-88.32	966	13-Jun-97	Mansfield
47	548	36.153	-88.3	1410	13-Jun-97	Mansfield
48	549	36.08	-88.367	1254	13-Jun-97	Vale
49	550	36.02	-88.27	939	13-Jun-97	Vale
50	551	36.167	-88.505	919	30-Jul-97	McKenzie
51	552	36.167	-88.436	919	30-Jul-97	Henry
52	553	35.042	-89.796	640	01-Oct-97	Germantown
53	554	35.248	-89.766	669	01-Oct-97	Ellendale
54	555	36.182	-89.307	672	27-Feb-98	Lane
55	556	36.052	-89.32	629	27-Feb-98	Newbern
56	557	36.063	-89.503	725	28-Feb-98	Caruthersville SE
57	558	36.029	-89.483	747	28-Feb-98	Dyersburg
58	559	36.158	-89.459	773	27-Feb-98	Miston
59	560	36.205	-89.366	697	27-Feb-98	Lane
60	561	35.321	-89.667	847	19-Jun-98	Arlington
61	562	35.322	-89.551	930	19-Jun-98	Gallaway
62	563	36.104	-88.97	836	14-Jul-98	Dyer
63	564	36.042	-88.881	940	14-Jul-98	Dyer
64	565	35.938	-88.958	1136	14-Jul-98	Trenton
65	566	35.796	-88.945	1130	14-Jul-98	Humboldt
66	567	35.627	-88.948	915	15-Jul-98	Adair
67	568	35.536	-88.939	1088	15-Jul-98	Westover
68	569	35.735	-88.377	1094	15-Jul-98	Lexington
69	570	35.921	-89.329	695	06-Aug-98	Bonicord
70	571	35.592	-89.04	1293	02-Oct-98	Denmark
71	572	35.505	-89.11	1140	02-Oct-98	Denmark
72	573	35.544	-89.183	1038	02-Oct-98	Sunnyhill
73	574	35.537	-89.343	1344	02-Oct-98	Brownsville
74	575	35.532	-89.343	1185	02-Oct-98	Brownsville
75	576	35.579	-89.467	1342	02-Oct-98	Turnpike
76	577	35.539	-89.545	847	02-Oct-98	Gift
77	578	35.591	-89.582	679	02-Oct-98	Gift
78	579	35.683	-89.555	840	03-Oct-98	Ripley S
79	580	35.785	-89.504	705	03-Oct-98	Ripley N
80	581	35.857	-89.592	741	03-Oct-98	Ripley N
81	582	35.906	-89.405	667	03-Oct-98	Fowlkes
82	583	35.185	-89.063	1043	15-Jul-98	Middlesburg

OBJECTID	ELEVATION_	ARRAY	OFFSET_1	OFFSET_2
1	325	A	20	200
2	369	A	20	200

3	275	A	20	200
4	285	A	20	200
5	376	C	0	0
6	360	B	20	400
7	329	B	20	400
8	345	C	0	0
9	350	C	0	0
10	340	C	0	0
11	435	C	0	200
12	380	C	0	0
13	410	C	0	0
14	550	C	0	0
15	425	C	0	0
16	480	C	0	400
17	380	C	0	0
18	400	C	0	0
19	299	C	400	0
20	290	C	0	400
21	310	C	0	0
22	330	C	0	0
23	300	C	0	0
24	300	C	0	0
25	323	C	0	0
26	300	C	0	0
27	350	C	0	0
28	340	C	0	400
29	370	C	0	0
30	450	C	0	0
31	510	C	0	0
32	387	C	0	0
33	396	C	0	0
34	430	C	0	0
35	480	C	0	0
36	465	C	0	0
37	510	C	0	0
38	440	C	0	0
39	355	C	0	0
41	405	C	0	0
42	385	C	0	0
43	395	C	0	0
44	310	C	0	0
45	385	C	0	0
46	460	C	0	0
47	485	C	0	0

48	415	C	0	0
49	510	C	0	0
50	460	C	4	0
51	540	C	4	0
52	300	B	20	400
53	300	B	20	400
54	280	B	20	320
55	283	B	20	320
56	280	B	20	320
57	270	B	20	320
58	272	B	20	320
59	300	B	20	320
60	270	C	20	0
61	295	C	20	0
62	326	C	20	0
63	353	C	20	0
64	372	C	0	20
65	340	C	20	0
66	390	C	20	0
67	480	C	20	0
68	500	C	20	20
69	280	B	0	96
70	410	B	0	400
71	340	B	0	400
72	320	B	0	400
73	370	B	0	400
74	350	B	0	400
75	300	B	0	400
76	280	B	0	400
77	270	B	0	400
78	300	B	0	400
79	350	B	0	400
80	250	B	0	400
81	290	B	0	400
82	500		20	140

Street–Tennessee sites.

OBJECTID	SITE	SOIL TYPE	LAT	LONG	V_{30} (m/s)	LAYER 1 (m)
1	1	Qfo	38.641	-83.73	295.1002	24
2	2	Qfo	38.644	-83.737	262.9146	22
3	3	Qfo	38.644	-83.752	384.8595	21
4	4	Qfo	38.645	-83.76	382.4179	20
5	5	Qfm	38.637	-83.732	435.7905	14
6	6	Qwo	38.641	-83.753	372.8813	8
7	7	Qfm	38.641	-83.742	388.1296	7
8	8	Qfm	38.639	-83.747	427.1646	5
9	9	Qfm	38.637	-83.741	385.6809	3
10	10	Qwo	38.643	-83.734	254.4409	4
11	11	Sharpsburg	38.201	-83.924	558.8298	5

OBJECTID	LAYER 2 (m)	VEL 1 (m/s)	VEL 2 (m/s)	VEL 3 (m/s)	BED VEL (m/s)	Layer 3 (m)
1		250			1060	
2		211			813	
3		300			1132	
4		284			1246	
5		283			826	
6	20	240	440		1200	
7	13	177	455		1090	
8	7	123	456		1265	
9	9	146	250	620	1200	8
10	14	130	191	720	1090	6
11		170			1030	

Lin–Maysville, KY, sites.

OBJECTID	SITE	LAT	LONG_	V30	NEHRP_SITE	ELEVATION_
1	1	35.379	-90.03	198	D	68.6
2	2	35.381	-90.066	200	D	70.1
3	3	35.32	-90.05	272	D	105.2
4	4	35.284	-90.049	0	*	91.5
5	5	35.338	-89.954	220	D	76.2
6	6	35.279	-89.942	223	D	73.2
7	7	35.333	-89.89	0	D	83.8
8	8	35.293	-89.846	270	D	77.7
9	9	35.286	-89.762	216	D	76.2
10	10	35.321	-89.667	252	D	82.3
11	11	35.195	-90.219	199	D	67.1
12	12	35.193	-90.23	180	D	67.1
13	13	35.24	-90.115	205	D	67.7
14	14	35.145	-90.103	193	D	64
15	15	35.156	-90.057	188	D	62.5
16	16	35.241	-90.013	266	D	70.1
17	17	35.196	-89.986	225	D	68.6
18	18	35.22	-89.969	238	D	97.6
19	19	35.161	-89.92	181	D	77.7
20	20	35.192	-89.909	266	D	71.6
21	21	35.188	-89.87	256	D	77.7
22	22	35.169	-89.856	0	*	77.7
23	23	35.158	-89.849	344	D	86.9
24	24	35.132	-89.812	204	D	83.8
25	25	35.209	-89.8	292	D	89.9
26	26	35.167	-89.755	0	*	99.1
27	27	35.248	-89.766	209	D	91.5
28	28	35.201	-89.65	0	*	103.5
29	29	35.029	-90.338	199	D	62.5
30	30	35.081	-90.227	181	D	65.2
31	31	35.005	-90.113	213	D	71.6
32	32	35.034	-90.068	0	*	74.7
33	33	35.058	-90.002	264	D	75
34	34	35.125	-89.983	0	*	93
35	35	35.035	-89.966	326	D	88.4
36	36	35.05	-89.91	0	*	89.9
37	37	35.083	-89.904	315	D	80.8
38	38	35.023	-89.884	0	*	93
39	39	35.076	-89.857	263	D	83.8
40	40	35.061	-89.834	210	D	88.4
41	41	35.079	-89.903	287	D	115.9
42	42	35.042	-89.796	217	D	91.5
43	43	35.031	-89.763	0	*	93

44	44	35.19	-89.655	0	*	93
45	45	35.02	-89.652	0	*	112.8
46	46	34.958	-90.185	194	D	62.8
47	47	34.894	-90.167	187	D	64
48	48	34.977	-90.118	304	D	93
49	49	34.961	-90.009	218	D	82.3
50	50	34.94	-89.958	0	*	99.1
51	51	34.971	-90.118	0	*	117.4
52	52	34.991	-89.854	0	*	112.8
53	53	34.959	-89.856	0	*	99.9
54	54	34.957	-89.835	0	*	120.4
55	55	34.984	-89.799	0	*	123.5
56	56	34.9	-89.795	0	*	89.9
57	57	34.828	-90.334	173	E	61.9
58	58	34.847	-90.293	193	D	62.2
59	59	34.822	-90.234	189	D	59.5
60	60	34.847	-90.227	179	E	61
61	61	34.861	-90.203	205	D	61
62	62	34.803	-90.149	258	D	73.2
63	63	34.83	-90.085	237	D	80
OBJECTID	**L1__M_**	**L2__M_**	**L3__M_**	**L4__M_**	**V1__M_S_**	**V2__M_S_**
1	11	31	88		165	224
2	15	65	0		134	397
3	10	33	0		192	344
4	11	16	0		165	480
5	7	19	0		125	294
6	10	9	31		136	291
7	10	21	0		152	498
8	8	16	30		172	321
9	4	7	19	36	127	215
10	9	19	20		198	282
11	5	11	36	36	130	189
12	15	20	26		133	299
13	27	39	0		195	388
14	8	25	0		153	213
15	9	19	37		163	195
16	7	9	17	24	171	258
17	15	31	0		175	315
18	10	17	29		157	304
19	24	64	0		155	562
20	6	6	23	23	161	265
21	9	22	0		160	350
22	18	0	0		154	380
23	9	12	19		211	396

24	24	23	0		182	449
25	9	25	30		203	353
26	9	0	0		151	291
27	28	0	0		206	392
28	21	0	0		288	426
29	11	23	0		161	227
30	7	30	0		152	192
31	17	26	27		166	350
32	7	12	0		131	366
33	9	15	14		165	286
34	8	10	0		233	371
35	9	48	0		195	443
36	6	12	0		145	303
37	11	23	0		176	582
38	10	0	0		192	312
39	4	10	30		148	273
40	32	0	0		210	544
41	12	25	0		187	445
42	8	11	0		174	219
43	6	0	0		208	974
44	13	13	0		161	449
45	2	7	0		142	373
46	4	26	25	19	168	197
47	7	23	27		142	207
48	8	30	0		180	430
49	10	15	18		142	268
50	9	0	0		288	488
51	9	13	0		269	472
52	8	0	0		237	548
53	3	6	0		176	273
54	4	0	0		187	551
55	4	12	0		182	528
56	11	0	0		318	702
57	8	20	0		149	186
58	11	39	0		143	242
59	15	30	58		139	285
60	17	32	0		148	232
61	17	18	30		170	281
62	18	20	0		203	375
63	17	27	0		197	324

OBJECTID	V3__M_S_	V4__M_S_	V5__M_S_
1	536		
2	0		
3	494		

4	0		
5	490		
6	363	612	
7	579		
8	406	495	
9	254	348	613
10	383	499	
11	266	516	
12	464	547	
13	0		
14	484		
15	305	536	
16	377	448	
17	575		
18	475		
19	1165		
20	340	483	
21	427		
22	0		
23	602		
24	546		
25	496		
26	0		
27	0		
28	0		
29	472		
30	508		
31	492		
32	0		
33	379	475	
34	473		
35	0		
36	472		
37	0		
38	0		
39	336		
40	0		
41	659		
42	267		
43	0		
44	0		
45	478		
46	405	565	680
47	302		

48	571		
49	409	555	
50	0		
51	0		
52	0		
53	403		
54	0		
55	737		
56	0		
57	398		
58	599		
59	607	937	
60	580		
61	468	599	
62	486		
63	587		

Wood–Memphis, TN, sites.

OBJECTID	SITE	LAT	LONG_	V30	DEPTH_TO_B	H_LAYER_1_	H_LAYER_2_
1	1	37.746	-88.337	705.56	11	2	9
2	2	37.751	-88.36	753.00	7.5	7.5	0
3	3	37.755	-88.36	753.83	7	7	0
4	4	37.755	-88.36	753.83	7	7	0
5	5	37.758	-88.377	849.89	4.5	4.5	0
6	6	37.758	-88.377	849.89	4.5	4.5	0
7	7	37.759	-88.379	674.56	8	2	6
8	10	37.788	-89.125	278.74	27	3.5	23.5
9	11	37.788	-89.13	485.63	18.5	3	15.5
10	12	38.128	-87.358	675.17	0	2	0
11	13	38.12	-87.356	748.70	16	3.5	12.5
12	14	38.226	-87.391	753.29	14	4	10
13	15	38.226	-87.391	753.29	14	4	10
14	16	38.09	-87.281	832.07	6	3	3
15	20	38.253	-87.35	932.74	6.5	1.5	5
16	21	38.363	-87.365	250.26	25.5	1.5	5
17	22	38.335	-87.455	580.19	3.5	3.5	0
18	25	38.284	-87.363	730.34	10	2	8
19	26	38.336	-87.445	388.93	13	5	8
20	30	38.304	-87.35	434.82	8	1.8	6.2
21	31	38.337	-87.341	314.29	21	1.5	3.5
22	32	38.353	-87.293	779.94	4	4	0
23	33	38.352	-87.282	705.01	2.5	2.5	0
24	34	38.352	-87.275	883.06	4.5	1.5	3
25	35	38.353	-87.278	690.11	16	2.5	13.5
26	36	38.352	-87.275	883.06	4.5	1.5	3
27	37	38.167	-86.945	1043.82	15	1	2
28	38	37.926	-87.708	774.24	11.5	3	8.5
29	39	38.765	-87.435	678.97	4.5	4.5	0
30	41	38.801	-87.473	580.12	14	2	12
31	42	38.605	-87.011	594.84	0	3	0

OBJECTID	H_LAYER_3_	VELOCITY_1	VEL_2__M_S	VEL_3__M_S	VEL_4__M_S
1		259	498	1136	
2		289	1620	0	
3		282	1536	0	
4		282	1536	0	
5		256	1439	0	
6		256	1439	0	
7		142	287	2109	
8		146	291	1035	
9		156	428	1817	
10		201	812	0	
11		232	761	1636	

12		232	781	1636	
13		232	781	1636	
14		216	630	1379	
15		174	721	1415	
16	19	127	179	243	2318
17		137	1013	0	
18		149	713	1217	
19		158	437	1080	
20		127	182	1060	
21	16	127	181	278	1333
22		355	956	0	
23		159	1025	0	
24		167	766	1210	
25		157	669	1900	
26		167	766	1210	
27	12	256	400	1038	1813
28		208	636	1688	
29		202	1164	0	
30		208	372	1626	
31		219	735	0	

Woolery–Wabash Valley sites.

OBJECTID	SITE	LAT	LONG_	V30	VS2__M_S_	VS3__M_S_
1	LOU01	38.245	-85.638	1195.99	4118	
2	LOU02	38.287	-85.687	368.94	253	1899
3	LOU03	38.36	-85.633	275.38	592	
4	LOU04	38.313	-85.643	257.98	277	446
5	LOU05	38.268	-85.722	186.39	232	
6	LOU06	38.238	-85.74	600.91	825	
7	LOU07	38.162	-85.703	857.05	1498	
8	LOU08	38.181	-85.67	981.8	2310	
9	LOU09	38.261	-85.83	251.41	265	
10	LOU10	38.24	-85.781	253.56	272	
11	LOU11	38.245	-85.825	345.3	439	
12	LOU12	38.183	-85.86	270	378	
13	LOU13	38.155	-85.895	290.3	330	
14	LOU14	38.213	-85.777	246.9	265	
15	LOU15	38.198	-85.82	254.19	310	

OBJECTID	DEPTH1__M_	DEPTH2__M_
1	7	
2	3	18
3	18	
4	6	21
5	5	
6	6	
7	5	
8	3	
9	3	
10	4	
11	10	
12	15	
13	10	
14	4	
15	9	

Wang–Louisville, KY, sites.

Appendix B

The following maps show the results from interpolation of both the DSP and V_{30} attributes using each of the applicable techniques available in Geostatistical Analyst 9.1. The prediction error statistics for each map are included. It is evident that interpolation of DSP values was successful; each of the derivative maps have RMS values less than 1. The interpolation of the V_{30} attribute, however, was unsuccessful for all techniques. RMS values for V_{30} derivative maps ranged from 79 to over 100, a few orders of magnitude higher than those achieved by interpolation of the DSP attribute.

DSP Interpolated Maps

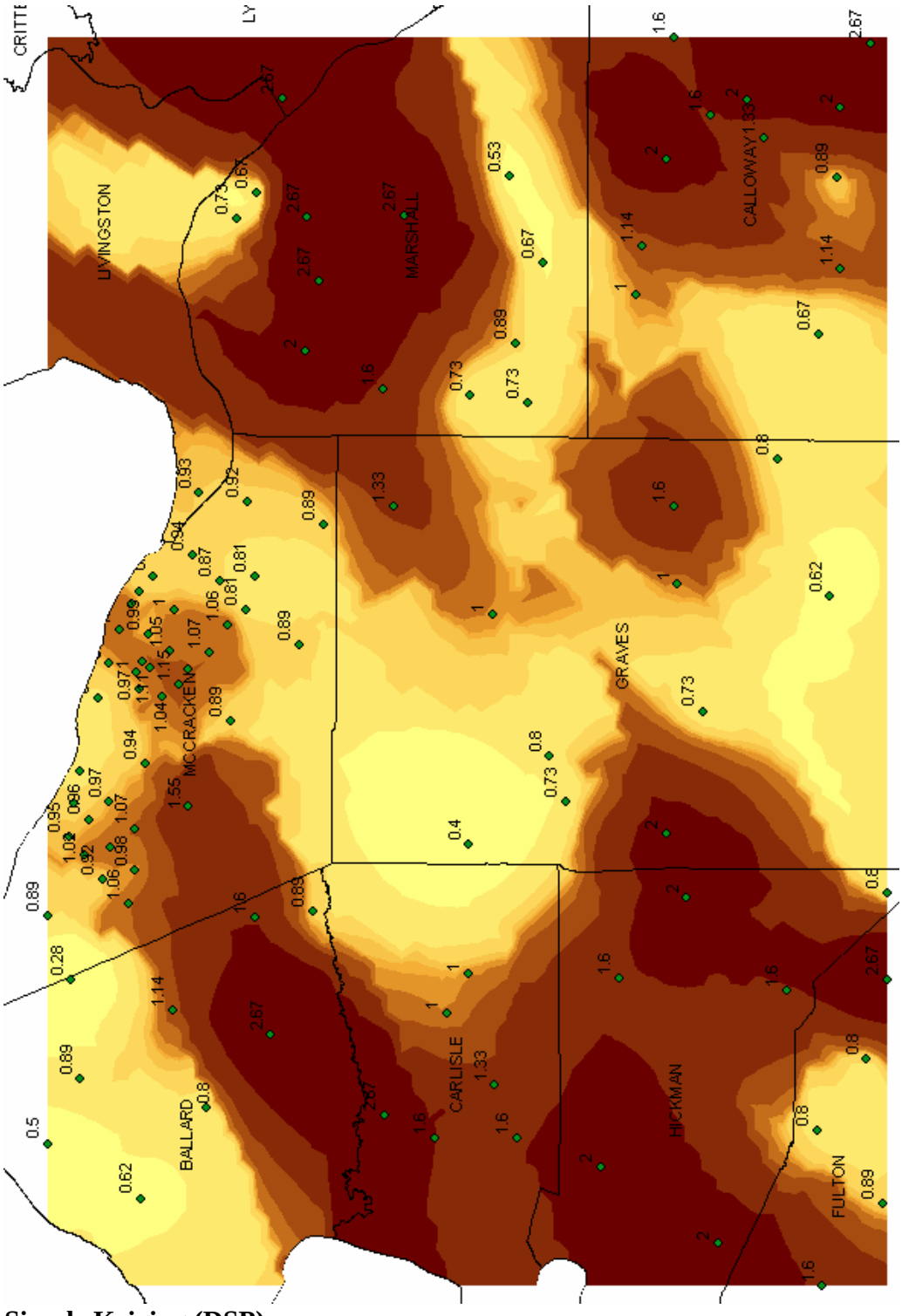

Simple Kriging (DSP)

Mean:	-0.008543
Root-Mean-Square:	0.4149
Average Standard Error:	0.2829
Mean Standardized:	-0.02485
Root-Mean-Square Standardized:	1.369

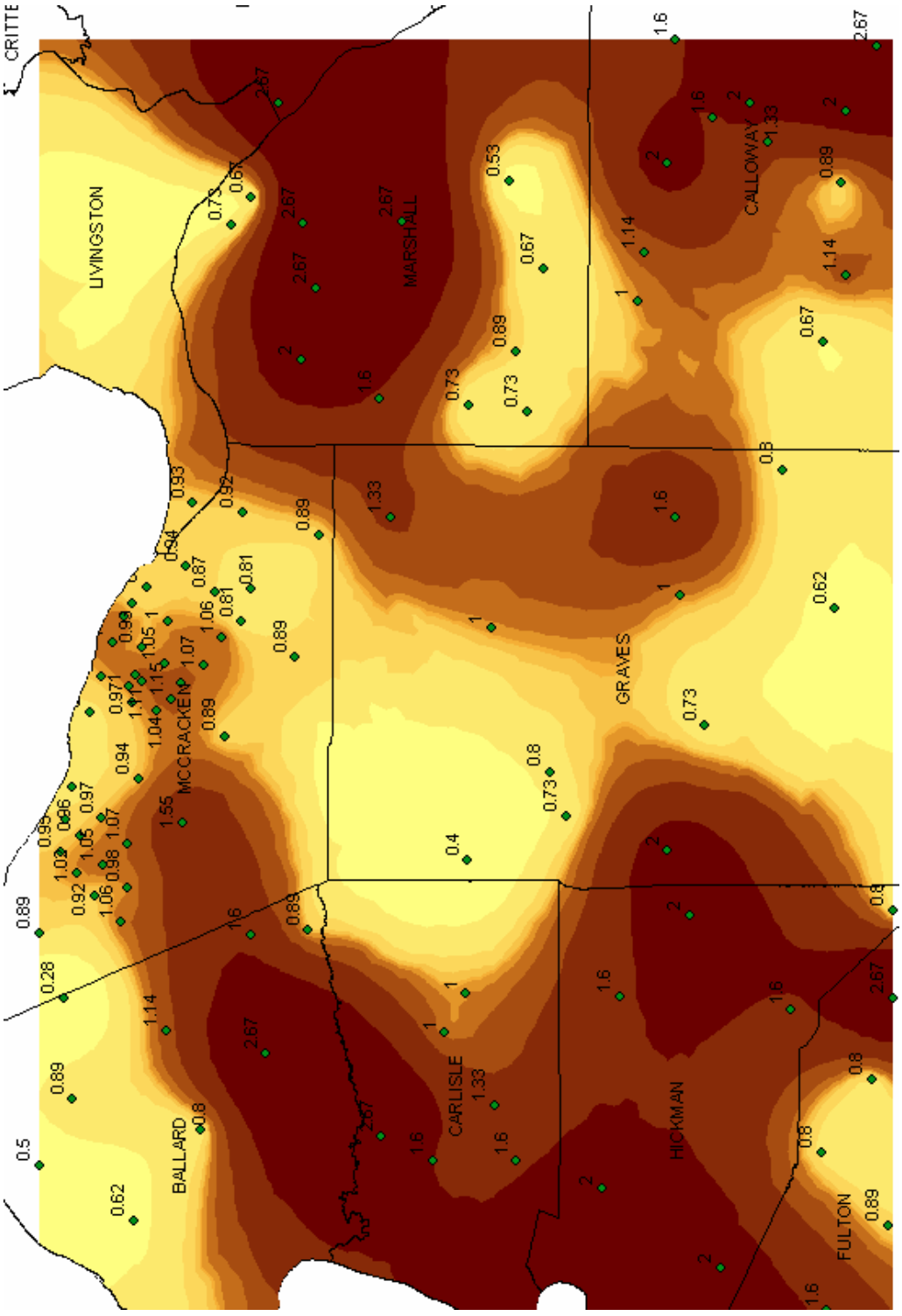

Simple Cokriging (DSP)

Mean:	0.0007828
Root-Mean-Square:	0.3787
Average Standard Error:	0.2761
Mean Standardized:	0.004697
Root-Mean-Square Standardized:	1.221

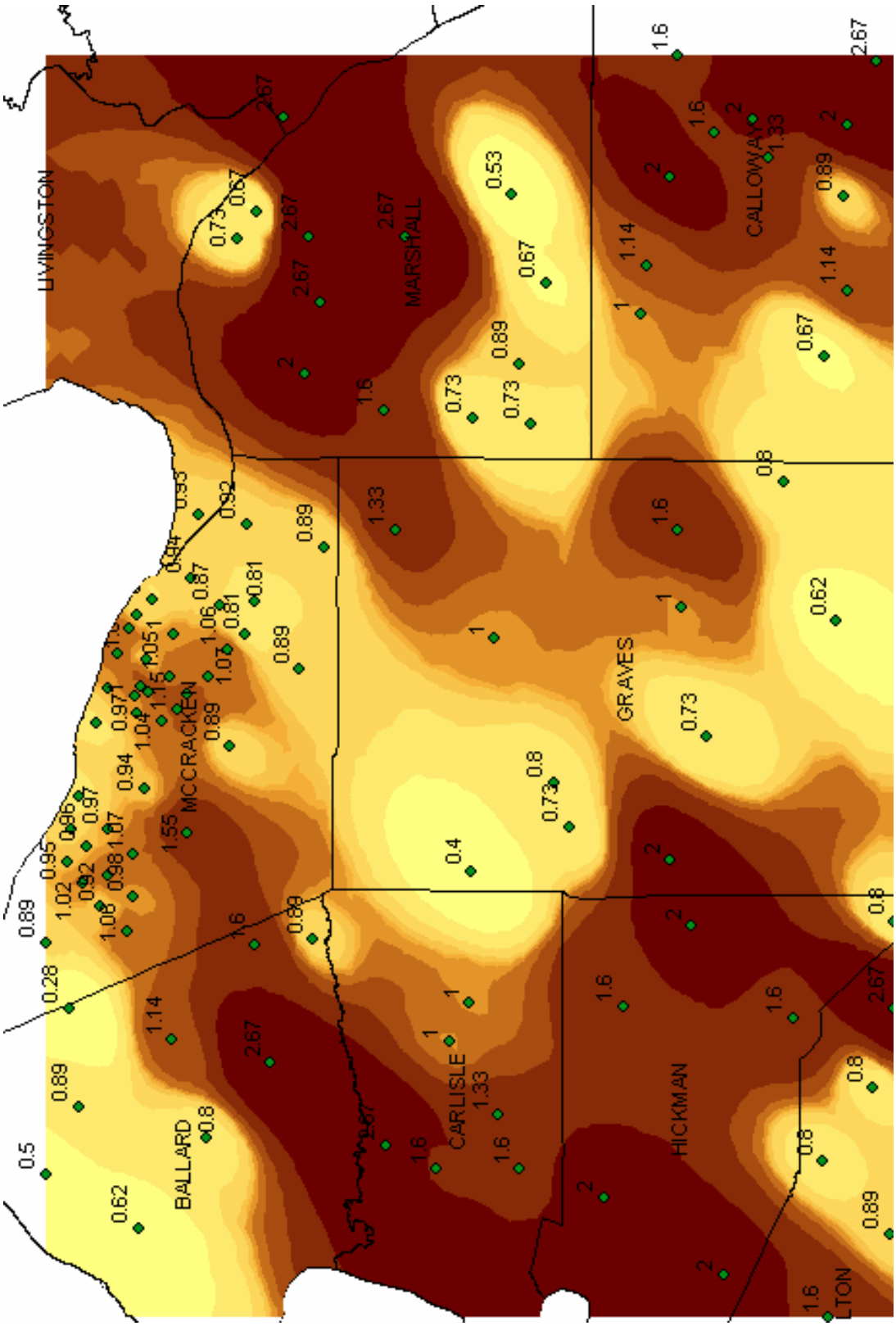

Inverse Distance Weighted (DSP)

Mean: -0.01489

Root-Mean-Square: 0.4577

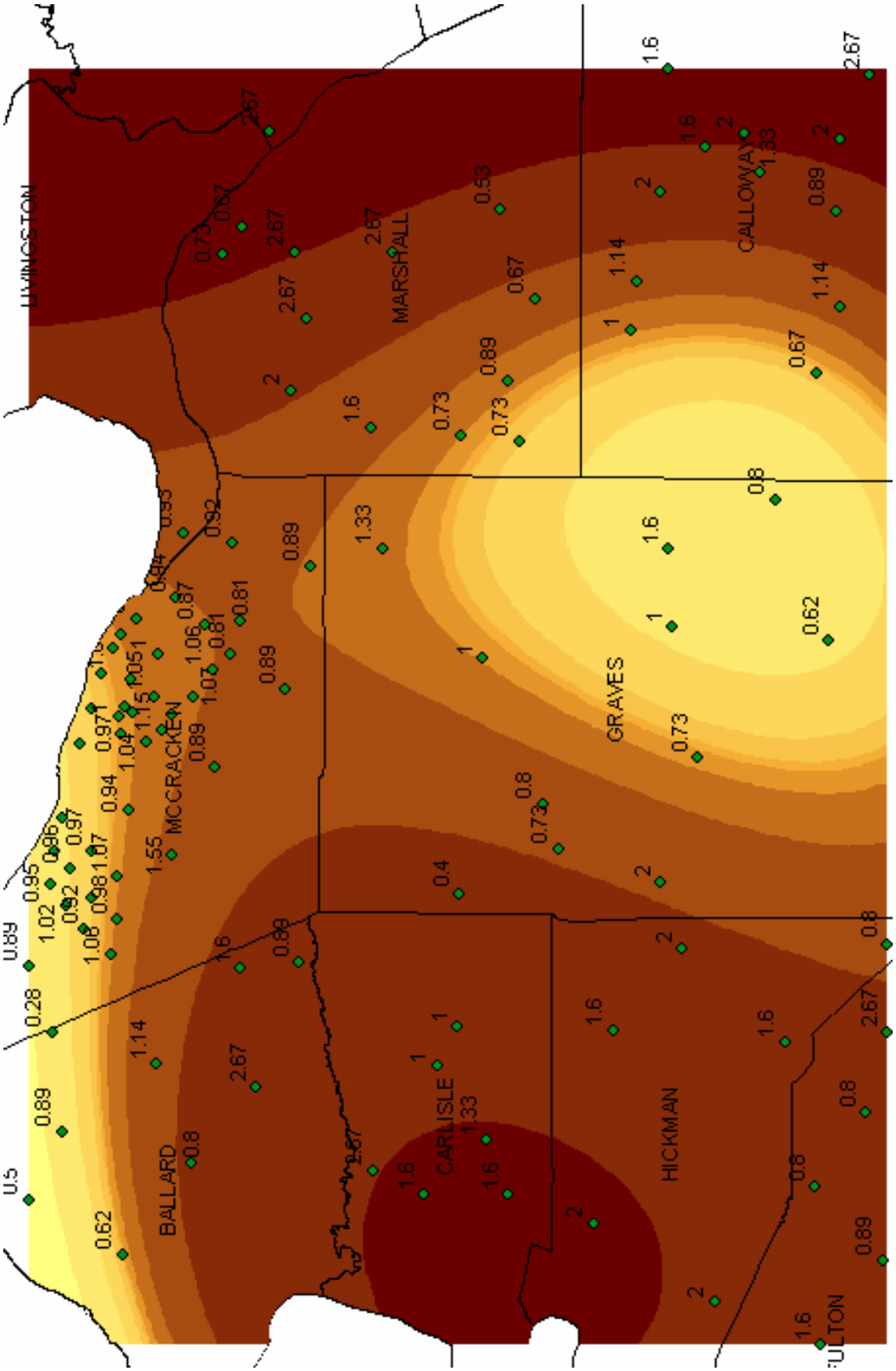

Global Polynomial (DSP)

Mean:	0.001094
Root-Mean-Square:	0.5298

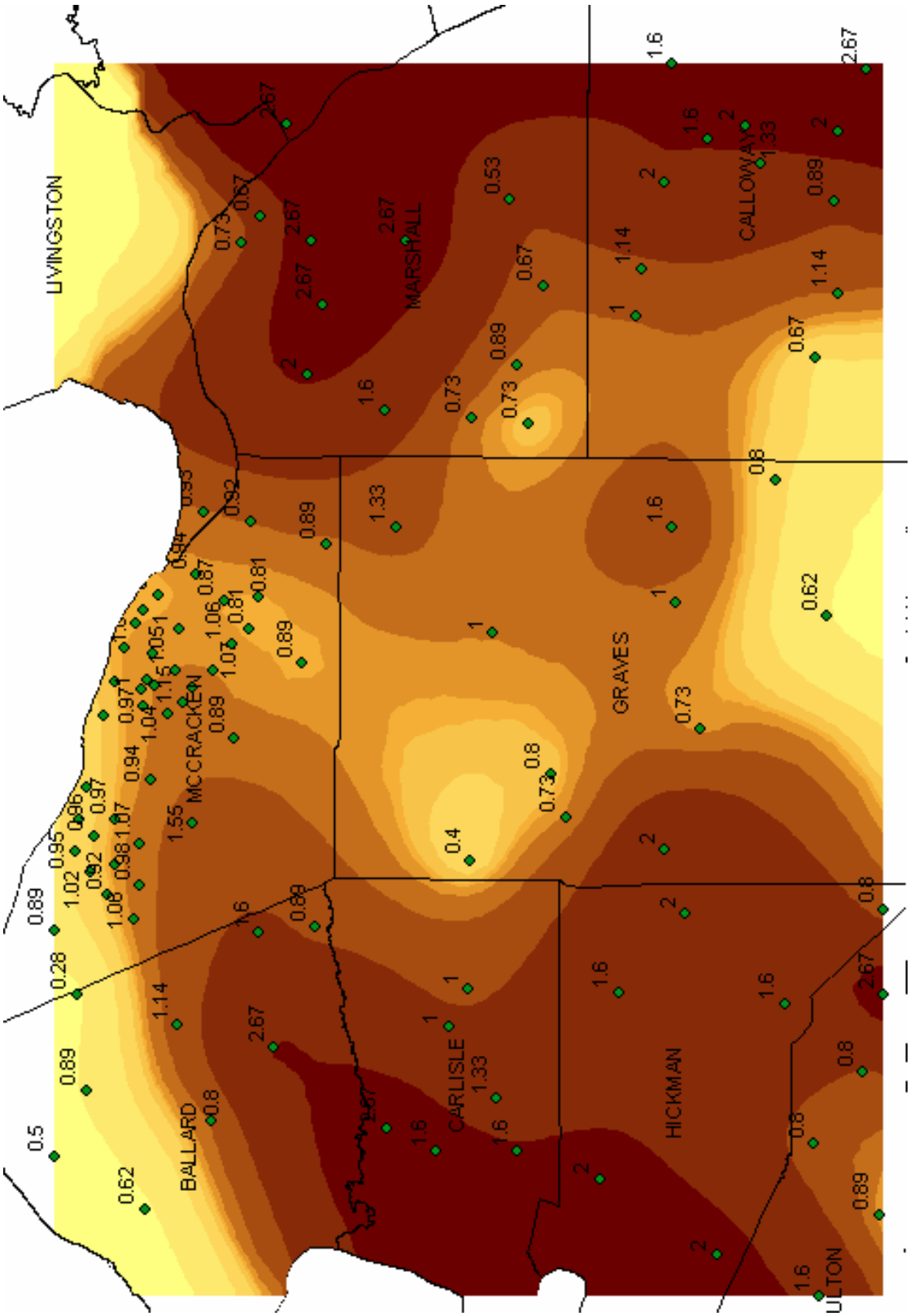

Local Polynomial (DSP)

Mean: 0.004424

Root-Mean-Square: 0.5117

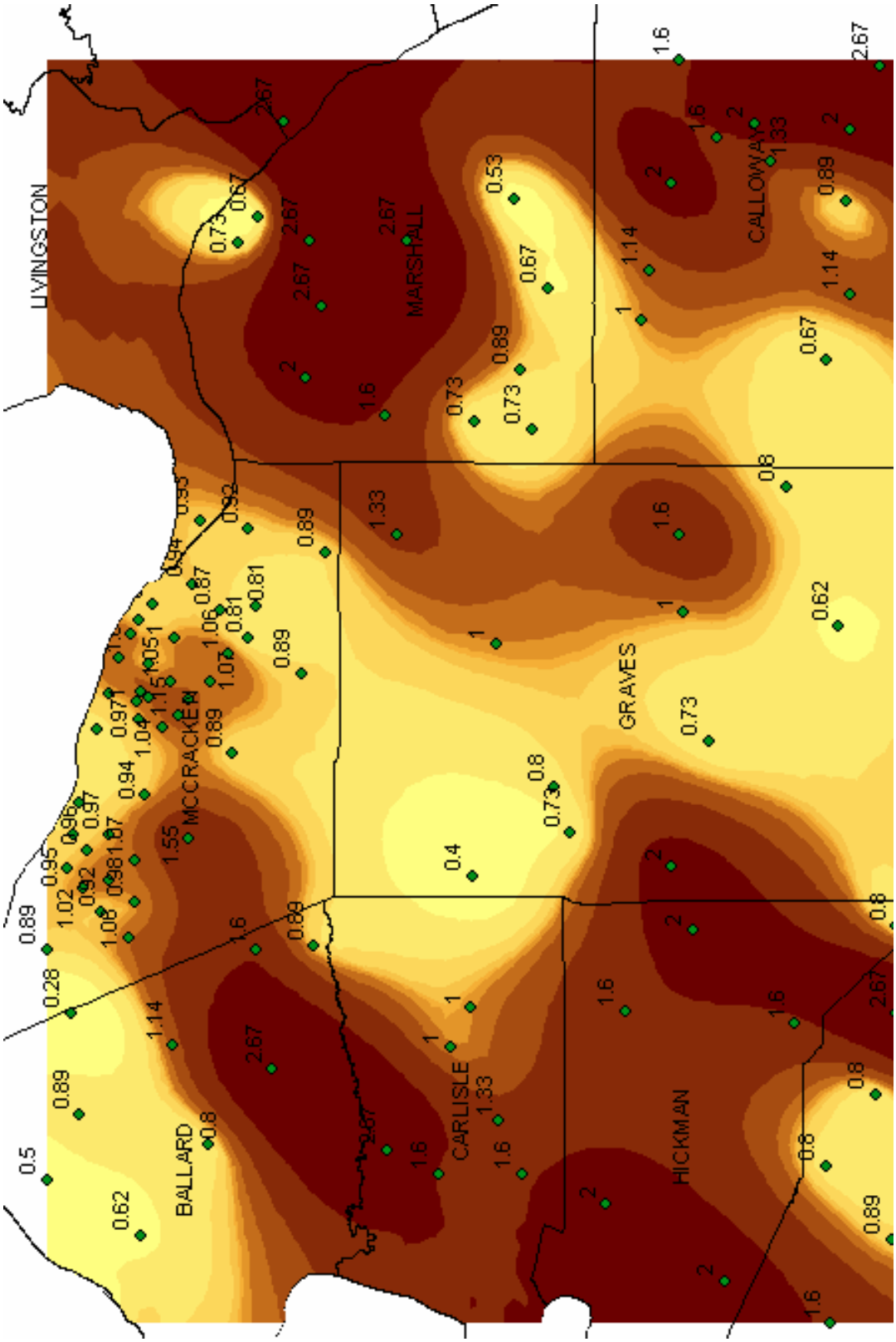

Spline with Tension (DSP)
Mean: 0.9071
Root-Mean-Square: 78.38

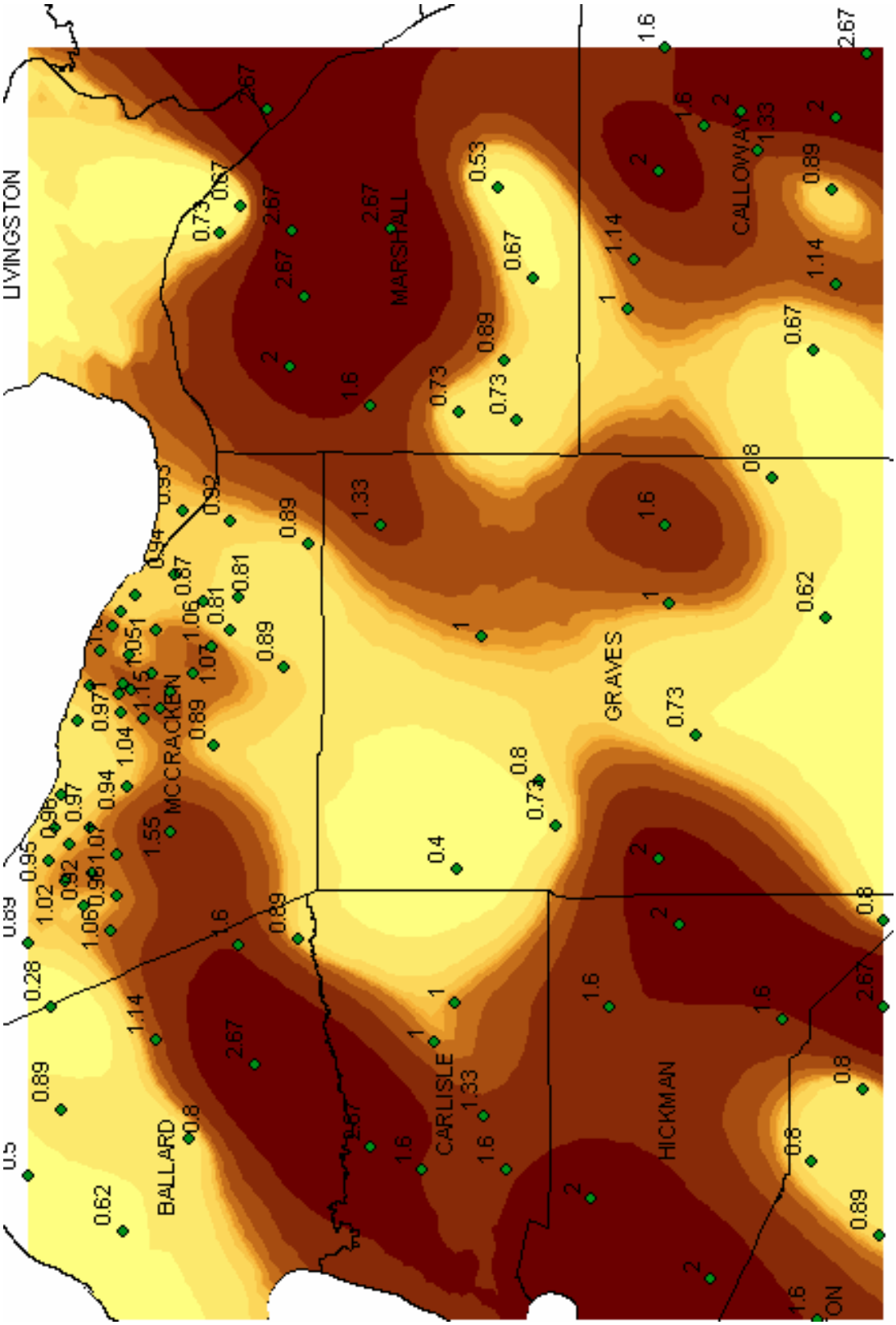

Multiquadric Spline (DSP)

Mean: -0.007199

Root-Mean-Square: 0.4681

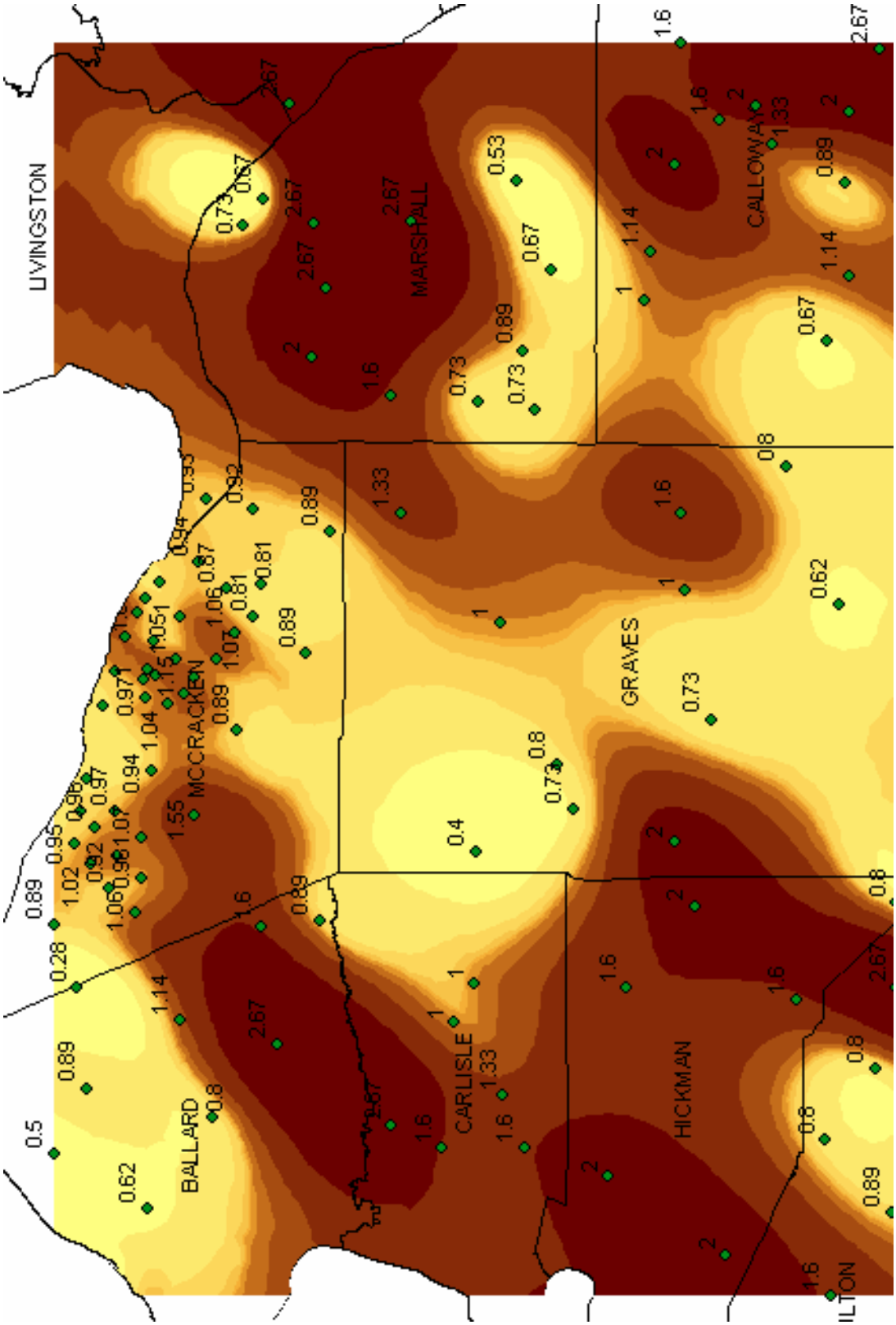

Inverse Multiquadric Spline (DSP)

Mean: -0.01416

Root-Mean-Square: 0.463

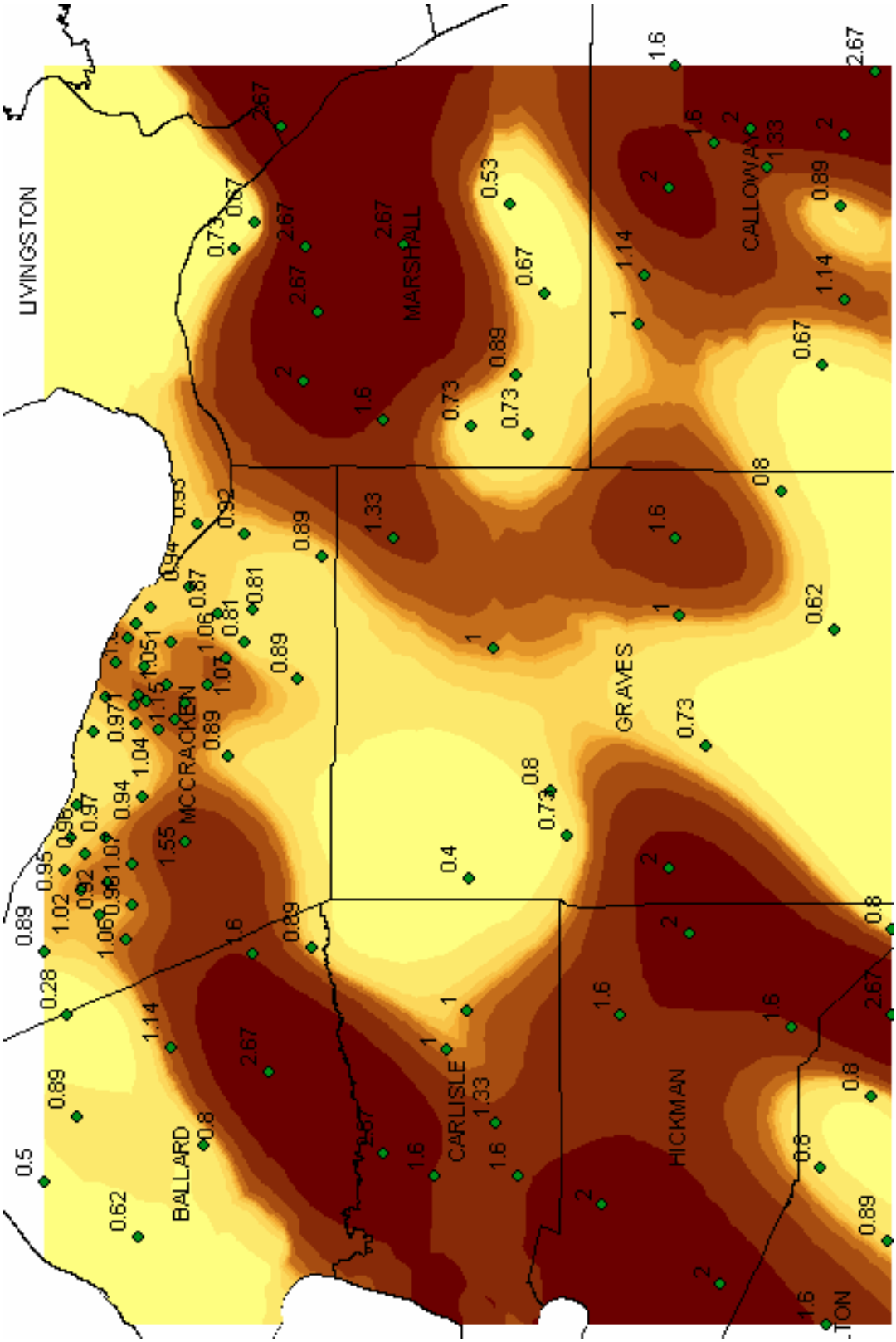

Thin Plate Spline (DSP)

Mean: -0.007255

Root-Mean-Square: 0.5315

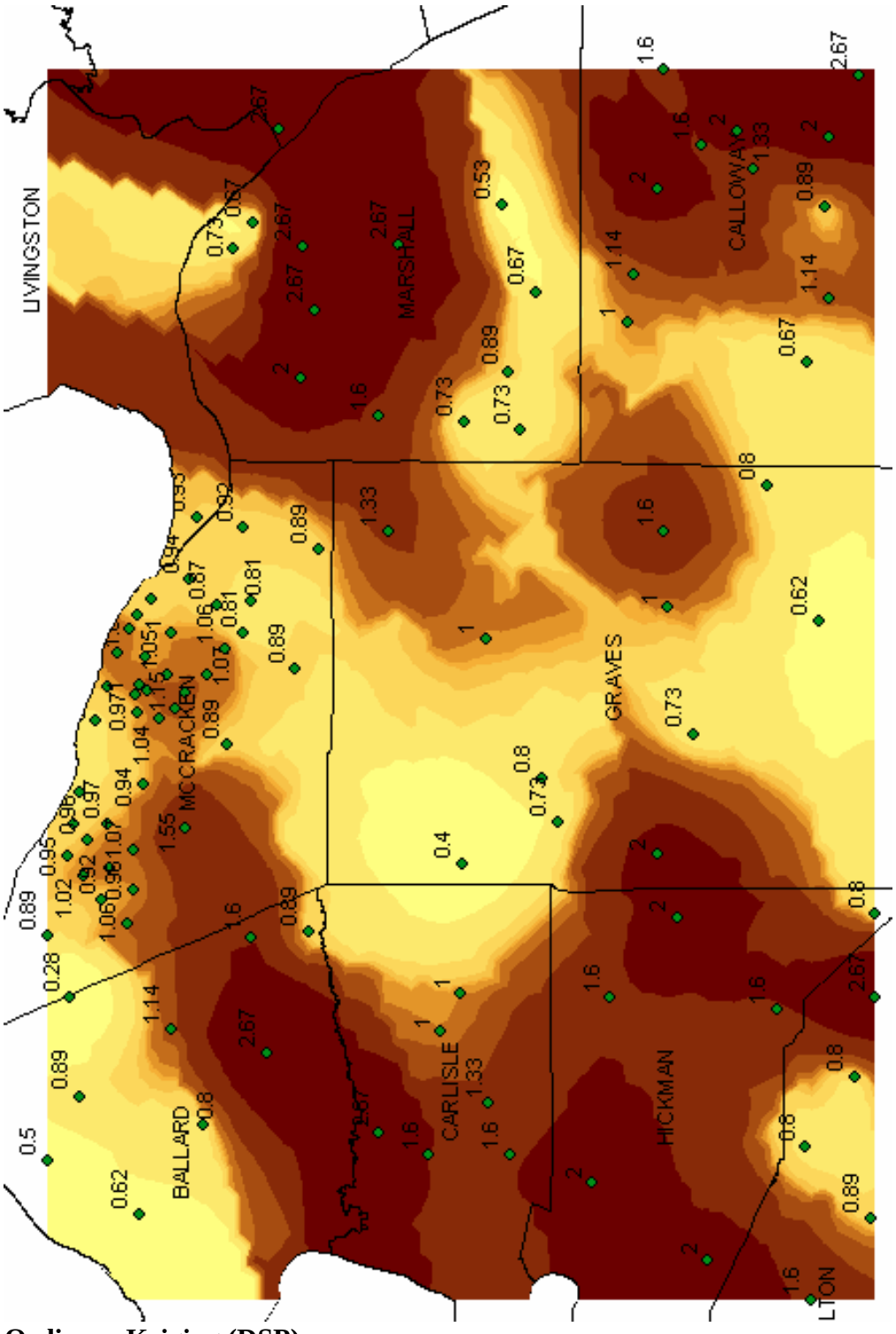

Ordinary Kriging (DSP)

Mean:	0.01556
Root-Mean-Square:	0.4341
Average Standard Error:	0.3018
Mean Standardized:	0.04384
Root-Mean-Square Standardized:	1.304

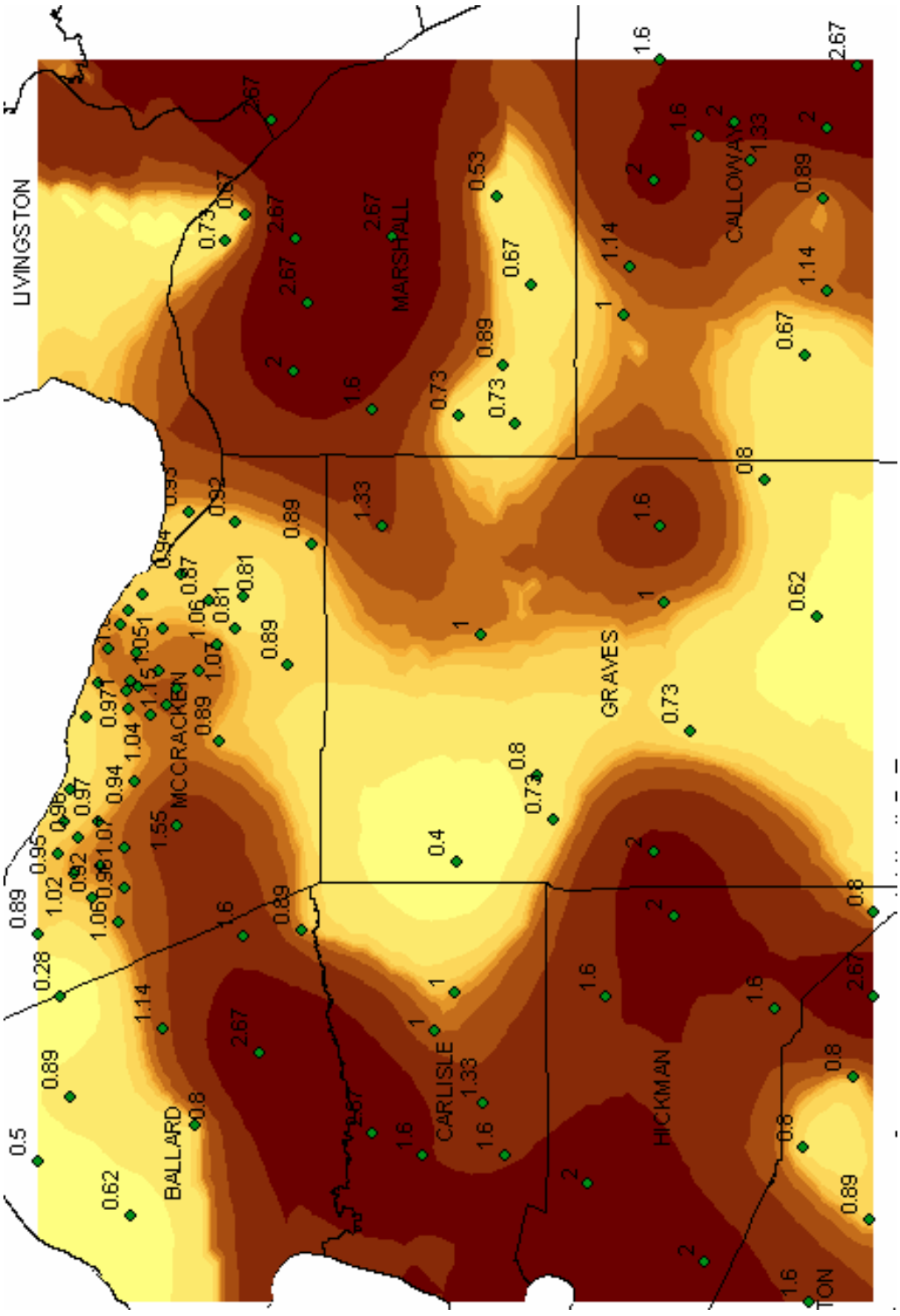

Ordinary Cokriging (DSP)

Mean:	-0.004087
Root-Mean-Square:	0.3601
Average Standard Error:	0.2831
Mean Standardized:	-0.01107
Root-Mean-Square Standardized:	1.147

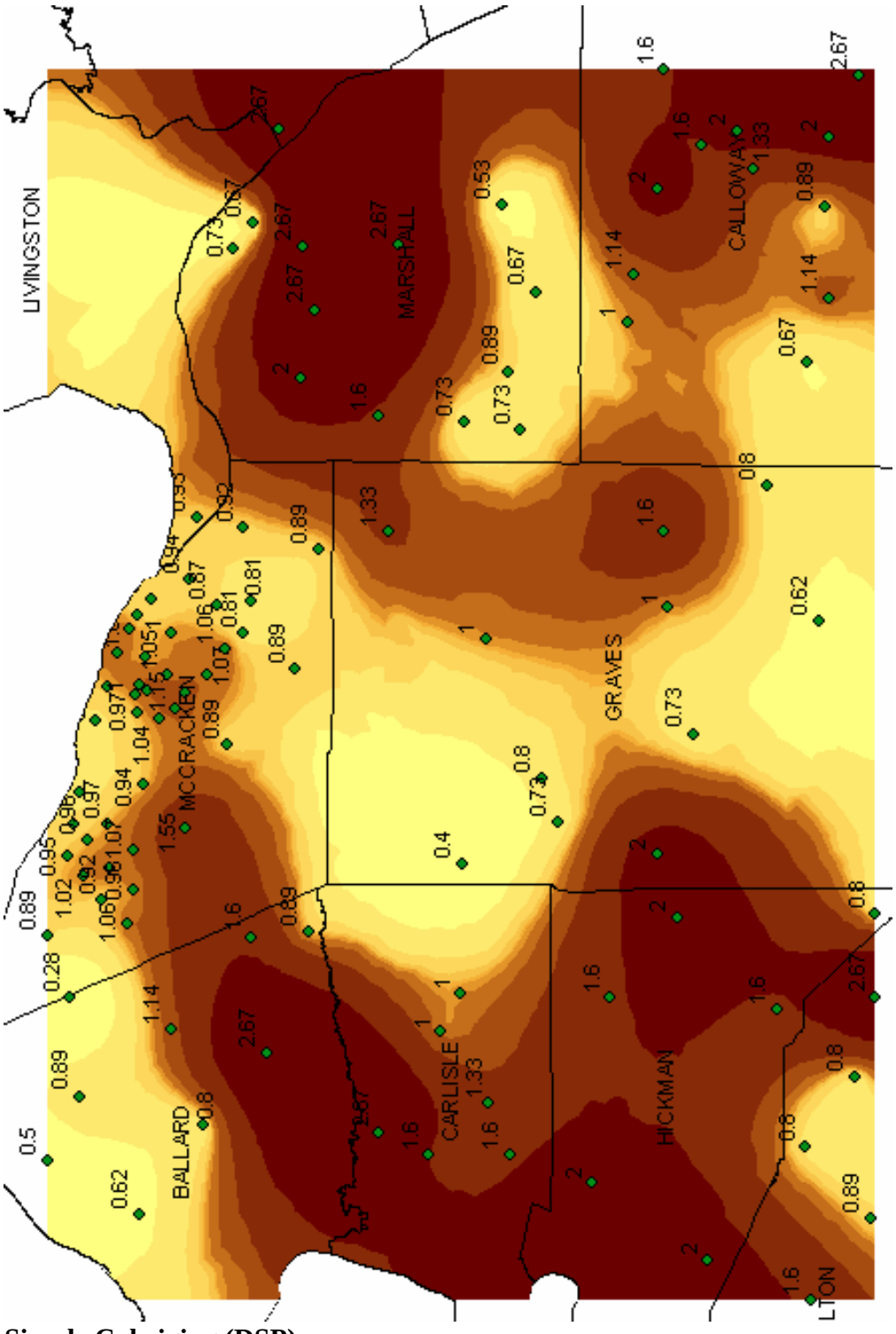

Simple Cokriging (DSP)

Mean:	0.0007828
Root-Mean-Square:	0.3787
Average Standard Error:	0.2761
Mean Standardized:	0.004697
Root-Mean-Square Standardized:	1.221

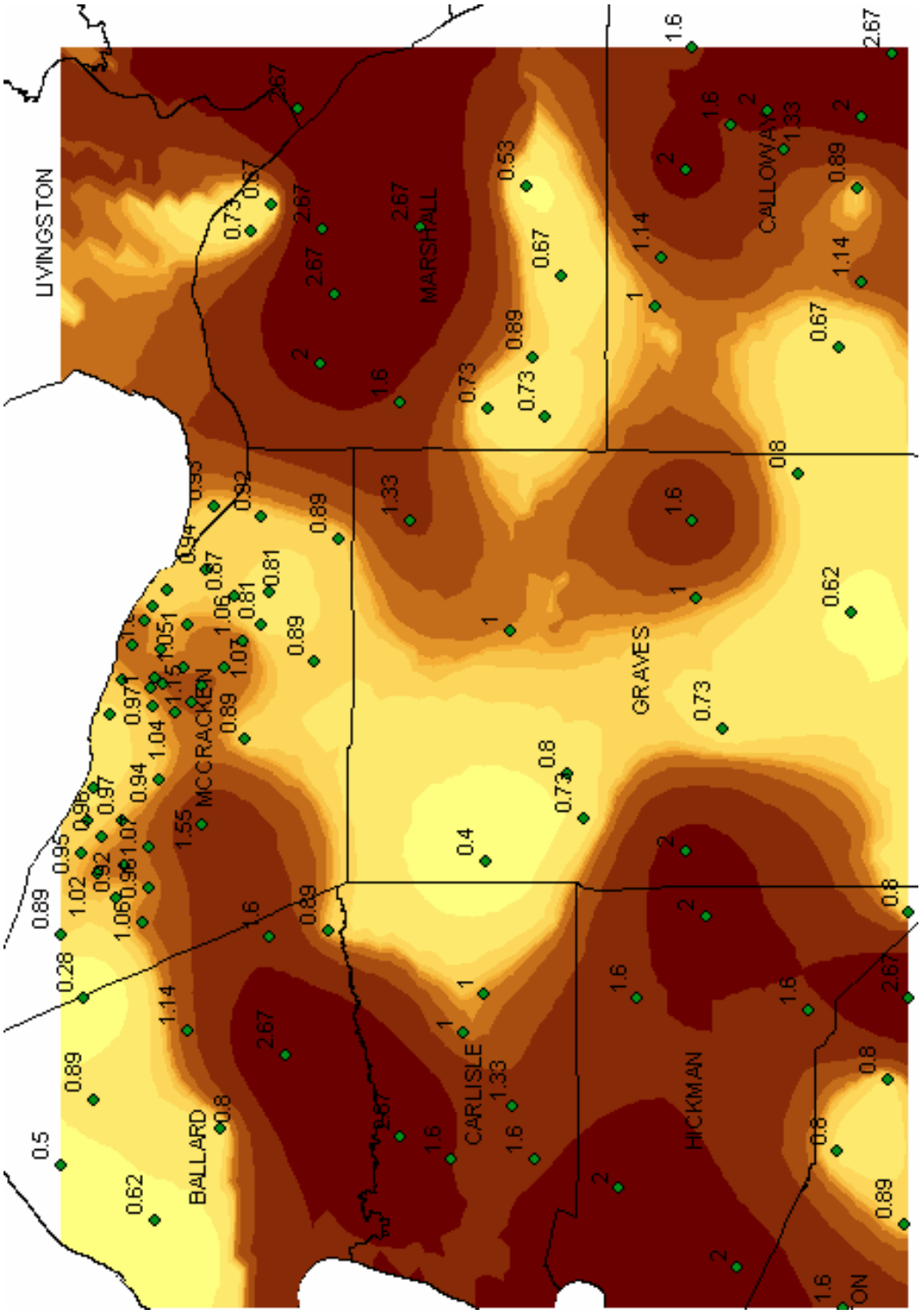

Universal Kriging (DSP)

Mean:	-0.002872
Root-Mean-Square:	0.4519
Average Standard Error:	0.2254
Mean Standardized:	-0.00163
Root-Mean-Square Standardized:	1.795

V_{30} Interpolated Maps

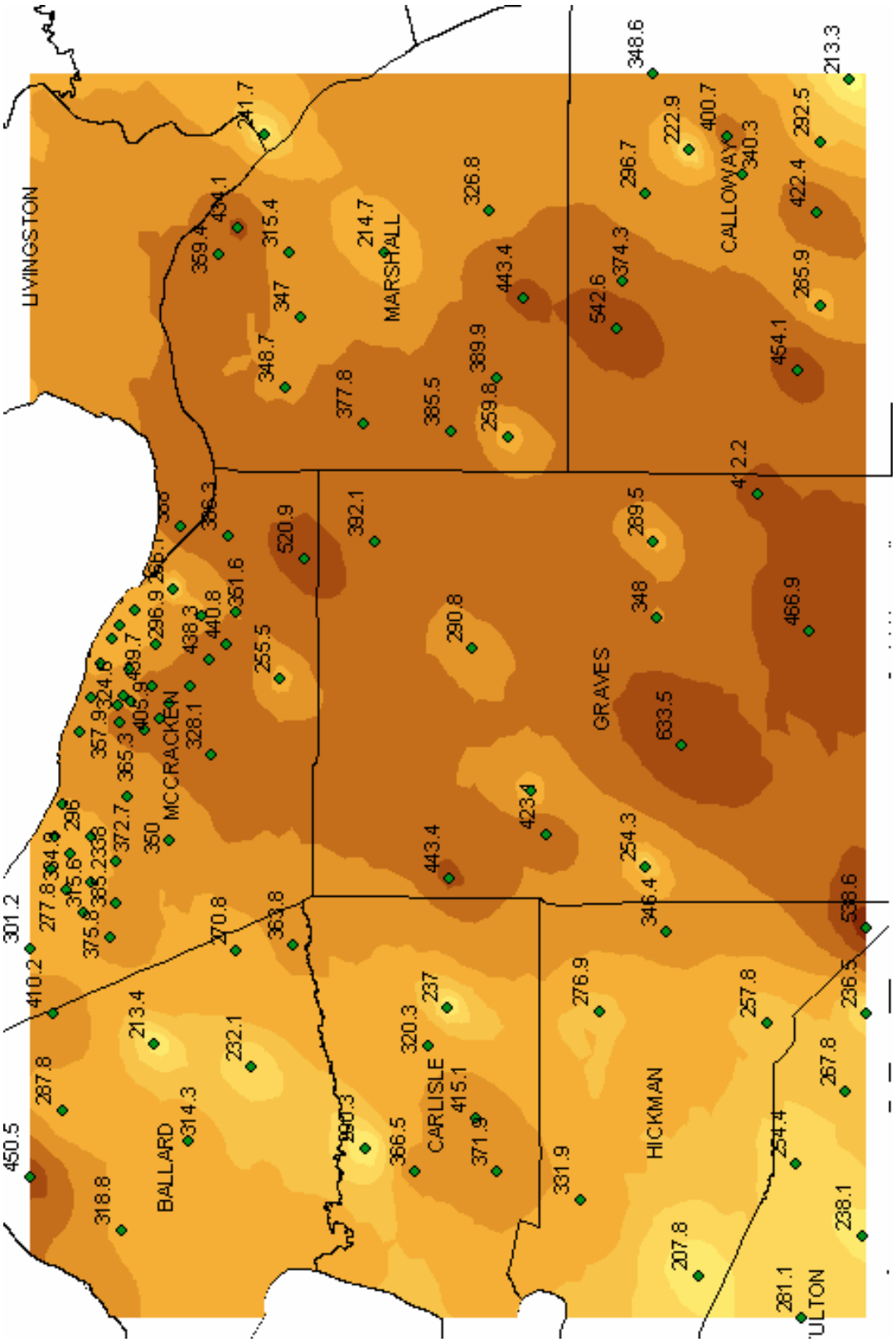

Inverse Distance Weighted (V_{30})

Mean: 1.173

Root-Mean-Square: 79.59

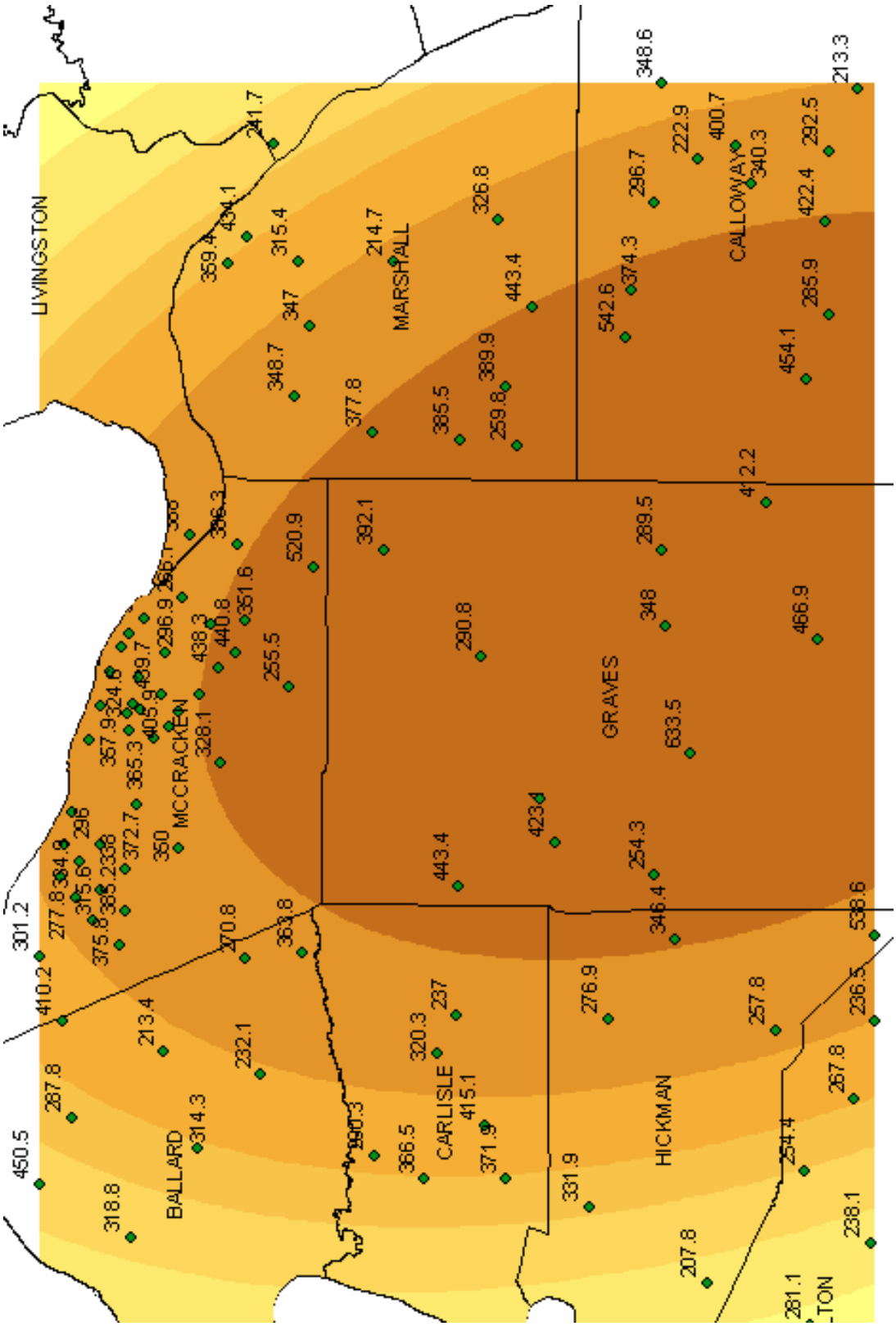

Global Polynomial (V_{30})

Mean: -0.1828

Root-Mean-Square: 80.77

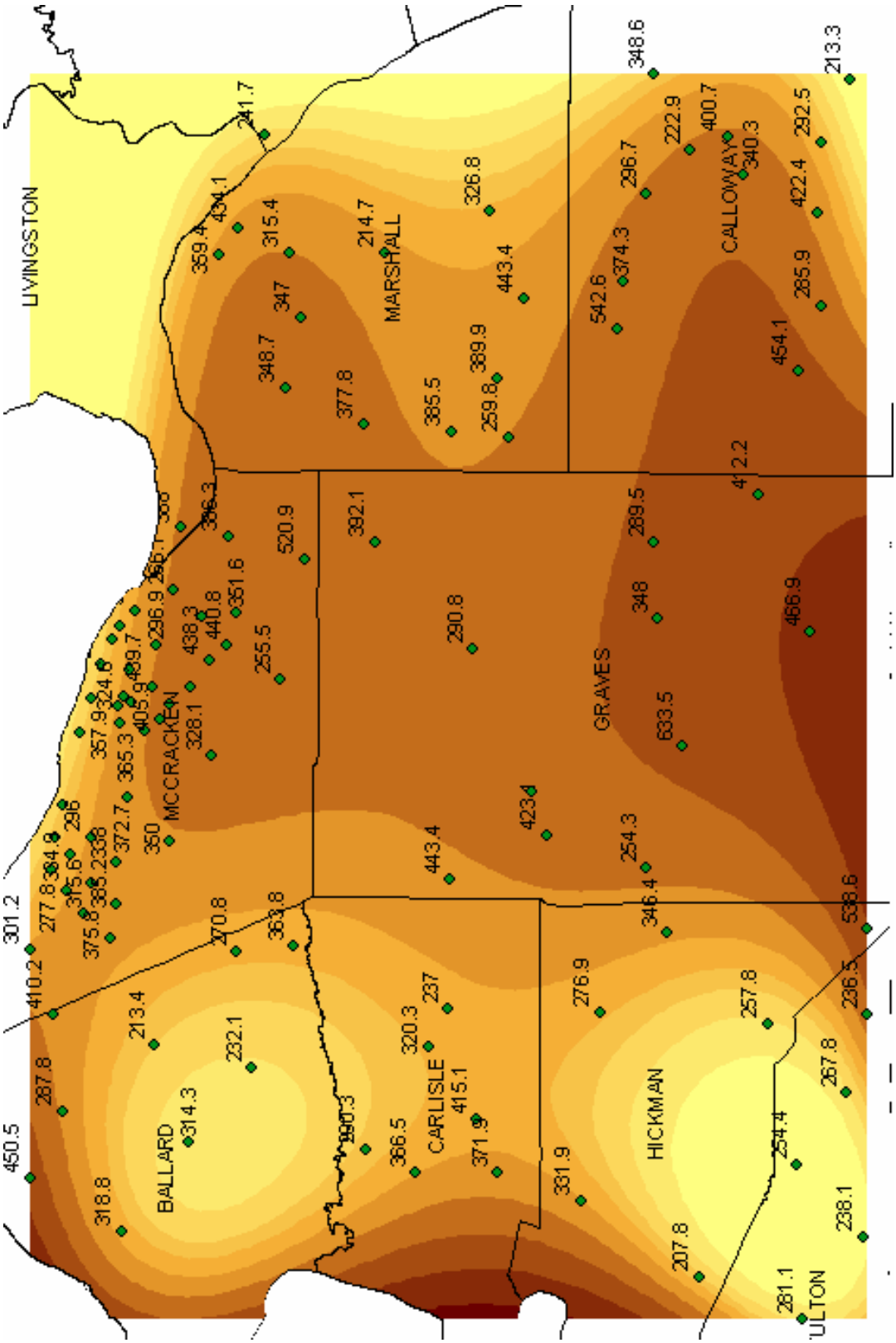

Global Polynomial using higher-order polynomial (V_{30})

Mean: -1.194

Root-Mean-Square: 87.54

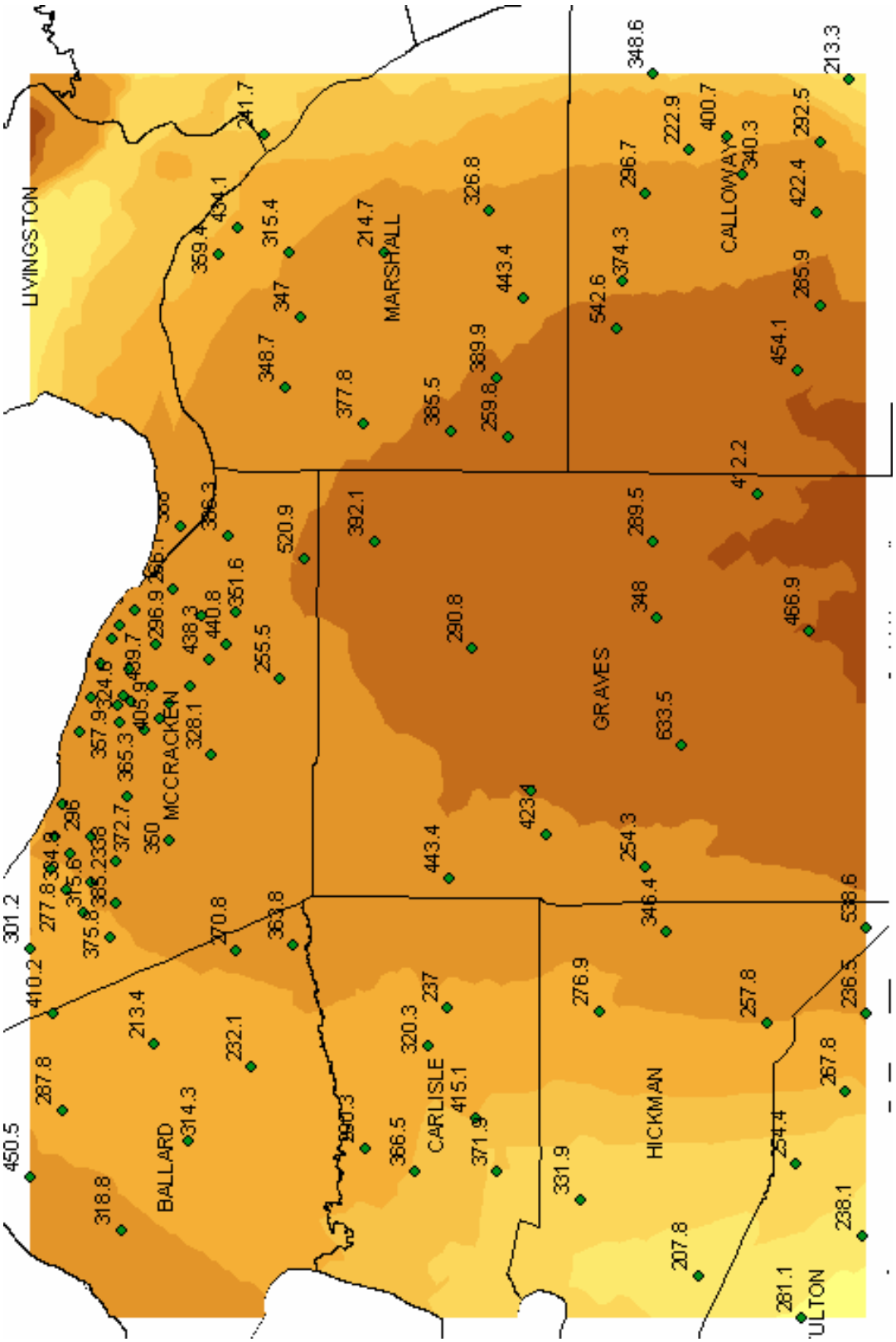

Local Polynomial (V_{30})

Mean: -7.123

Root-Mean-Square: 80.09

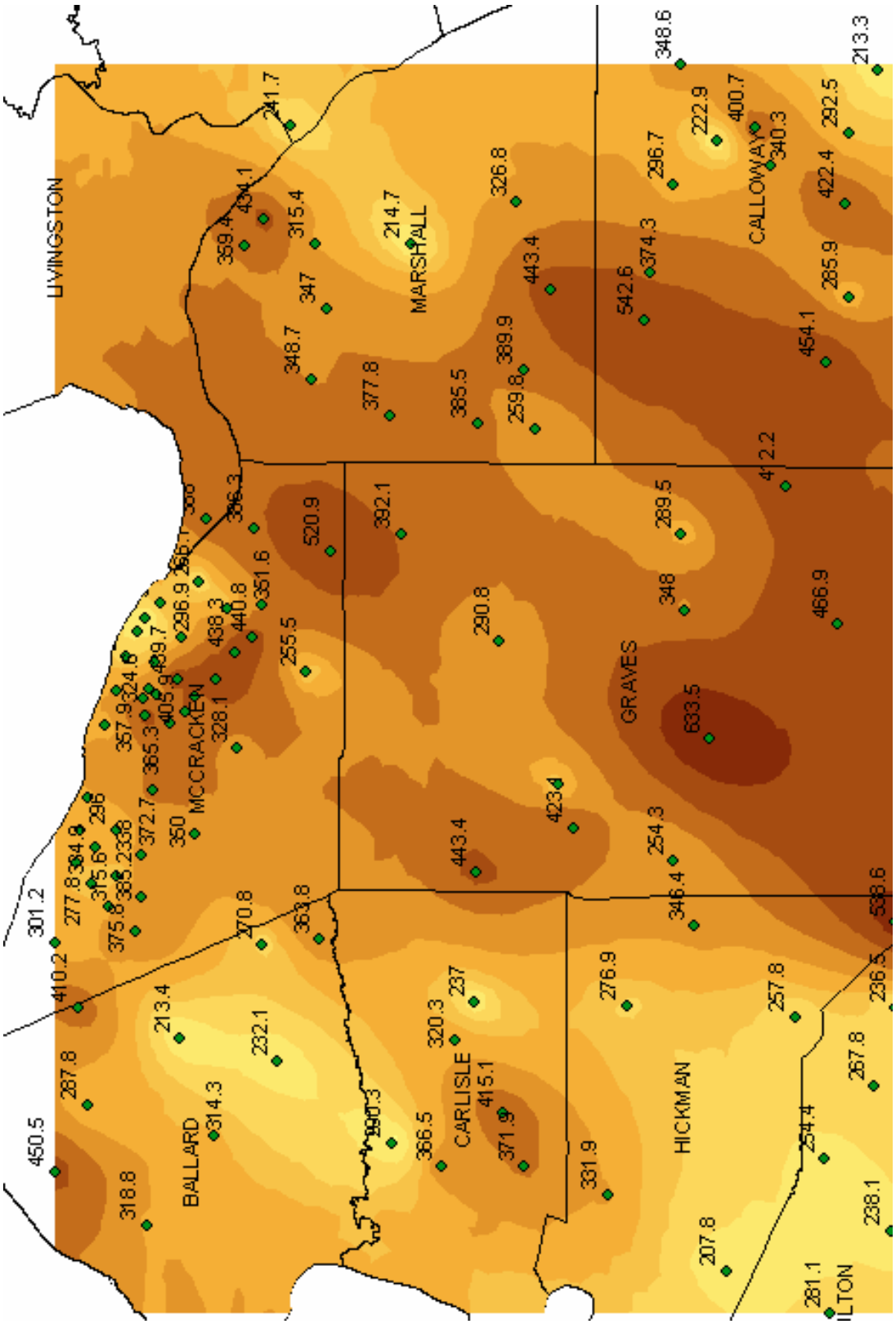

Completely Regularized Spline (V_{30})

Mean: 1.076

Root-Mean-Square: 78.78

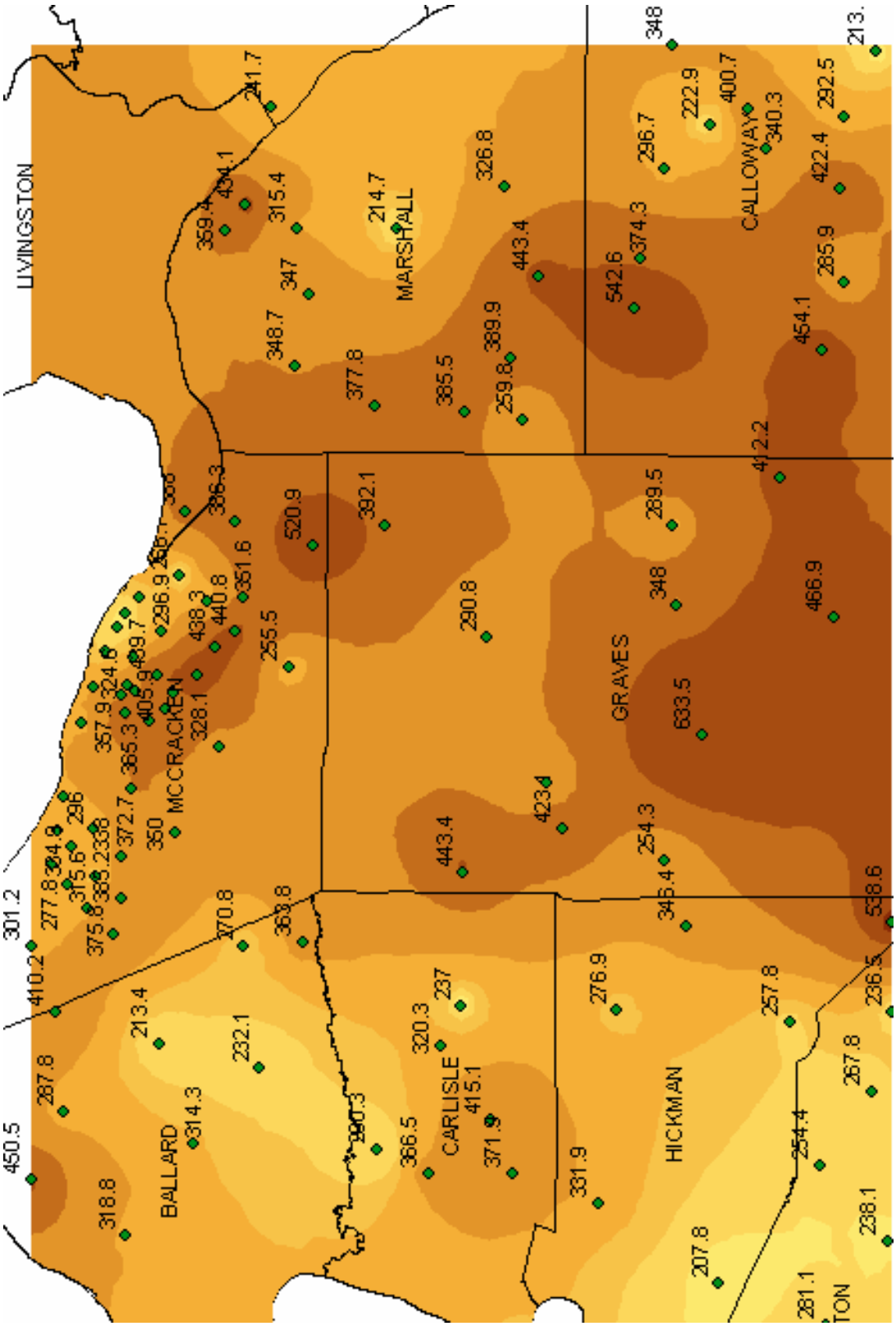

Spline with Tension (V_{30})
Mean: 0.9071
Root-Mean-Square: 78.38

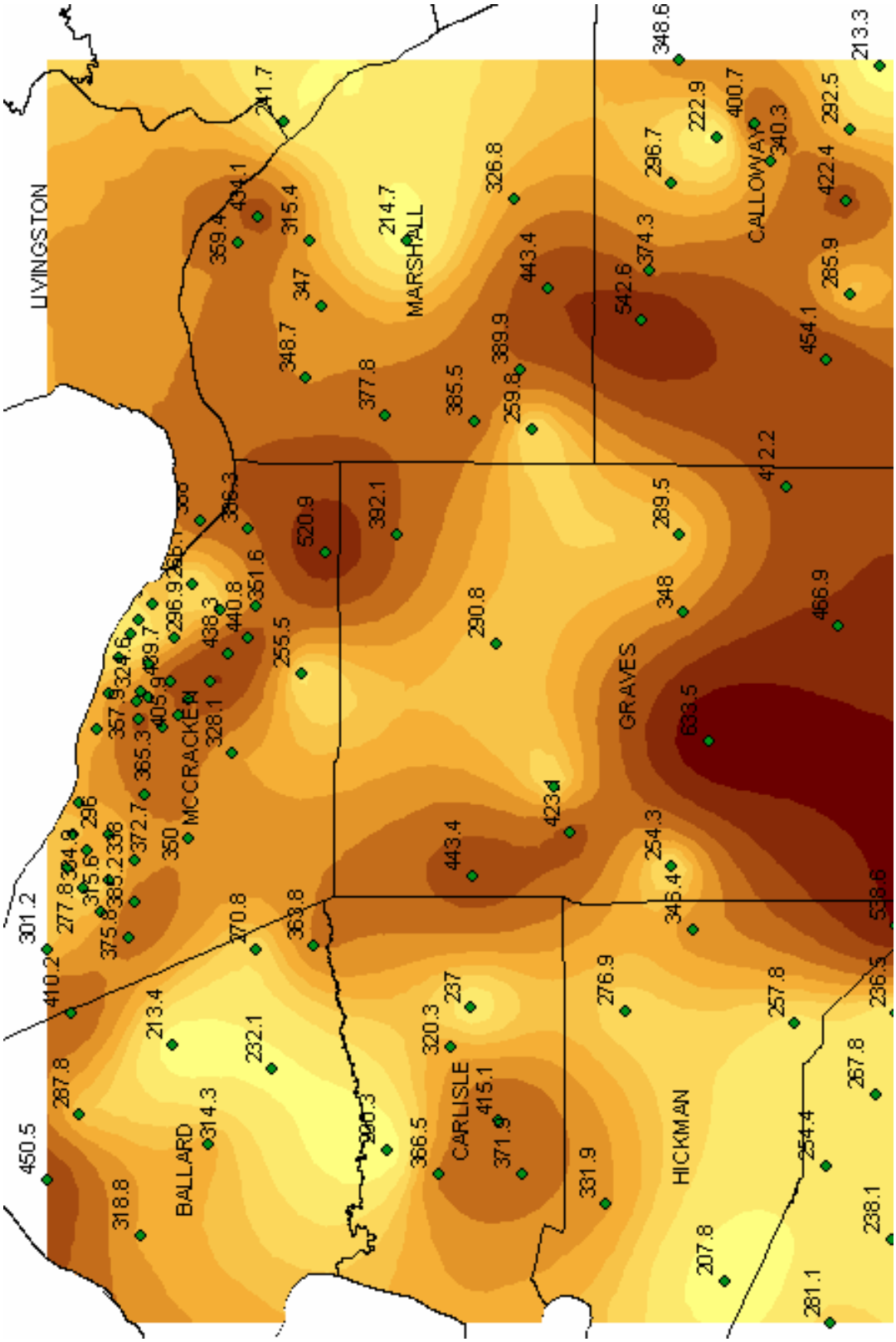

Multiquadric Spline (V_{30})

Mean: 0.4201

Root-Mean-Square: 84.18

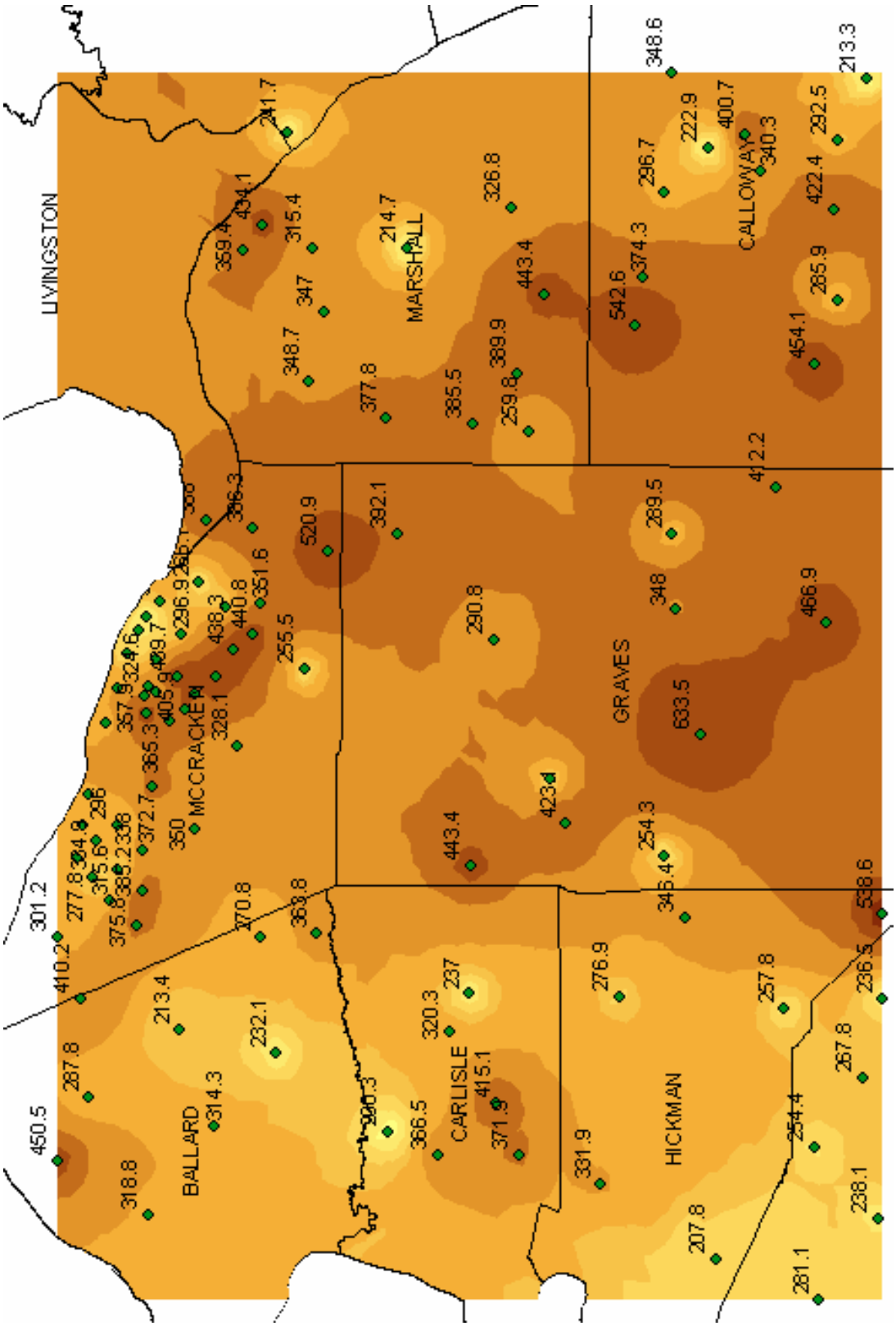

Inverse Multiquadric Spline (V_{30})

Mean: 1.932

Root-Mean-Square: 77.85

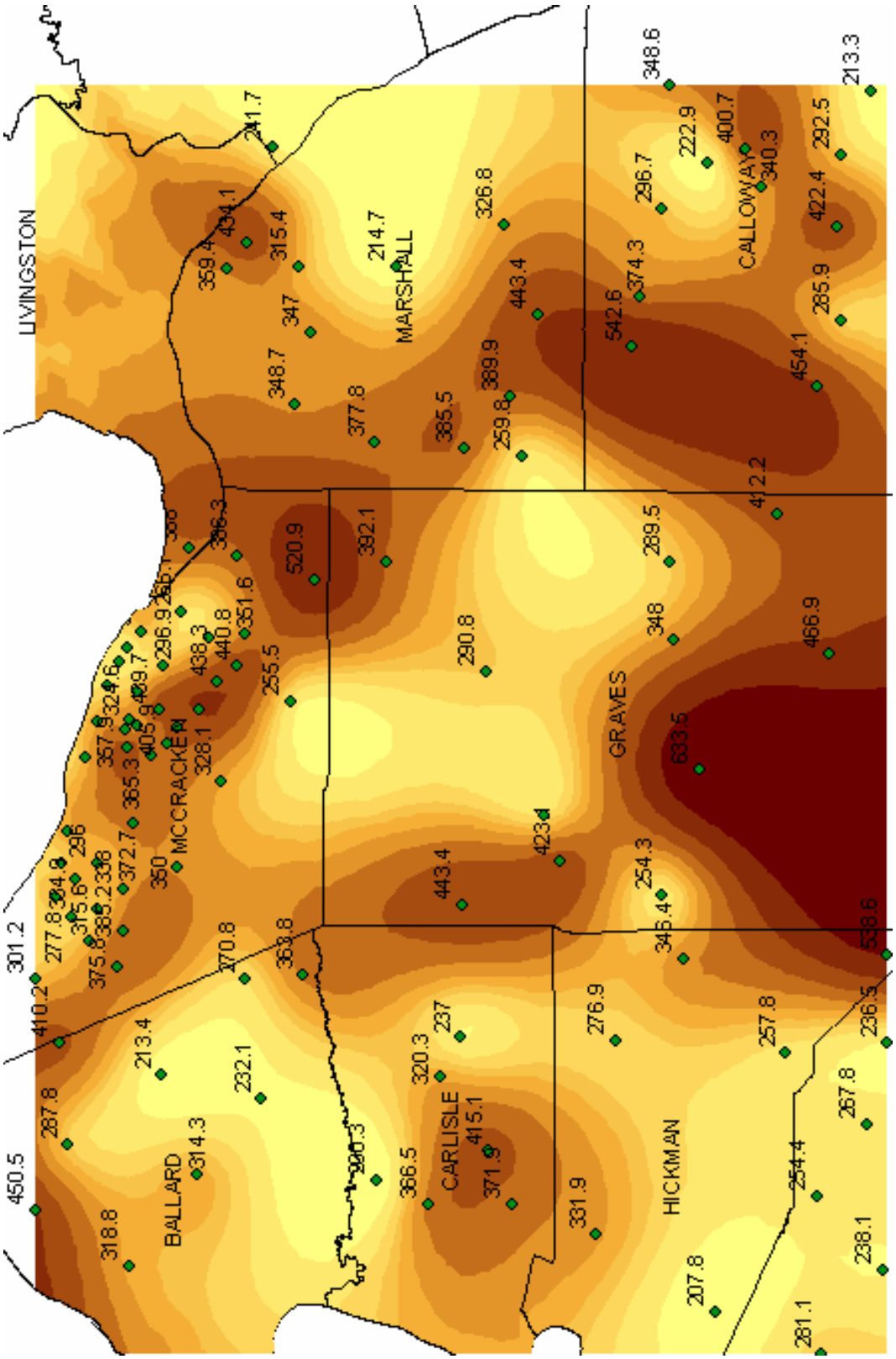

Thin Plate Spline (V_{30})

Mean: 1.153

Root-Mean-Square: 98.79

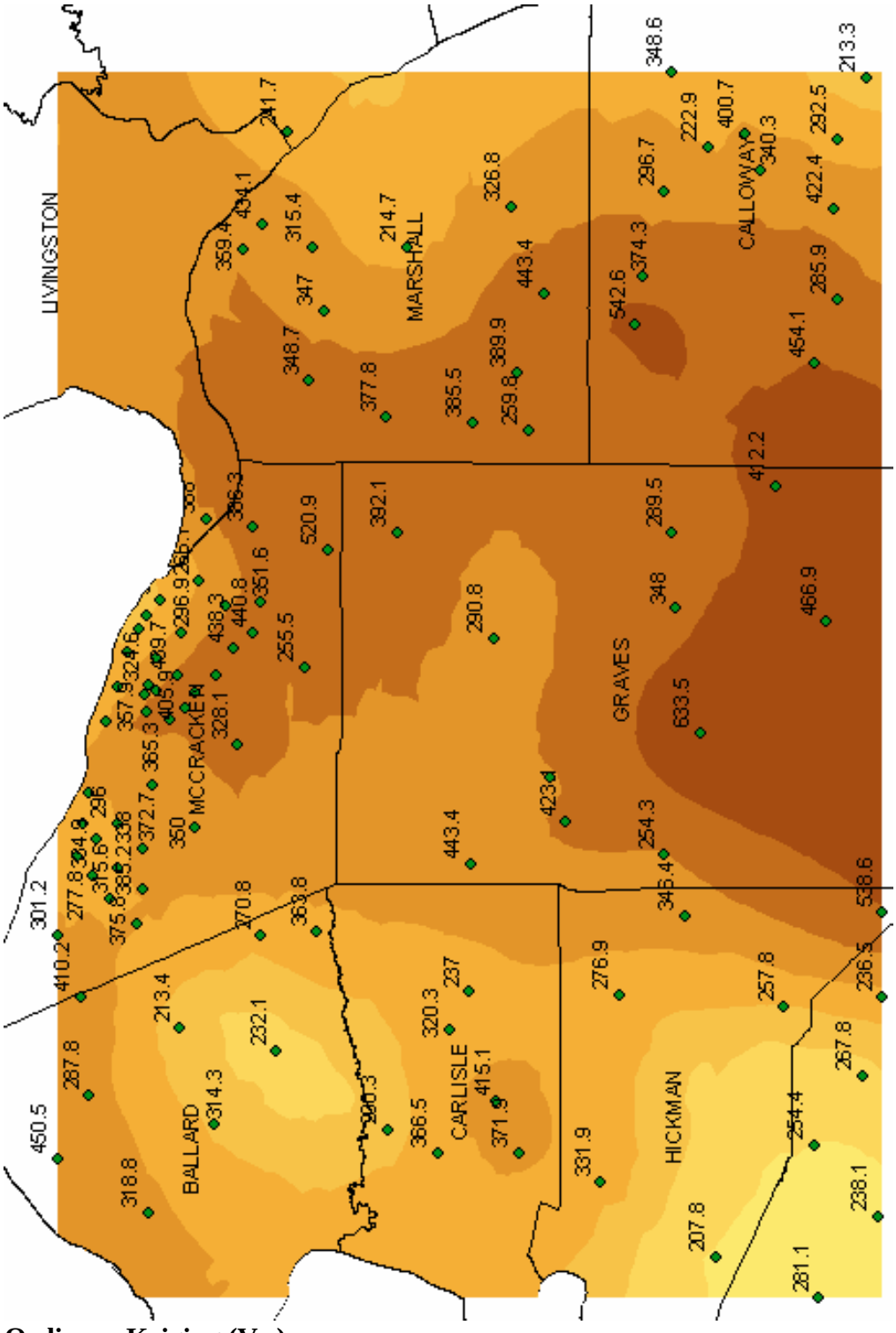

Ordinary Kriging (V_{30})

Mean:	0.6137
Root-Mean-Square:	79.55
Average Standard Error:	68.96
Mean Standardized:	0.008499
Root-Mean-Square Standardized:	1.133

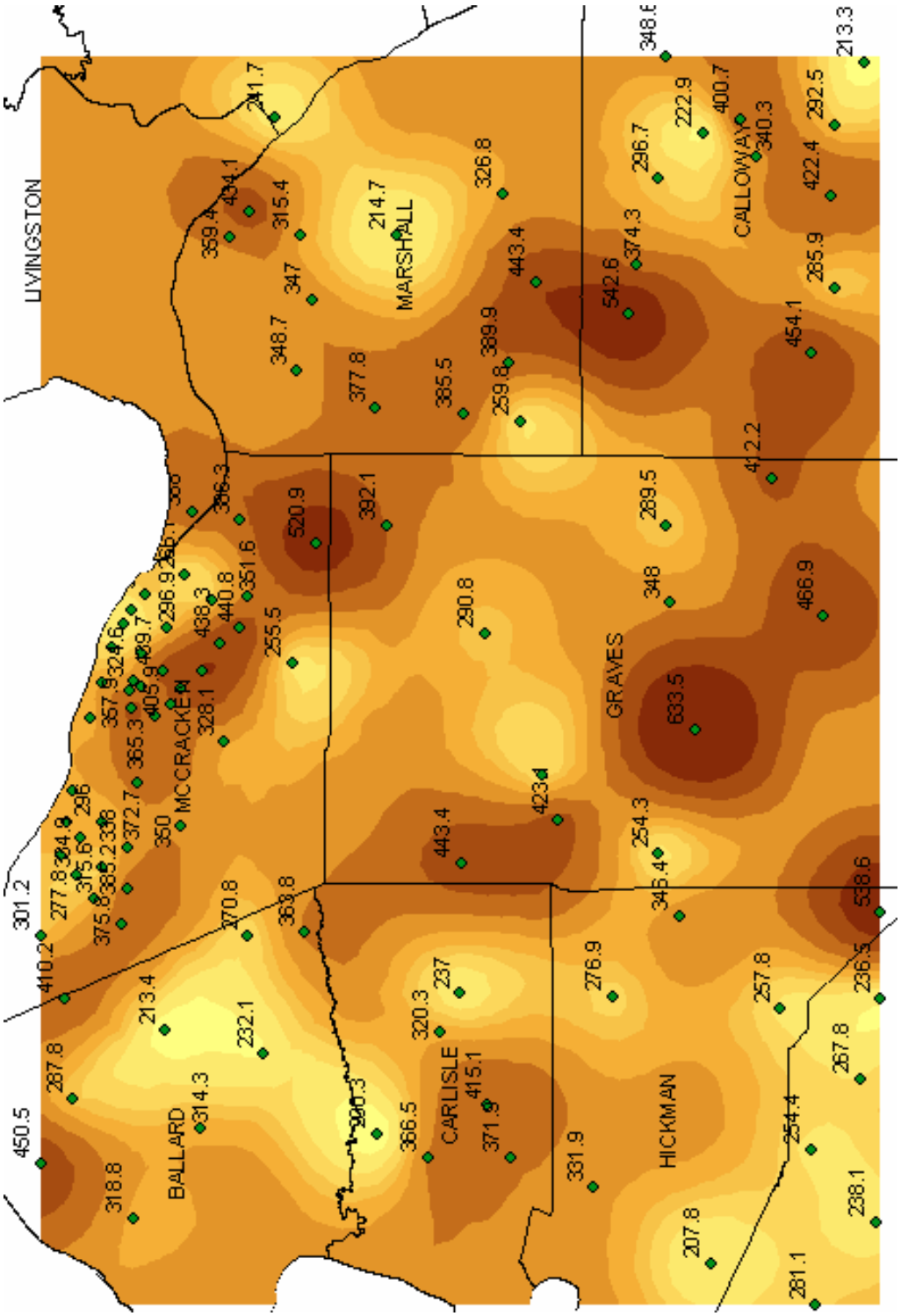

Simple Kriging (V_{30})

Mean:	1.155
Root-Mean-Square:	80.36
Average Standard Error:	64.16
Mean Standardized:	0.01027
Root-Mean-Square Standardized:	1.21

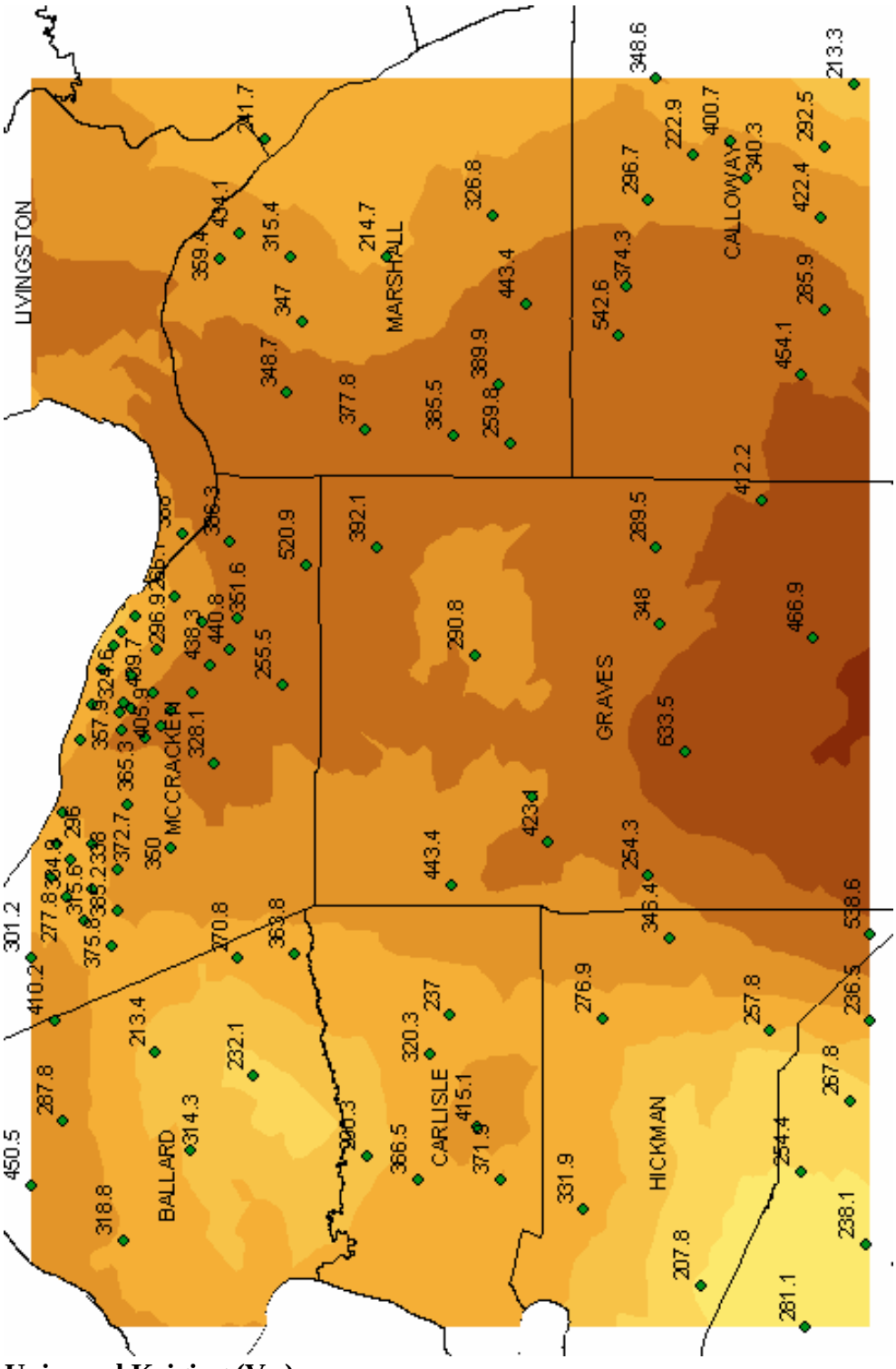

Universal Kriging (V_{30})

Mean:	0.09248
Root-Mean-Square:	79.32
Average Standard Error:	68.29
Mean Standardized:	0.001597
Root-Mean-Square Standardized:	1.143

References

Al-Yazdi, Ali Ahmed. 1994. Paleozoic bedrock depth investigation in the Jackson Purchase Region of western Kentucky using the P-wave seismic reflection technique for the purpose of regional 1-D site effects estimation. University of Kentucky, Thesis.

Arlinghaus, Sandra L. 1996. Practical Handbook of Spatial Statistics. CRC Press, Boca Raton, FL.

BSSC. 1997. NEHRP Recommended Provisions for Seismic Regulations for New Buildings, Part 1 — Provisions. 1997 Edition, Building Seismic Safety Council, Washington, D.C.: 337 pp.

Carr, James R. 1995. Numerical Analysis for the Geological Sciences. Upper Saddle River, New Jersey: Prentice-Hall, Inc.

Carver, Steve. 1997. Innovations in GIS 5. Taylor and Francis, Inc. Bristol, Pa.

Christakos, G., Bogaert, P., and Serre, M. 2001. Temporal GIS: Advanced Functions for Field-Based Applications. Berlin: Springer-Verlag.

Cressie, Noel A. 1991. Statistics for Spatial Data. New York: John Wiley and Sons.

Davis, John C. 1986. Statistics and Data Analysis in Geology (2nd Edition). New York: John Wiley and Sons.

Deutsch, Clayton V., and Journel, Andre G. 1998. GSLIB: Geostatistical software library and user's guide (2nd Edition). New York: Oxford University Press, Inc.

Dowdy, Therese C. 1998. Application of a GIS to a hydrogeologic investigation of the Inner Bluegrass karst region in Scott County, Kentucky. University of Kentucky, Thesis.

ESRI Virtual Campus Web Course. 2004. Creating, Editing, and Managing Geodatabases for ArcGIS 8.3. campus.esri.com/index.cfm. (Accessed March, 2005).

ESRI. 2006. www.esri.com. Accessed February, 2006.

Foresman, Timothy W. 1998. The History of Geographic Information Systems. Upper Saddle River, N.J.: Prentice Hall, Inc.

Goovaerts, Pierre. 1997. Geostatistics for Natural Resources Evaluation. New York: Oxford University Press, Inc..

Haining, Robert. 1990. Spatial data analysis in the social and environmental sciences. Cambridge [England]: Cambridge University Press, 409 pp.

Harris, James B. 1992. Site amplification of seismic ground motions in the Paducah, Kentucky, area. University of Kentucky, Thesis.

Hernandez, Michael J. 1997. Database Design for Mere Mortals: A Hands-On Guide to Relational Database Design. Reading, Mass.: Addison Wesley Longman, Inc.

Higgins, Brian A. 1997. Site amplification of earthquake ground motions in unconsolidated sediments in Henderson, Kentucky. University of Kentucky, Thesis.

Hoffer, Jeffrey A., Prescott, Mary B., and McFadden, Fred R. 2005. Modern Database Management (7th Edition). Upper Saddle River, N.J.: Pearson Education, Inc.

Hohn, Michael E. 1999. Geostatistics and Petroleum Geology. Dordrecht, The Netherlands: Kluwer Academic Publishers.

Isaaks, Edward H., and Srivastava, R. Mohan. 1989. An Introduction to Applied Geostatistics. New York: Oxford University Press.

Johnston, A.C., and Nava, S.J. 1985. Recurrence rates and probability estimates for the New Madrid Seismic Zone. Journal of Geophysical Research, 90, 6737–6753.

Journel, Andre G. 1989. Fundamentals of Geostatistics in Five Lessons. Washington, D.C.: American Geophysical Union.

Kanevski, Mikhail, and Maignan, Michel. 2004. Analysis and Modelling of Spatial Environmental Data. New York: EPFL Press.

Kim, Dong-Soo, Chung, Choong-Ki, Sun, Chang-Guk, Bang, Eun-Seok. 2002. Site assessment and evaluation of spatial earthquake ground motion of Kyeongju. Soil Dynamics and Earthquake Engineering 22, 371–387.

Laslett, G.M. 1994. Kriging and splines: An empirical comparison of their predictive performance in some applications. Journal of the American Statistical Association, 89 (426), 391–409.

Lin, T. 2003. Local soil-induced amplification of strong ground motion in Maysville, Kentucky. University of Kentucky, Thesis.

Middleton, Gerard V. 2000. Data analysis in the earth sciences using MATLAB. Upper Saddle River, N.J.: Prentice Hall.

Nuttli, O.W. 1973. The Mississippi Valley earthquakes of 1811 and 1812, intensities, ground motion, and magnitude. Seismological Society of America Bulletin, 63, 227–248.

Olive, W.W. 1972. Geology of the Jackson Purchase Region, Kentucky: Roadlog for the Geological Society of Kentucky field excursion: Kentucky Geological Survey, Ser. 10, 11 p.

O'Sullivan, David, and Unwin, David J. 2003. Geographic Information Analysis. Hoboken, NJ.: John Wiley and Sons.

Ott, Thomas, and Swiaczny, Frank. 2001. Time-Integrative Geographic Information Systems. Berlin: Springer-Verlag.

Petry, Frederick E., Robinson, Vincent B., and Cobb, Maria A. 2005. Fuzzy Modeling with Spatial Information for Geographic Problems. Berlin: Springer-Verlag.

Riccardi, Greg. 2001. Principles of Database Systems with Internet and Java Applications. Boston: Addison Wesley Publishing Company.

Royle, A., Clark, Isobel, Brooker, P.I., Parker, H., Journel, A., Rendu, J.M., Sandefur, R., and Mousset-Jones, Pierre. 1980. Geostatistics. New York: McGraw-Hill, Inc.

Rutledge, Alex. 2004. High resolution geophysical investigation of late quaternary deformation in the lower Wabash Valley Fault System. Thesis. University of Kentucky.

Schabenberger, Oliver, and Gotway, Carol A. 2005. Statistical Methods for Spatial Data Analysis. Boca Raton, Fla.: Chapman and Hall/CRC, 488 p..

Schwalb, H. R., 1969, Paleozoic geology of the Jackson Purchase Region, Kentucky, with reference to petroleum possibilities: Kentucky Geological Survey, ser. 10, Report of Investigations 10, 40 p.

Shi, Wenzhong, Fisher, Peter F., and Goodchild, Michael F. 2002. Spatial Data Quality. London: Taylor and Francis.

Street, R. 1982. A contribution to the documentation of the 1811–1812 Mississippi Valley earthquake sequence. Earthquake Notes, 53 (2), 39–52.

Street, R. 1996. Dynamic site periods in the northern Mississippi Embayment area of western Kentucky and southeastern Missouri. Contract report to U.S. Geological Survey.

Street, R., Woolery, E., Harik, I., Allen, D., and Sutterer, K. 1997. Dynamic Site Periods for the Jackson Purchase Region of Western Kentucky. (KYSPR96-173). Research Report KTC-97-1. Kentucky Transportation Center.

Street, R., Woolery, E., Wang, Z., and Harik, I. 1997. Soil classifications for estimating site-dependent response spectra and seismic coefficients for building code provisions in western Kentucky. Engineering Geology, 46, p. 331–347.

Street, R., Woolery, E., Wang, Z., and Harris, J. 2001. NEHRP soil classifications for estimating site-dependent seismic coefficients in the Upper Mississippi Embayment. Engineering Geology, 62, 123–135.

Street, R., Wiegand, J., Woolery, E. W., and Hart, P. 2005. Ground-motion parameters of the southwestern Indiana earthquake of 18 June 2002 and the disparity between the observed and predicted values. Seismological Research Letters, 76 (4).

Wang, Z. 1993. Qs estimation for unconsolidated sediments and site amplification of strong ground motion in western Kentucky. University of Kentucky, Thesis, 94 p.

Wang, Z., Cordiviola, S., and Kiefer, J. 2004. Earthquake Hazard Assessment for Louisville Metropolitan Area, Kentucky. Kentucky Geological Survey Final Report. USGS.

Wheeler, R. 1997. Boundary separating the seismically active Reelfoot Rift from the sparsely seismic Rough Creek Graben, Kentucky and Illinois. Seismological Research Letters, 68, 586–598.

Wood, Steve. 2000. Ground-response analysis of the near-surface sediments in the Memphis, Tennessee, metropolitan area. University of Kentucky, Thesis.

Woolery, Edward W., Schaefer, Jeffrey A., and Wang, Zhenming. 2003. Elevated lateral stress in unlithified sediment, Midcontinent, United States—Geotechnical and geophysical indicators for a tectonic origin. Tectonophysics, 368, 139–153.

Zeiler, Michael. 1999. Modeling Our World: The ESRI Guide to Geodatabase Design. Environmental Systems Research Institute.

Zhang, Jingxiong, and Goodchild, Michael. 2002. Uncertainty in Geographical Information. New York: Taylor and Francis, Inc.

VITA

-Born February 10, 1977, in Santa Maria, California.

Education

-University of Kentucky, Lexington, Kentucky, 2000 – 2004
Bachelor of Science – Geology

Experience

-Research Assistant, Kentucky Geological Survey, 2001 – 2006
-Kentucky Army National Guard, 1999 – 2004
-United States Army, 1996 – 1999

Honors and Activities

-Presented thesis research poster at the Seismological Society of America sectional meeting, 2005
-Presented research findings at the Seismological Society of America sectional meeting, 2005
-Recipient of Graduate School Pirtle academic scholarship, 2005 and 2006
-Attended field camp as a student, Montana; 6-week structural geology mapping course, 2004

David M. Vance